Haalbaarheidsstudie naar de toepassing van grid-verstijfde glass-fiber ondersteuningspilaren

Projectnummer - TEW0414010
Project periode: 1 Mei 2015 - 31 Januari 2016

Uitgevoerd door ATG Europe BV

Contents

Chapter 1

Summary

Cost is a design driver in any commercial business, and this is not different in the wind energy industry. The potential of cost savings on wind turbine towers through lightweight composite designs has been shown in the past. However composite grid-stiffened (or lattice) structures, which were shown to lead to significant weight reductions in aerospace applications, have not yet been under investigation for applications in wind turbine towers.

This report describes a feasibility study performed by ATG Europe wherein the structural efficiency of lattice composite structures applied to wind turbine support towers was put to test. Apart from the weight advantages of lattice structures and additional motivation for the study was the aerodynamically semi-transparent nature of a lattice composites. This feature offers potential additional benefits through reducing the interaction between the rotor blade and the tower. The feasibility of lattice composite support tower structures has been determined based on the objectives to:

1. Design a full scale composite lattice tower structure fulfilling the design requirements obtained from references.
2. Show manufacturability of representatively scaled samples of the structure.
3. Evaluate the real life mechanical performance and behaviour of composite lattice geometries under typical wind turbine design loads.
4. Obtain the cost figures for the lattice composite design in comparison to a reference conventional tower, based on the costs related to the process of tower production up to the assembly on-site.

To achieve these objectives a literature review was performed focussing on state of the art in wind turbine design as well as production and analysis of grid-stiffened composites. A reference wind turbine, international regulations and design load references were identified as a good starting point for tower design. Literature on grid-stiffened composite structures supported the expected weight saving potential of these structures.

The reference turbine chosen to be used in this project is the "NREL 5MW reference turbine", weighing 347.5 tonnes and featuring a cost of 510k EURO. It is a virtual open source turbine based on properties of real life wind turbines and wind turbine design studies. The design loads used in this project were based on loads in normal wind turbine operations with a once in 50 year extreme loading occurrence probability.

An analytical smeared stiffness optimisation method was used to obtain an expected range of suitable composite lattice configurations for the selected reference. The outer bounds of this range, featuring extreme grid configurations, were used as input for the design of small scale glass fibre reinforced polymer samples for manufacturing method development and testing. Through a number of iterations a manufacturing method was established which enabled visual defect-free production of samples.

In order to get a more refined performance prediction than the analytical models could offer, numerical simulations and optimizations of the structure were performed. Here, design constraints included a minimum natural frequency constraint of 0.222 Hz, that has been determined based on the rotor operating frequencies. All dimensions of the lattice tower were based on dimensions of the reference tower except for the base diameter. Here an additional base diameter constraint of 4.4m was implemented to reduce excessive land based transportation costs for the tower sections.

Based on the initial optimization results it was found that a glass fibre design could not satisfy the stiffness, manufacturing and 4.4m base diameter constraints simultaneously. Additional preliminary calculations indicated that a carbon fibre reinforced polymer version of the tower could meet the design requirements, at the same time being cheaper than the glass fibre version due to significantly lower weight and decreased transportation costs. Following this modification, the design of the carbon fibre reinforced tower has been optimized using an in-house optimization approach tailored for lattice towers. The application of the optimisation approach led to an optimal

design featuring a tower weight of 134.5 tonnes, a material strength factor of safety of 2.41, and a natural frequency of 0.225 Hz.

In order to validate the analysis approach and the performance of vacuum infused lattice a mechanical test sample featuring a scaled section of the composite lattice tower has been designed for testing purposes. Six samples of similar geometry were tested for analysis validation. After correlating the tests, the average error for predicting stiffness of the samples using the selected analysis method was 3.8% with a standard deviation of 4.7%. The failure load found through analysis was 67 kN, whereas the test data showed a spread in failure load from 44 kN to 76 kN.

The cost of the full scale structure has been determined based on the production process starting with the manufacturing tower sections up to installing it on-site. This has been done by estimating material, production and possible savings on transport and assembly costs. The material cost has been determined based on the weight of the optimised design, the production cost has been compared with research performed on wind turbine blade production cost, while the transport and assembly savings were based on a wind turbine logistics reference study. It has been found that the material cost dominates the total cost of the composite tower, and that the composite tower is 675k Euro more expensive than the steel reference tower. Looking at the generated energy cost this increase boils down to an increase in cost of off-shore wind energy of 1.8-3.0% which has to be compensated by the potential additional benefits of a composite lattice tower to make the composite structure economically interesting. Such benefits are e.g. the transparent nature of the structure which has a lower impact on the blade than a steel tower and hence reduces the blade fatigue loads significantly. This can result in direct weight savings in the blades and the tower as well as it could remove the limitations on the maximum achievable rotor span related to fatigue issues. In turn this could enable manufacturing of larger wind turbines than ever before.

Based on the results of this study it has been shown that a geometrically feasible structure can be designed that complies to all design constraints. The manufacturability of small scale samples has been demonstrated, and the real life compression behaviour of small representative samples has been tested. Based on these tests the prediction of stiffness, strength and out-of-plane deflection have been improved. A cost estimation of the process of manufacturing tower sections up to installing the composite lattice tower on-site shows that the cost of off-shore wind energy increases by 1.8-3.0% in comparison to steel towers for 5MW wind turbines. These increases can be potentially offset by additional benefits of composite lattice towers.

The final conclusion therefore is that a composite lattice tower for wind turbines shows to be structurally very promising, however further research is required into additional benefits of the structure to determine the final economic potential of the structure.

In case of questions or to request additional information please contact Leonid Pavlov:
leonid.pavlov@atg-europe.com

Chapter 2

Introduction

The reduction of cost is as in every industry, a driver in the design process of wind turbines. To reduce cost in wind turbine tower transport and assembly, light weight fibre reinforced lattice structures have shown potential in former research projects [6, 7]. Both studies determine the structural performance of composite wind turbine tower alternatives for steel towers through Finite Element Analysis (FEA). Polyzois et al. included both a static and a dynamic test campaign on tower sections [6]. Lim et al. showed that based on production cost a fibre reinforced tower could be an economic alternative for a 2MW turbine [7].

With regard to saving weight, composite grid stiffened and lattice structures have shown to achieve high strength to weight ratios [8], and weight savings compared to equivalent aluminium concepts up to 30-40% [9, 10] in aerospace industry. However research on neither composite grid stiffened nor composite lattice structures for wind turbine towers is known to the author.

Based on the potential cost reduction in wind turbines through lightweight composite wind turbine tower designs, and with the notion that the airflow transparent nature of a composite lattice geometry can potentially have a secondary benefit in decreasing the tower blade interaction based cyclic loading on the blade [11], a feasibility study on fibre reinforced polymer lattice structure for wind turbine towers is proposed.

The feasibility of this fibre reinforced lattice structure is assessed based on the results flowing out of the following project objectives:

1. Design a full scale composite lattice tower structure fulfilling the design requirements obtained from references.
2. Show manufacturability of representatively scaled samples of the structure.
3. Evaluate the real life mechanical performance and behaviour of composite lattice geometries under wind turbine typical design loads.
4. Obtain a relative cost figure for the composite design in comparison to a reference tower, based on the cost related to the process of tower production up to the assembly on-site.

These project objectives are achieved by performing: global design and analysis of the structure, manufacturing and testing of scaled samples and comparing the cost of a composite design to the cost of a steel reference. It is expected that a composite lattice structure can be designed to feature a lower weight than a steel reference tower. Therefore this design can decrease transport and assembly cost for wind turbine towers. It is furthermore expected that the material costs of the composite structure are of large influence on the total cost, which makes the economic potential highly dependent on the final weight of the tower. Considering industry preferences, glass fibre is expected to be the most cost efficient reinforcing fibre for such a composite lattice tower.

Chapter 3

Literature study

This literature study was performed with the objective to facilitate a knowledge basis for the design of an open lattice composite wind turbine tower. This is done by describing the ingredients required to perform such a design process. These ingredients can be subdivided in three main groups: Design criteria for wind turbines, analysis methods for grid stiffened structures and production methods for grid stiffened structures.

The main applicable information is first summarized per topic and a subsequent synthesis of relevant information is performed. This synthesis served as a backbone for developing the project logic.

3.1 Literature review

This section discusses information gathered from literature on topics relevant to composite lattice wind turbine tower design and manufacturing.

3.1.1 State of art in wind turbine design

Wind turbine towers are the support structures of wind turbines. All the forces and moments of the complete system have to be taken care of by the tower in order to keep the turbine attached to its foundation. Therefore it is required to know what load cases can be expected on the tower, what safety factors are to be taken into account and what regulations apply.

As for nearly every engineering structure, regulations apply on wind turbines. The operating conditions and design safety factors are dictated by the international regulations on wind turbines. These regulations are written by the International Electrotechnical Commission (IEC) under the code: IEC 61400 [12]. The structural design requirements are given in a format of wind condition classifications. These wind conditions are wind turbine site specific and are based on two parameters, reference wind speed and a turbulence factor. Reference wind speed is defined as an extreme average wind speed over a 10 minute time span with a recurrence interval of 50 years. The turbulence factor is defined as a ratio between the standard deviation of the wind speed and the average wind speed. The final design load cases are in turn based on these site specific wind condition.

The reference wind speeds and turbulence factors can be used in wind turbine specific aero-elastic tools to obtain design loads. An open source tool available for these type of calculations is the Fatigue, Aerodynamics, Structures and Turbulence code (FAST) written by the National Renewable Energy Laboratory (NREL) in the US. This code is widely used in wind turbine design and is accepted for certification purposes [13]. In order to obtain these design loads from such an aero-elastic tool a reference wind turbine is required. However since wind turbines are produced by commercial companies, extensive data on commercially available wind turbines is not readily available.

A solution for this problem can be found in other research performed by the NREL. The NREL developed a 5MW reference wind turbine which is widely used in wind turbine research and development for comparative purposes [14]. This open source wind turbine model contains all the data on nearly all the aspects of wind turbine design (aerodynamic, structural, electric etc.). This enables the usage of this reference turbine in combination with the FAST tool to obtain design criteria.

The most important design criterion for wind turbines stated by the international regulations is the so called design load case 1.1 [12]. This design load case covers the expected 10 minute average extreme loads with a recurrence interval of 50 years. The data required for this design load case

for the NREL 5MW reference turbine [14] has been simulated extensively by research institute SANDIA [2]. In this research the average wind speed and turbulence intensity in a 10 minute interval is recorded for 96 years worth of simulations. The loads found based on the simulated wind parameters can be translated to probabilities of exceedance in 10 minute intervals. Using this data the extreme design loads for a 50 year occurrence interval can be determined for the NREL reference wind turbine tower and can be used as the basic design load case for a typical 5MW wind turbine.

With the basics on design criteria described, cost determination of wind turbine towers is the topic left for discussion. As already mentioned detailed cost determination in the small amount of research found on composite wind turbine towers is scarce. However extensive research has been performed by NREL on the topic of wind turbine cost. These studies enable the determination of transport and assembly cost of both the NREL 5MW reference wind turbine and a composite tower design through a cost break down for tower transport and assembly based on tower geometry and weight as provided by Smith [15]. The study shows that keeping the diameter of the tower below $4.4m$ has very big influences on land based transportation cost. This diameter can therefore be used as a design constraint in the project to reduce wind turbine tower cost. The manufacturing cost of the steel reference wind turbine can be determined using a manufacturing cost scaling model based on basic wind turbine parameters such as hub height, rotor swept area and turbine rated power. Such a study is performed by Fingersh et al. [16]. With the reference turbine tower and tower transport and assembly cost figures based on the research indicated in this section, the composite tower material and production costs are left to be determined in the project based on the final tower design.

3.1.2 Composite grid stiffened and lattice structures

The envisioned type of structure in this project is an open lattice composite structure, which is designed based on the requirements as described in 3.1.1. This type of structure has its own properties and typical analysis methods. In this section the specific properties of grid stiffened composite structures and analysis methods available are be reviewed.

Properties of composite lattice structures

Composites have superior properties in axial fibre direction but this is not always optimally used in a lot of composite applications today. Often aluminium structures are replaced by topologically equivalent composite versions, in aerospace industry. This is sometimes referred to as black aluminium [10].

Composite grid stiffened and lattice structures try to improve the efficiency of structures using the superior properties of fibres in axial direction by the use of rib type structures with a unidirectional lay-up [10, 17, 18]. Grid stiffened structures are therefore considered to be interesting structural alternatives in aerospace applications. It is found that composite grid stiffened structures achieve higher strength to weight ratios [8] and application of these structures in spacecraft payload fairings and interstages has shown weight savings up to 30-40% in comparison to aluminium equivalents [9, 18]. This design concept improves the buckling behaviour of the cylindrical structures by adequate usage of hoop ribs in the grid. When these composite lattice structures are loaded in compression the hoop ribs are be slightly loaded in tension. This resists buckling and therefore stabilizes the structure [19].

Besides weight savings due to more efficient fibre loading, a few other advantages for composite lattice structures can be identified: the lay-up can be completely automated through, for instance, filament winding [18, 20]. Due to the open structure, inspection and repairs can easily be carried out compared to sandwich solutions [18,20]. And the grid gives the structure an increased damage tolerance by means of redundant load paths [20, 21].

A side note has to be made on shortcomings of grid stiffened composites. As for all composite structures it is hard to predict failure accurately [20]. Furthermore grid stiffened structures require complex manufacturing processes and tooling compared to for instance sandwich structures due to the complex geometry of grid stiffened composite structures [20].

Analysis methods

Two types of structural analysis methodologies for grid stiffened composites can be identified. Smeared stiffness and direct stiffness approaches. The smeared stiffness approach, smears the stiffness of the grid over a virtual skin which has equivalent properties with respect to the real system. The direct stiffness methods directly takes the grid into account as is and therefore is more detailed in geometric representation. Both methods have their advantages and shortcomings, smeared stiffness approaches are generally simpler to evaluate than discrete models [18], but do show inaccurate results in failure prediction [22].

A smeared stiffness or sometimes also called equivalent stiffness model for grid structures with or without skins is for instance developed by Reddy et al. [23]. The smearing approach took compression, tension and transverse shear effects into account. But did not consider torsion of the ribs and the eccentricity of the geometry. In an effort to improve the smearing model Jaunky et al. included skin stiffener interaction effects [24]. Other improvements are made by Chen and Tsai [18] expanding the model by including torsion effects of the ribs. And by Zhang et al. who also took eccentricity into account, further reducing the error made on unsymmetrical cross-sections [25].

The application of a smeared method in optimization is for instance performed by Vasiliev and Rasin using a smeared stiffness method to obtain optimal parameters by analytical minimization of safety factors [9]. And the method proposed by Jaunky is used to optimize composite structures with a genetic algorithm in references [26, 27].

As mentioned before smeared stiffness approaches can be inaccurate for certain types of structures, Gürdal and Gendron acknowledge this inaccuracy for sparse grids and propose a FEM approach where the grid is modelled as discrete elements [21]. Such discrete methods are used in multiple studies to assess local behaviour of grid stiffened structures. The discrete analysis method can be sub-divided in a few sub groups. The first group is the so-called stiffened element methods as for instance defined and described by [28–31]. Using the stiffened element method the elements themselves account for being stiffened by a grid, and take the effect the grid has on the structure into account. The usage of stiffened element methods is therefore very convenient, but the elements are considered questionable because they have a discontinuity in the second derivative while the displacement is described by continuous functions [28].

Another approach is the layerwise method which is developed to take thickness effects into account while using shell elements for the skin and beam elements for the stiffeners. It is for instance used by Kassegne et al. and Guo et al. to determine local effects more accurately [32, 33]. Of course detailed analysis of grid stiffened structures can also be done using solid elements. This is for instance done by Jadhav et al. using solid elements to model the ribs and shell elements for the skin, in an effort to optimize composite panels for impact energy absorption through parametric optimization [34].

Numerous other researches have been performed using the above described techniques. The research described in this section is used to show the different modelling techniques and the potential of the modelling techniques found. The accurate results on local behaviour of these methods in the papers cited in this section show the advantages of the discrete modelling approach when detailed results are required. This accuracy is however at the cost of computational time compared to smeared stiffness analysis.

3.1.3 Manufacturing of composite grid stiffened and lattice structures

The manufacturing of composite lattice structures requires special approaches in order to produce the ribs. Typically wet filament winding or fibre placement is used in combination with a tool to keep the ribs in place to obtain the desired geometry. The details in manufacturing approaches are further elaborated in this section.

Manufacturing methods

Some distinctions in production methods considering mould type can be made. The simplest form is free forming which uses supports for the tows at the ends of a structure between which the fibres are wound. However while it is relatively cheap it leads to poor rib quality [19]. In order to improve the quality by keeping the fibres in place the ribs can also be placed in elastic coating applied around a mandrel which can be removed after curing [19].

A problem acknowledged for grid stiffened composites is the build-up of fibres in the nodes, where the ribs intersect. This typically leads to high fibre volume in the nodes and low fibre volume in the ribs [1,19]. For production processes requiring an elevated cure temperature, such as prepreg fibre placement and wet filament winding, improvements in this area are made with two different tooling methods, hybrid tooling and expansion block tooling. A hybrid tool consists of two parts, a rigid base with grooves in which an expansion tool made of a high thermal expansion material is placed [1], see Figure 3.1 [1] for a schematic example. The expansion tool gives compaction to the rib during curing, increasing the fibre volume fraction.

This production method however has a limitation to rib thickness, because the walls of the expansion tool needs to be very wide for providing adequate compaction for thick ribs. In order to overcome this problem, expansion block tooling is developed. In this approach, complete expansion blocks are used instead of grooves filled with expansion material [1], see Figure 3.2 [1] for a schematic example.

Besides wet filament winding and prepreg fibre placement a new manufacturing method is developed using dry winding and vacuum infusion [35]. The feasibility of this production process is also demonstrated by Shroff et al. [36]. This process enables room temperature curing, making

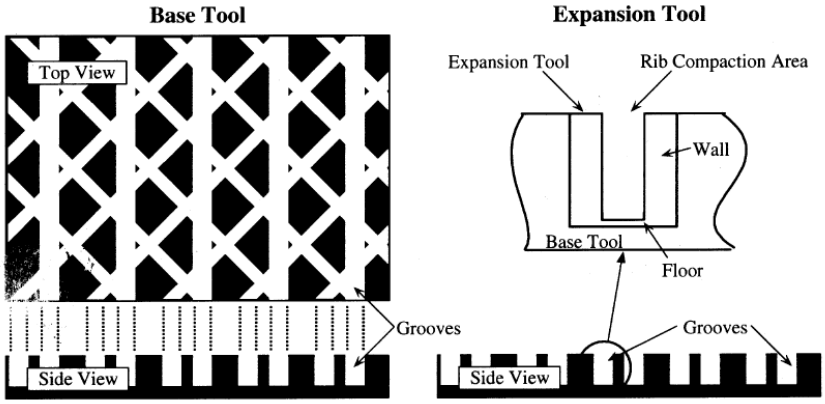

Figure 3.1: Schematic view of the base and expansion tool. The left side shows the base tool with the grooves in which an expansion tool can be placed. The expansion tool is integrated as shown at the right side of the picture [1]

.

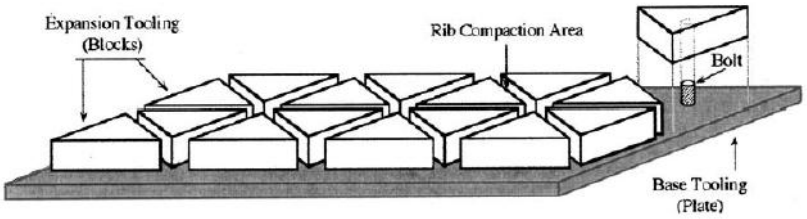

Figure 3.2: Schematic view of expansion block tooling with the expansion blocks on top of the tooling base [1]

.

the production process less expensive and less dependent on autoclave or oven availability. It should be noted that expansion based tooling cannot be used in this production method, since the expansion of the tool is based on thermal effects during curing. Furthermore post-curing should be considered to enhance resin properties for room temperature cured epoxies. See the following section for post-curing considerations.

Post-curing influences

The curing strategy influences the production cost of the tower. In order to minimize these costs an out-of-autoclave (OOA) curing process would be very beneficial. An OOA process could be achieved with vacuum infusion of resin in dry fibres. The need for and type of post-cure performed after the infusion and room temperature curing influences both cost and mechanical performance of the material. From a cost perspective it would be optimal to only have a room temperature cure omitting the necessity of post-cure equipment. The influences this has on the mechanical characteristics are however important to consider.

Post-curing an epoxy influences the degree of cure of the material, and with that the glass transition temperature (T_g), and the mechanical properties. Little information is available on the direct effect on T_g by post-curing epoxies. But for vinyl ester laminates it is shown that post-curing increases the degree of cure and with that enhance the mechanical properties dominated by matrix behaviour [37]. Cain et al. showed that the T_g increases and that shear strength, shear modulus and especially the amount of cycles of fatigue improve by post-curing [37]. For epoxies the positive dependence of T_g on degree of cure is originally shown by Venditti et Gillham [38]. The problem induced by a lower T_g is the decrease in stiffness of the epoxy at temperatures close to the T_g. This results in risks for structural stability when the structure heats up due to for instance solar radiation.

But besides the lower T_g another effect depending on post-cure and influencing the mechanical properties is water absorption. Water absorption is dependent on the free volume of the epoxy which is influenced by the degree of cure [39]. Epoxies absorb water when submerged but also

from humidity in he air [40]. Water absorption has a few effects on the mechanical properties. It reduces the T_g of the material and therefore affects the stiffness negatively [40]. Water absorption is reported to reduce the failure stress and inter laminate shear strength of the composites in salt water tests [41]. And test results do also report worse results in fatigue when these tests are performed in salt water [42]. The results worsen even more when the samples have been aged for 15 weeks in salt water at 60°C decreasing the maximum stress and fatigue life significantly.

Two effects on the amount of water absorption due to post-cure can be seen. The first is a decrease in water absorption for an increase in post-cure temperatures due to the higher cross-linking after post-cure [39]. However the second effect is an increase in water absorption for higher post-cure temperatures which is trigged by the higher glass transition temperature of these materials [39]. With the higher glass transition temperature the material transforms to the glass state at a higher temperature after post-cure. Further cooling results in slower increase in density than would be the case for the same epoxy with a lower glass transition temperature. This results in a larger free volume at ambient temperature in the epoxy which is cured at higher temperatures [39]. The two effects together lead to an optimal post-curing temperature for minimizing the combined effect.

3.2 Literature Synthesis

In the previous section, information is provided on the current state of the art in wind turbine design, the properties and analysis methods of composite lattice structures and manufacturing methodologies and considerations for these structures. The results found are combined and linked to the research project under consideration in this section.

Wind turbine regulations, a wind turbine reference model and open source wind turbine modelling software which is suited for certification is identified. Besides that previous research has been found on which cost estimations can be based and from which design loads can be extracted. This information is the basis of the design process. Based on this data, requirements on the structure can be made and design loads can be determined.

The envisioned design concept is a composite lattice structure. Due to the efficient usage of unidirectional fibres in the lattice, a high strength to weight ratio can be achieved. This in turn enables the weight optimization of wind turbine towers. Dependent on the sparseness of the composite lattice grid, the required detail in local effects and optimization strategy, an analysis method is to be chosen for the composite lattice tower optimisation. For fast calculations a smeared stiffness approach can be used, but it has to be taken into account that this method only accurately predicts global failure. A discrete analysis method can also take the local effects into account, but is computationally more expensive. Using a smeared stiffness method to obtain a preliminary design which can then in a second step be optimised in detail using FEM in combination with an inhouse build Abaqus and Catia based genetic algorithm, is seen as an appropriate design methodology for this project. It enables a quick method to come up with a first design, which can be used as a basis to assess the details of the structure in a second design step.

Samples of the final structure need to be manufactured for testing. Multiple manufacturing methodologies are described to produce the envisioned structure of which prepreg fibre placement or wet filament winding on expansion based tooling, and dry winding in combination with vacuum infusion are the most relevant methods. Dry winding in combination with vacuum infusion is preferred due to the low cost process related to this manufacturing method. When using vacuum infusion the use of post-curing should be evaluated to achieve a good balance between enhanced material properties and production cost. Since the post-cure influences are very epoxy dependent the influences of a post-cure can best be real life tested using representative post-cured and non-post cured test coupons. This study however does not go into further detail on a post curing evaluation. This is left as a recommendation for further research.

Chapter 4

Basic tower geometry considerations

In this chapter the basic geometry aspects of the wind turbine and the composite lattice structure are provided. This information serves as the basic design input required and used throughout the entire project.

4.1 The reference wind turbine and terminology

The reference turbine used in this study is the so called NREL 5MW reference turbine [14]. This reference turbine is virtual turbine which is based on the properties of real life wind turbines and wind turbine design studies. The main reason for using this wind turbine design as a reference, is because the study determining the design of this turbine is as an open-source available. This also triggered that the tower has been used as a baseline in other wind turbine researches which is amongst others of use in determining the design loads in section 6.1. The tower specific geometric properties of the reference turbine are given in table 4.1. The other basic properties of the reference turbine which are further used in this study are given in table 4.2. The tower outer dimensions are taken as design constraints for the composite tower such that the composite tower can function as replacement of the reference turbine's steel tower.

Table 4.1: Reference wind turbine tower geometric properties as used in this study

Tower height (m)	87.6
Tower base diameter (m)	6
Tower base thickness (m)	0.027
Tower top diameter (m)	3.87
Tower top thickness (m)	0.019

Table 4.2: Basic reference wind turbine properties used in this study

Rating (MW)	5.0
Rotor Orientation	Upwind
Rotor configuration	3 Blades
Cut-in rotor speed (rpm)	6.9
Rated rotor speed (rpm)	12.1
Hub Height(m)	90.0
Individual blade mass (Tonnes)	17.74
Hub mass(Tonnes)	56.78
Rotor mass (Tonnes)	110.0
Rotor Centre of Mass (CM) X-position (m)	-5
Nacelle mass (Tonnes)	240.0
Nacelle CM X-position (m)	1.9
Tower mass (Tonnes)	347.5
Rated generator torque (Nm)	43096
Gearbox ratio (-)	97

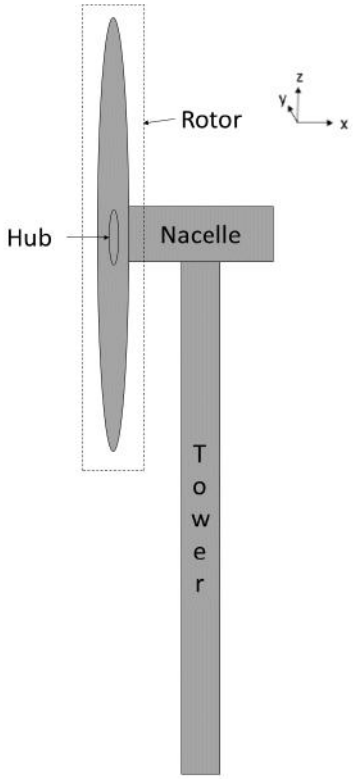

Figure 4.1: Schematic drawing of a wind turbine with part names

To make sure every reader of this report can understand the wind turbine terminology used a schematic drawing of a wind turbine is given in fig. 4.1. A small list explaining the specific terminology used in this report is given next:

- Hub: Part of the rotor to which all the blades are connected
- Rotor: Part of the wind turbine which contains all the blades and the hub.
- Nacelle: Part of the wind turbine which contains the generator and gearbox etc.
- Tower: The part connecting the nacelle to the foundation.
- Rating: The rating describes the maximum power a wind turbine can produce.
- Cut-in rotor speed: The minimum rotor speed (rpm) at which the turbine generates power.
- Rated rotor speed: The minimum rotor speed (rpm) at which the maximum power output of a wind turbine is achieved.
- Upwind/ downwind rotor orientation: Indicates the position of the rotor with respect to the tower and wind direction. An upwind rotor orientation means the rotor is positioned in front of the tower with respect to the wind direction. A downwind rotor orientation has the rotor positioned after the tower with respect to the wind direction.

4.2 Composite lattice geometry

For the composite lattice structures like the one under consideration in this study there are two grid structure lay-outs which are commonly used. One is the triangular grid orientation where all three rib types positive helical, negative helical and hoop rib come together in one node. The other is the tri-hexagon grid orientation in which only two ribs, come together in one node. Both types are shown in fig. 4.2. The triangular grid has the benefit that the amount of nodes in the grid is lower. But the complexity of the nodes is lower in the tri-hexagon grid type. Since complexity of the node is expected to have a large influence on the flow of resin in a vacuum infusion process, the tri-hexagon grid lay-out is selected early on in the project. Other grid types are therefore not further researched.

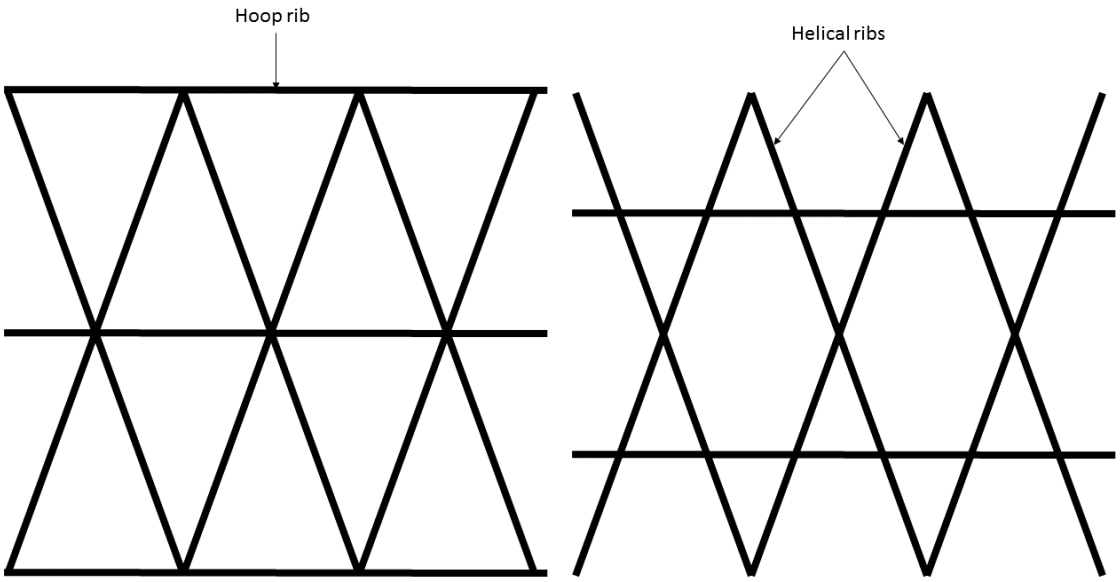

Figure 4.2: Schematic drawing of the grid layouts. Left a triangular grid, Right a tri-hexagonal (also known as kagome) grid

Chapter 5

Preliminary design and manufacturing method

In order to include manufacturing considerations in the final design of the tower, the manufacturing method was defined early on in the feasibility study through manufacturing tests. This chapter discusses the design considerations for manufacturing trial samples as well as main considerations regarding the manufacturing method used.

5.1 Preliminary design method

Early in the process of the feasibility study certain preliminary tower design iterations were performed in order to obtain a range of possible rib intersection angles in the structure. The main goal of the manufacturing tests besides determining the manufacturing method was to observe effects of resin flow over the nodes. Since the helical angle determines the length of the node, the range of helical angles possible in the design is desired as input for the test samples. Based on these initial tests manufacturing considerations can be taken into account in the detailed design process.

The preliminary design is based on an analytical optimisation as described by Vasiliev [43]. For detailed information on how the method works the reader is referred to the book written by Vasiliev [43]. In this section the results obtained with this method will be explained. The Vasiliev method is used to optimise the weight of the cylindrical composite lattice structure at the tower base, the highest loaded part of the tower, with constrains on strength and buckling failure only. Hence no deflection constraints are applied. Also the method only considers axial compressive loads and takes bending loads into account using the following equation for an equivalent compression load on a thin walled cylinder:

$$P = T + \frac{4M}{D} \tag{5.1}$$

Where P is the equivalent axial force, T is the applied axial force, M is the applied bending moment, and D is the cylinder diameter.

The equations do however not implement shear forces and torques in the model. Therefore the final loading situation in the model is one in which only an equivalent compressive load is applied as a distributed load over the outer edge of the grid. The loads used in the estimation of parameters are calculated using the base moments as described in section 6.1.1.

The Vasiliev optimisation method categorizes the most optimal design parameters based on three different loading ratios, the lower one where only local rib buckling and axisymmetric global buckling are critical. The middle one where also strength becomes critical. and the highest loading ratio where non-symmetric global buckling has to be taken into account instead of axi-symmetric buckling. Because of the high loading situation, the Vasiliev method estimates the most weight efficient design to be in the highest loading ratio range where material properties are determining the helical angle. This gives an optimal angle of 25.5°.

In order to obtain the second bound on the helical angle the Vasiliev method result for the region where the load is driving the helical angle is used. This does not give an weight optimal design set, but does results in an helical angle driven by the loading instead of material properties. The angle based on this calculation is 6.4°.

With this approach the helical angles driven by the two failure cases of importance, buckling and strength, are obtained. The two angles found are therefore considered to be the outer bounds of the range in which the helical angle is expected to be in the final design.

The Vasiliev optimisation result of 25.5° is used to determine the dimensions of the ribs. This optimisation method results in large rib heights of 0.818 m, which is considered undesirably large for a tower with a diameter of 4.5 m. To solve this a constraint on the rib height with a maximum of 0.2 m is added to the Vasiliev equations, while the angle was kept fixed at 25.5°. This constraint influences the required helical rib width through equations for the required structural strength. The required helical rib width can therefore be determined with the following equation:

$$\delta_h = \frac{P a_h}{2\pi D \bar{\sigma} h \cos\phi} \tag{5.2}$$

In which a_h is the shortest distance from helical rib to parallel helical rib $\bar{\sigma}$ is maximum material strength, and ϕ is the helical rib angle. a_h is given by:

$$a_h = \frac{2\pi}{n_h} D \cos\phi \tag{5.3}$$

In which n_h is the number of helical ribs. The equations lead to a helical rib width of 92.2 mm. The hoop rib width is determined in the next step using a few iterations in Abaqus to implement the effect of shear and torque loading in the evaluation on strength and buckling, a hoop rib width of 43.35 mm is determined in this way. A 2D picture of the geometry as described is given in fig. 5.1.

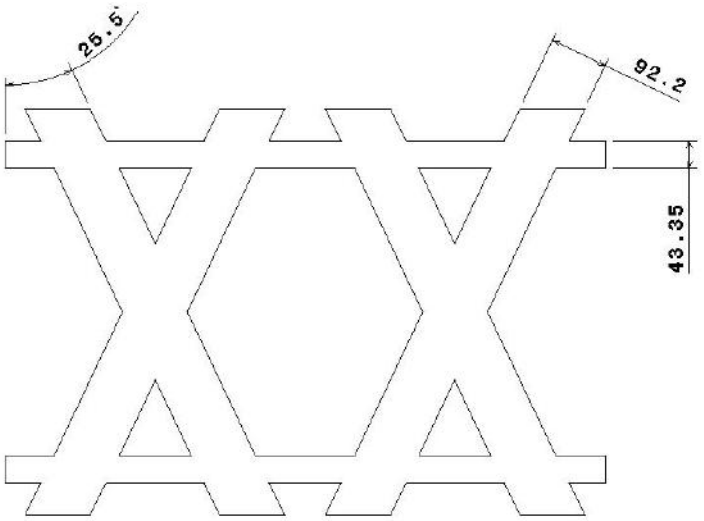

Figure 5.1: The final configuration of the preliminary design with a helical angle of 25.5°. The height of the rib of 200 mm is in the out-of-paper direction.

In order to simplify the grid geometry from an infusion point of view. The helical ribs are scaled close to the size of the hoop ribs, by decreasing the helical rib width by a factor of two. This is desired since little is known on the flow of resin in the ribs during infusion. Having the rib widths at dimensions close to each other would therefore make sure that effects of differences in rib width are not influencing the infusion and therefore makes it easier to understand what happens in the infusions when it is giving unexpected results. The effects of differences in rib width are therefore left to be researched later. However the infusions done for mechanical test sample production as described in section 8.2.1, did have differences in rib width. This therefore shows that on a small scale, the flow did not seem to be affected in a negative way by rib dimension differences.

Additionally all dimensions are scaled by a factor 6 to obtain sample geometries which are easily manufacturable by hand with not too much labour involved. This results in a rib height of

33.33 mm, a helical rib width of 7.68 mm and a hoop rib width of 7.23 mm. A pictures of the resulting samples are given in section 5.2 in figs. 5.2 and 5.3.

The analytical optimisation method described here has not been used further in the design process since it is not accommodating some basic input requirements like shear and torque loading, maximum deflection constraints, and uses rough assumptions. The Vasiliev method used here resulted in rib dimensions which are close to the final design as described in section 7.3. Therefore the rib geometries infused during the first manufacturing tests as described in section 5.2, are considered to be representative for the final optimised composite lattice geometry.

5.2 Manufacturing method determination

Based on the helical angle bounds found in the analytical design study, the manufacturability of the structure using vacuum infusion is tested.

5.2.1 Manufacturing considerations

Vacuum infusion is a process in which small details in the set-up can make big differences in the result. The results of a vacuum infusion are therefore difficult to predict. This is especially the case in the grid structure under consideration due to its changes in fibre volume fraction at the nodes and the multiple flow paths. The configuration leads to differences in permeability between different regions of the structure, influencing flow behaviour and increasing the risk of including air in the low fibre volume areas. To observe these properties, an infusion testing campaign was performed with the goal to obtain infused specimens which have no flaws which are visible to the human eye.

Geometry considerations

The testing campaign is set-up such that multiple effects in flow behaviour which are thought to be of importance can be observed. First a few rib infusions are performed with ribs of different sizes to observe size effects. Secondly a sample with the a single helical node and a small helical rib intersection angle is studied to observe the flow over a helical node. The geometry is shown in fig. 5.2.

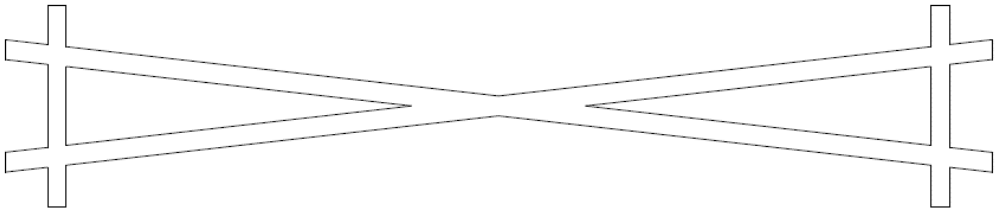

Figure 5.2: The small angle single helical node configuration

The small helical intersection angle of 6.4° is chosen for this single helical node sample, since this would represent an extreme angle from an infusion point of view, which can be a result of the optimization. A small helical intersection angle leads to a larger node volume, hence a larger region with lower permeability due to the higher fibre volume in the nodes. Therefore it is expected that this type of node is the hardest to infuse. Finally a multiple helical node sample with a the higher helical intersection angle of 25.5° is infused to observe the flow over regions with multiple helical nodes, and to validate that the infusion strategy works at different rib helical intersection angles. The geometry of this sample is shown in fig. 5.3.

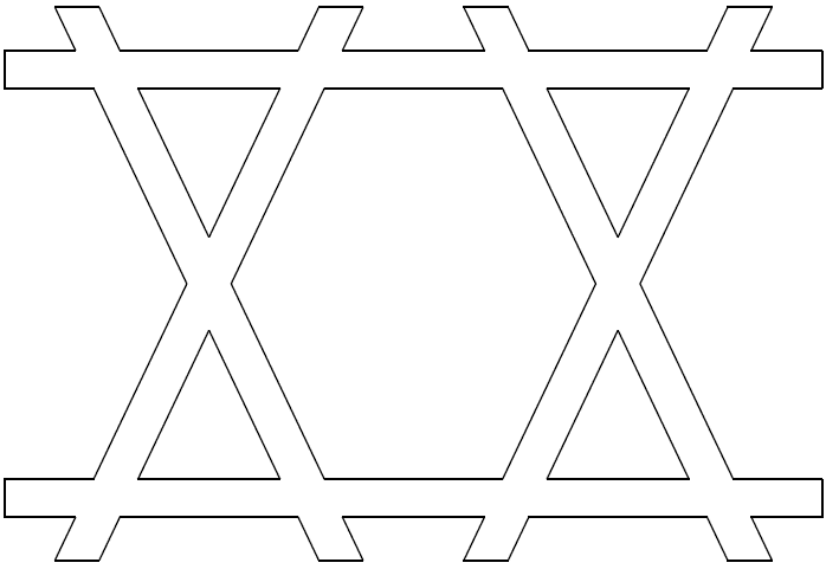

Figure 5.3: The high angle multiple helical node configuration

Mould considerations

To keep the fibres in place before and during infusion some kind of mould is required. For ease of production a silicon rubber mould is chosen. A silicon rubber mould can easily be created by pouring non-cured silicon rubber in the desired shape. And it can easily be removed from the infused sample when the resin has cured.

In order to pour the rubber in the right shape a male mould for the infusion samples should be created. This is done through 3D printing the ribs with an integrated outer wall, creating a closed part in which the rubber moulds can easily be poured. An example is shown in fig. 5.4

Winding considerations

The winding is done by placing the rubber mould on a wooden baseplate with nails placed such that they can be used to wind the fibres straight through the mould and around the nails. The way of winding is shown in fig. 5.5 The winding is considered completed when the mould is completely filled at the node locations. For the rib samples which do not have a node in the sample, a node is wound outside of the mould to ensure the fibre volume fraction in the rib is representative for a large scale structure. After winding is completed, a vacuum bag is created and infusion of resin is performed.

Manufacturing method trial samples

Upon a short development cycle of the manufacturing method, visual defect-free samples have been produced for scaled-down lattice tower sections. An example is shown in fig. 5.7.

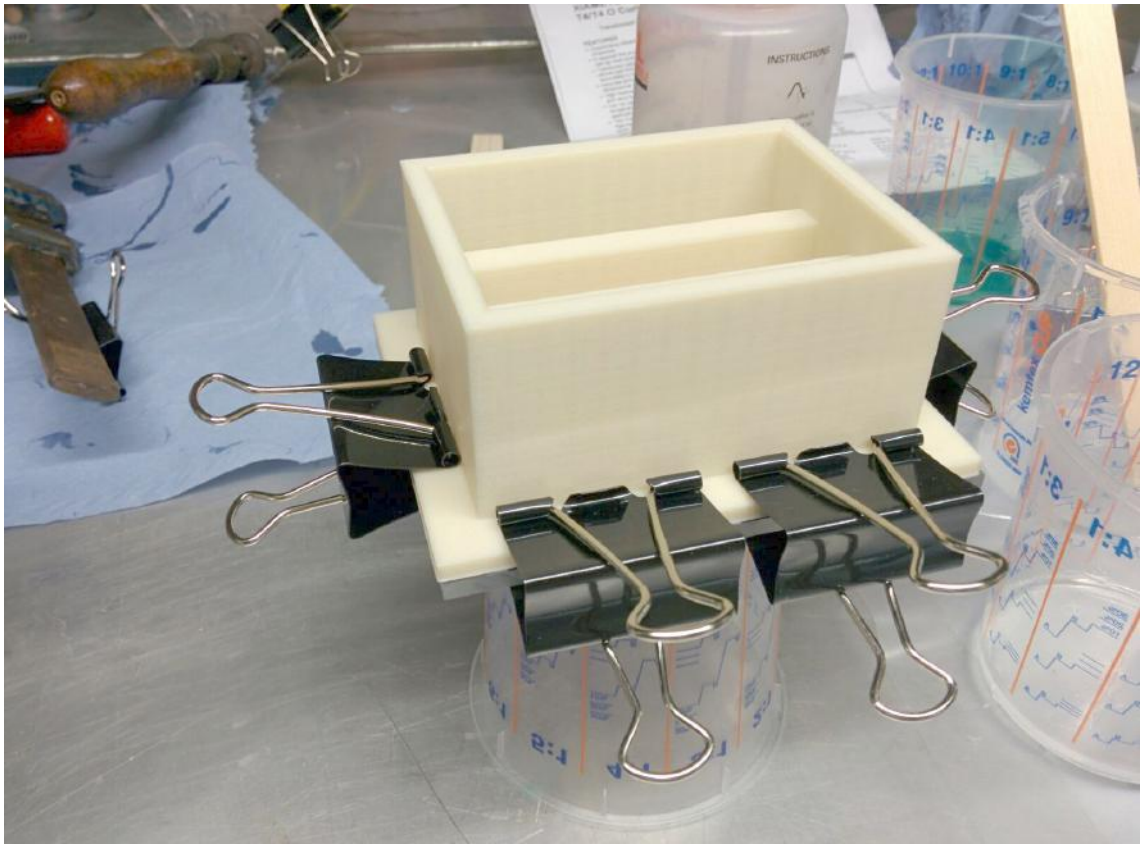

Figure 5.4: 3D printed negative for producing a rubber rib sample mould

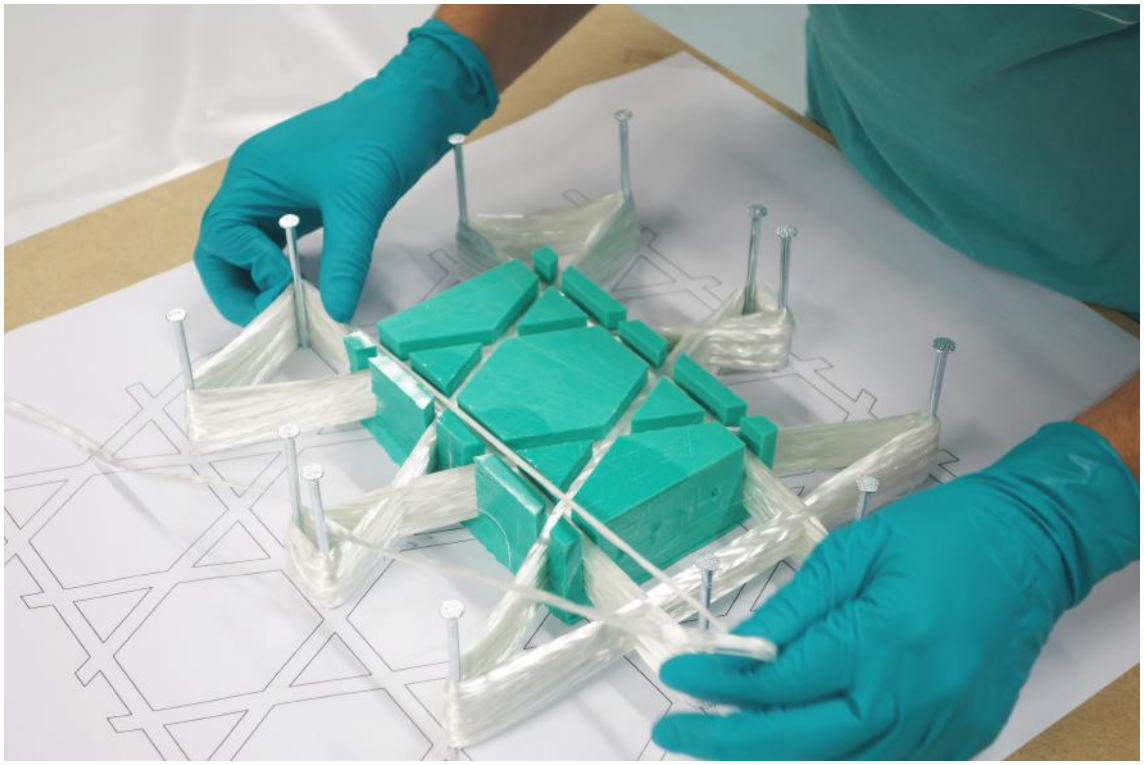

Figure 5.5: Picture showing the winding process of the high angle multiple helical node sample

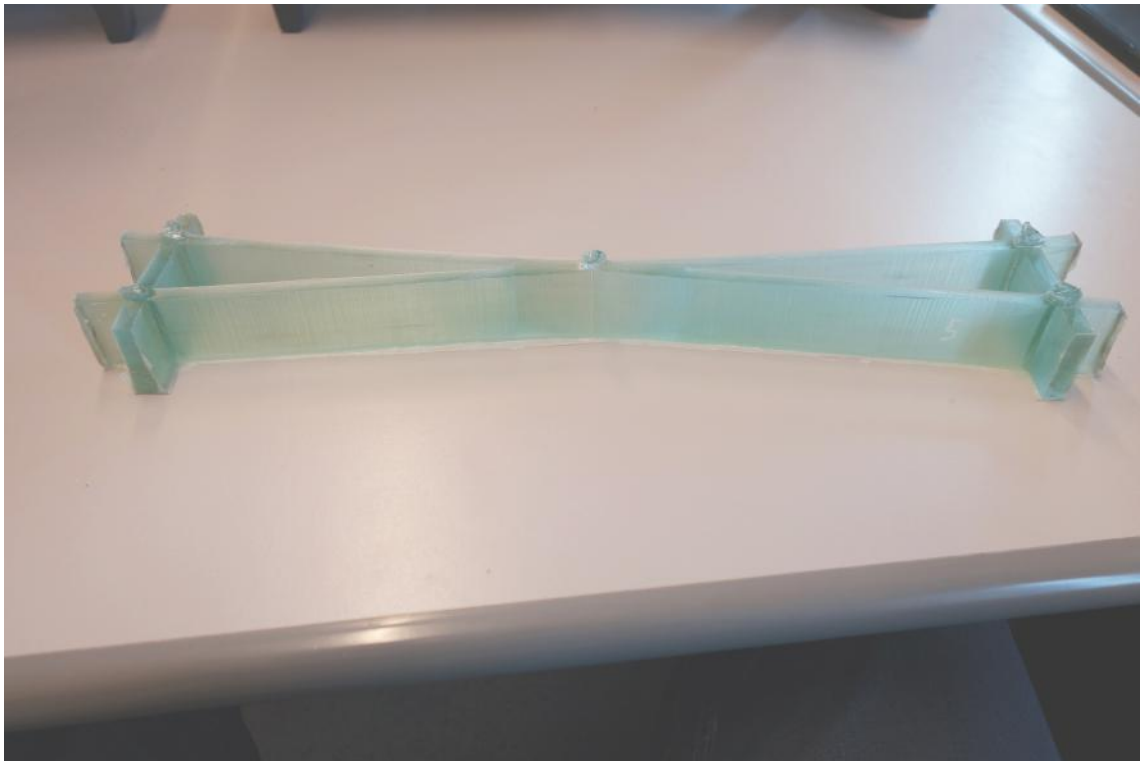

Figure 5.6: Picture showing the Final single helical node infusion sample

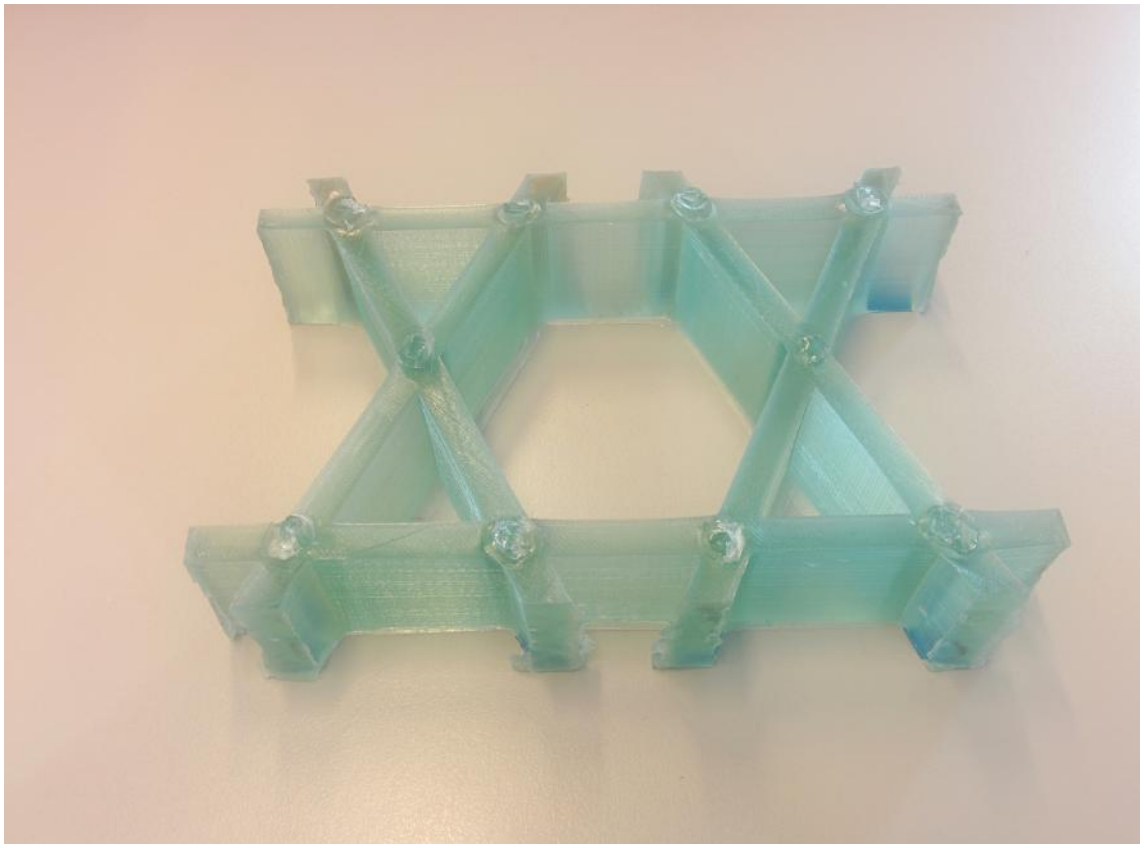

Figure 5.7: Picture showing the Final multiple helical node infusion sample

Chapter 6

Detailed design input determination

To be able to have a consistent way of designing and optimising a composite lattice tower, the final design inputs and requirements have to be settled first. The final design loads considered in the detailed design are given in section 6.1. In section 6.2 the materials under review and exact material property determination method is explained. And finally the cost influence on the design constraints is explained in section 6.3.

6.1 Design load determination

The structural criteria considered in this study are based on an expected ultimate load for this type of wind turbine in operation conditions and a natural frequency constraint based on the rotational speed of the rotor. Of course there are more loading situations like fatigue and gust wind etc. which are of importance in wind turbine tower design. Based on input obtained from specialists in the field of wind energy [44], it is decided that an quasi-static ultimate load analysis would be a representative load case for determining the initial structural feasibility. The method of load determination is described in section 6.1.1.The natural frequency constraint determination is explained in section 6.1.2.

6.1.1 Static loading determination

The ultimate design loads for a wind turbine are determined through a data set created by research institute Sandia for the NREL 5MW wind turbine [2].

The data is generated with the software package FAST. The wind turbine loads are representing the maximum loads measured in a wind turbine simulation with a duration of 10 minutes. These loads plotted as function of the cumulative probability for exceeding that load. The higher the load is the lower the cumulative probability that this load is exceeded. The basic static load case in wind turbine design is based on the once in 50 year expected maximum load. The probability of reaching this load in a 10 minute timespan can be calculated to be:

$$\frac{1}{50 * 365 * 24 * 6} = 3.805 * 10^{-7} \tag{6.1}$$

Comparing this probability to the probability distribution of loads given by the Sandia documentation, as shown in fig. 6.1, leads to the base moment data given in table 6.1 [2]. The coordinate system is as shown in fig. 6.2

Table 6.1: Once in 50 year expected base moments

M_x (Nm)	$4.26 * 10^7$
M_y (Nm)	$1.15 * 10^8$
M_z (Nm)	$1.18 * 10^7$

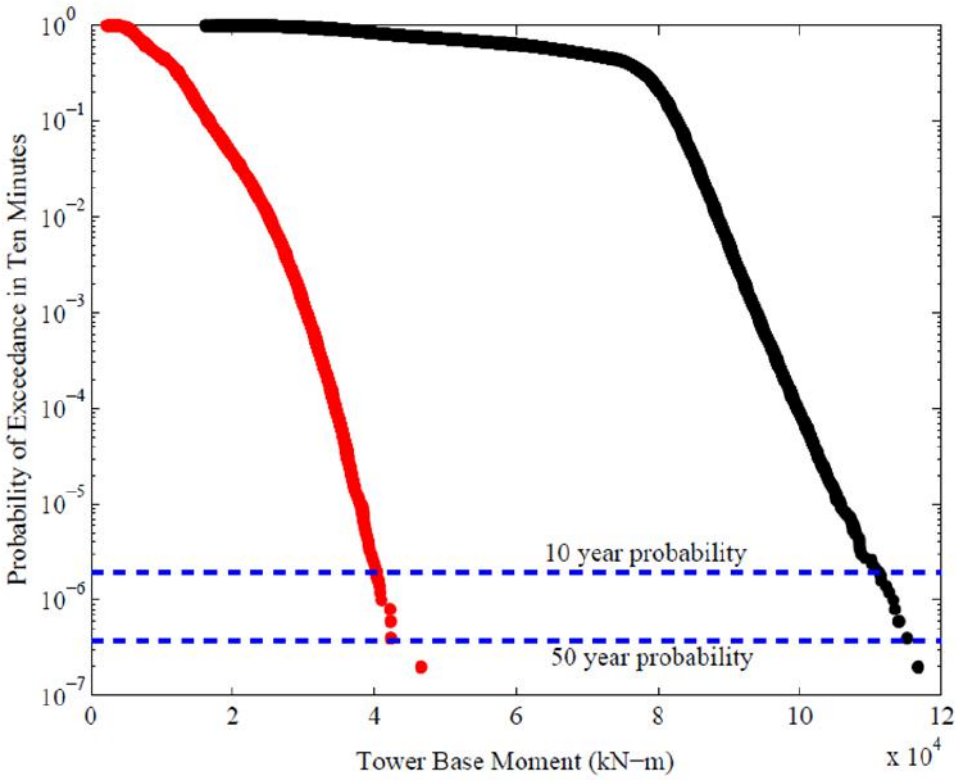

Figure 6.1: The tower base moments as given by Sandia [2]. Red shows the moments around y-axis and black shows the moment around x-axis

The assumption is made that in this situation all the moments on the tower base can be described by quasi-static equations related to the masses of the different parts and forces and moments acting on the combined rotor and nacelle centre of mass as shown in fig. 6.2. Since tower wind forces have a slight contribution to the tower base bending moment measured, it is assumed that wind forces on the tower itself can be described as an equivalent force acting at the tip of the tower. This assumption is made because based on the data available it was not possible to separate the loads induced by tower drag from the loads induced by the rotor. The assumption is however a conservative one, because when the base moment generated by wind drag on the tower could separately be taken into account, the force applied at the tower top would decrease. Since the force at the tower top is slightly overestimated due to this assumption, the bending moment distribution is also slightly overestimated.

The height of the centre of mass is assumed to be at the hub height. The turbine is symmetric in y-direction and the distance of the centre of mass from the middle of the tower in x direction can be obtained from NREL data on the 5MW reference turbine [2]. The forces acting on the centre of mass in this quasi-static model are a torque on the turbine shaft, the weight force of the rotor and nacelle and a force in x and y direction. The shaft torque and nacelle plus rotor weight data can be found in table 6.2 and table 6.3 respectively. The centre of mass X-coordinates of both the rotor and the nacelle with which the centre of mass location of the entire system on top of the tower is calculated is given in these tables too.

Table 6.2: Turbine properties required for quasi-static load calculation

Hub height (m)	90
Rated generator torque (Nm)	43096
Gearbox ratio (-)	97

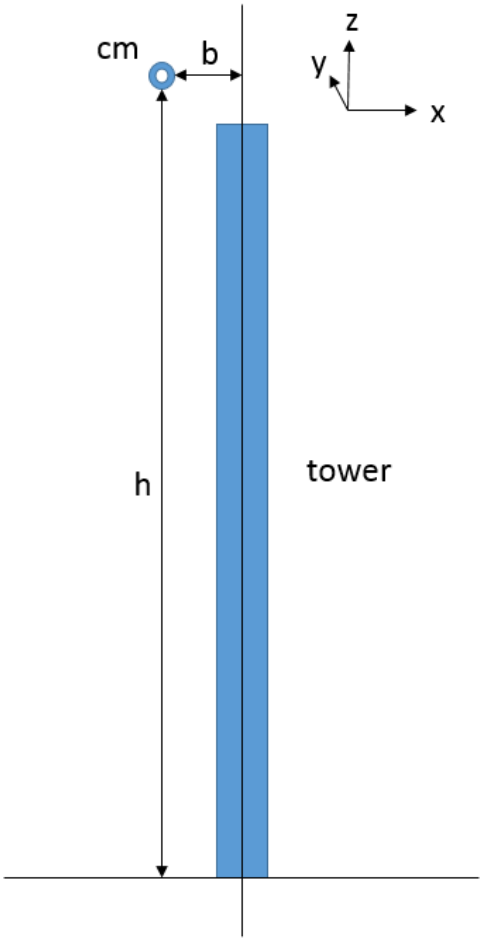

Figure 6.2: Schematic representation of the tower and the rotor/nacelle combined centre of mass

Table 6.3: Rotor and Nacelle mass properties required for the centre of mass estimation

Nacelle mass (kg)	240000
Nacelle CM X-position (m)	1.9
Individual blade mass (kg)	17740
Rotor hub mass (kg)	56780
Total rotor mass (kg)	110000
Rotor CM X-position (m)	-5
Combined Nacelle and rotor mass (kg)	350000
Combined Nacelle and rotor CM X-position (m)	-2.635

The data in table 6.3 is directly used as an input for mass of the nacelle and rotor in Abaqus, placed at the calculated centre of gravity position of 90m in Z-direction and -2.635m in X-direction. The generator torque multiplied with the gearbox ratio equals the torque induced by the rotor on the system. This completes the data required to calculate the forces and moments acting at the centre of mass as given in fig. 6.2 using the Sandia base moment data. The resulting forces, moments and gravity loads acting on the centre of mass are given in table 6.4.

No force is acting in z-direction since the force is z-direction is only influenced by the mass of system according to this quasi-static model. The mass of the system is defined as direct input in

Table 6.4: Rotor and Nacell center of mass forces and moments

F_x (N)	$1.29 \cdot 10^6$
F_y (N)	$-4.27 \cdot 10^5$
F_z (N)	0
M_x (N)	$4.18 \cdot 10^6$
M_y (N)	0
M_z (N)	$1.06 \cdot 10^7$
g (m/s^2)	9.81

Abaqus, and the effect of the mass on the stresses is taken into account by defining a gravity force on the system. This also directly takes the effect of the distributed tower mass into account. Last step is applying a safety factor on these forces and moments to comply with regulations [12]. This safety factor has a magnitude of 1.35 and needs to be applied to all forces and moments. This leads to the Abaqus input given in table 6.5.

Table 6.5: Design forces and moments with regulation safety factor

F_x (N)	$1.74 \cdot 10^6$
F_y (N)	$-5.76 \cdot 10^5$
F_z (N)	0
M_x (N)	$5.64 \cdot 10^6$
M_y (N)	0
M_z (N)	$1.44 \cdot 10^7$
g (m/s^2)	9.81

6.1.2 Natural frequency constraint determination

The natural frequency of the tower should not be in the range of the operating frequencies of the wind turbine. These operating frequencies are linked to the rotational speed of the wind turbine rotor and the blade tower passage frequency, and is therefore based on the cut-in and rated rotor speed of 6.9 and 12.1 rpm as given in table 4.2. These rotational speeds devided by the amount of seconds in a minute would give the frequency ranges of 0.115-0.202 Hz for rotational frequency and 0.335-605 Hz for blade tower passage frequency, in which the natural frequency of the wind turbine may not be.

There are three ways of avoiding to have the natural frequency in these frequency ranges, this is illustrated with a design space in fig. 6.3. Designing a flexible tower which has an natural frequency below 0.115 Hz would generally result in a tower with relatively high tower top displacements, this is considered undesirable. Designing a tower with a natural frequency above 0.605 Hz generally results in a very stiff design. But since this stiffness has to come from the material and geometry properties it generally leads to heavy designs. Therefore the design space in between the frequency ranges would generally result in the most optimal design which complies to the natural frequency restrictions. It turned out that avoiding to have the first natural frequency in the lower operating frequency region is driving the design. Therefore a minimum natural frequency constraint is used. In order to account for uncertainties in as-built properties of the tower a safety factor of 1.1 on the natural frequency constraint is applied in this study, this results in a minimal natural frequency constraint of 0.222 Hz.

6.2 Material selection and property determination

The selection of material in this project has been based on three basic practical criteria. The glass fibre and infusion epoxy resin should already be used in wind turbine industry to make sure the

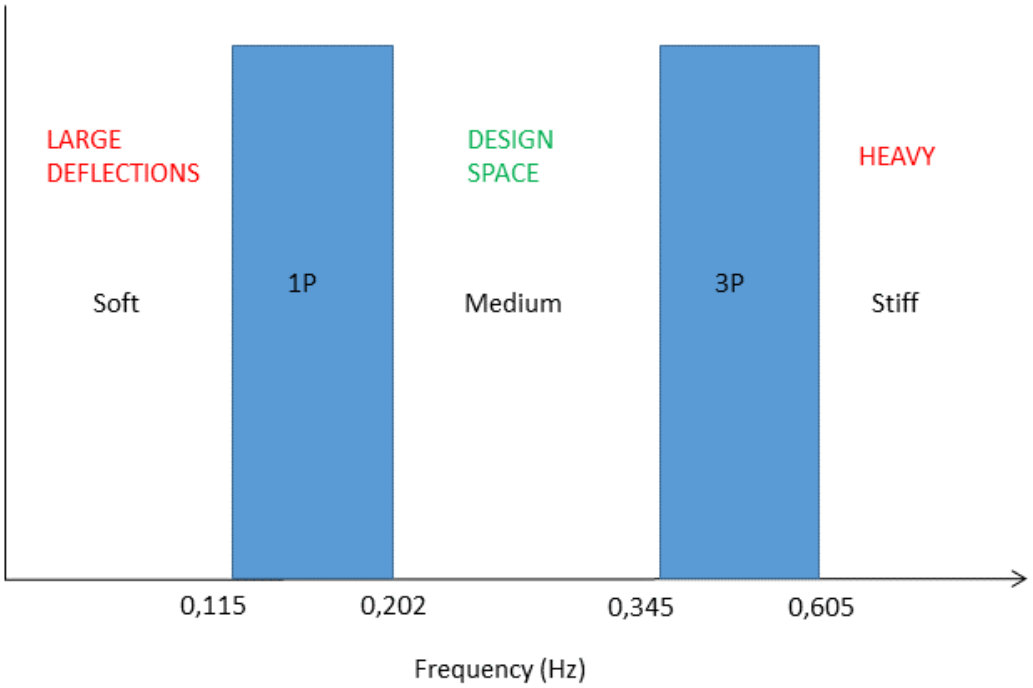

Figure 6.3: Natural frequency design space

materials are not new to the industry and can therefore be more easily accepted. Data has to be available for the material epoxy combination to base the material properties used in designing the tower and test samples on. And the material should be obtainable in small quantities to produce the test samples in this project. The glass fibre found based on these criteria is the Owens Corning SE1500 and the epoxy is a Momentive RIMR135 resin in combination with the RIMH137 hardener.

During the project it became clear that a carbon fibre design might be more interesting than initially thought. Therefore a carbon fibre is selected to base the properties on for the carbon fibre computations. The carbon fibre used for this purpose is the Toray T300 fibre [5].

In this section the laminate properties are determined for the tower design. The fibre volume fraction used in the model is determined based on the maximum fibre volume fraction possible in the ribs. This is done based on the filament diameter and the epoxy having to be between the filaments. When the filament are assumed to be tightly fitted in a rectangular packing, it can be shown that the filament cross-sectional area to total box area ratio is 0.785. When these boxes are stacked in layers the boxes in the rib would be alternating between being filled with a fibre to not being filled with a fibre from layer to layer. It can be shown that the fibre volume fraction in this lay-out would be 0.393. The rib fibre volume fraction is the fibre volume fraction which is being used in this project for optimising the wind turbine tower model, in which the ribs are represented by shell elements. Therefore this volume fraction of 0.393 is used in this section to determine the material properties.

Based on the rib volume fraction and the material properties found [3, 5, 45], the fibre weight fractions for glass fibre and carbon fibre can already be determined. The material densities and resulting carbon and glass fibre weight fractions are given in table 6.6.

Further composite properties based on the carbon fibre are given in section 6.2.2. But first the way the properties of the glass fibre are determined is described in section 6.2.1.

6.2.1 Glass fibre laminate properties

The glass fibre laminate properties are based on two sources of data. One in which the neat resin properties are given by the manufacturer [3], and one in which tests results on the fibre infused with the RIMR 135 resin is given [4]. The neat resin properties used in the calculations in this section are given in table 6.7. The glass fibre laminate properties used in this section are given by

Table 6.6: Material densities and resulting weight volume fractions

Epoxy density (kg/m^3)	1131
Glass fibre density (kg/m^3)	2620
Carbon fibre density (kg/m^3)	1760
Glass fibre weight fraction (-)	0.747
Carbon fibre weight fraction (-)	0.502

uni-directional(UD) test data and laminate test data as given in tables 6.8 and 6.9.

Table 6.7: RIMR-135 Neat resin properties [3]

Modulus (GPa)	2.7-3.2
Tensile strength (MPa)	60-75
Compressive strength (MPa)	80-90

Table 6.8: Dry filament wound UD lay-up infused properties at 2 mm thickness [4]

Fibre volume fraction (-)	0.638
UD tensile strength (Mpa)	1430
UD tensile modulus (GPa)	48
UD compressive strength (MPa)	850
UD compressive modulus (GPa)	53.7

Table 6.9: Dry filament wound 0-90 lay-up infused properties at 4 mm thickness [4]

Fibre volume fraction (-)	0.623
+-45 tensile strength (Mpa)	133
+-45 tensile modulus (GPa)	14.2
0-90 tensile strength (MPa)	673
0-90 tensile modulus (GPa)	27.1

The goal is to obtain the separate fibre and resin properties based on the test data given, to be able to calculate the properties of a lay-up at different volume fractions. The problem however is that resin properties are given in ranges. It is therefore assumed that the given resin strengths are equal to the lowest values given in the ranges. The modulus is assumed to be equal in tension and compression. The exact epoxy modulus can be obtained by comparing the test data from the two tests. The fibre modulus can be obtained from UD axial test data as a function of resin modulus by using a so-called slab model based on the cumulative stiffness of resin and fibre in a lay-up. The cumulative stiffness equation is:

$$\frac{E_t A_t}{L} = \frac{E_f A_f}{L} + \frac{E_r A_r}{L} \tag{6.2}$$

In this equation E is the material modulus, A is the cross-sectional area and L is the length of the sample under consideration. The sub-scripts t, f and r represent the total, fibre and resin

properties respectively. In this equation the cross-sectional area and length can be rewritten to f, leaving:

$$E_t = E_f f + E_r(1 - f) \tag{6.3}$$

Knowing the relation between fibre and resin modulus, the properties in transverse direction of the lay-up can be obtained from the data in two ways. First it can be obtained by using the separate fibre and resin properties and the following cumulative stiffness equation:

$$\frac{L_t}{E_{90}A} = \frac{L_f}{E_f A} + \frac{L_r}{E_r A} \tag{6.4}$$

Where the sub-script 90 indicates the properties of the 90° angle lay-up. The lengths in this equation can be rewritten to fibre volume fraction f, leaving:

$$\frac{1}{E_{90}} = \frac{f}{E_f} + \frac{1 - f}{E_r} \tag{6.5}$$

Secondly it can also be obtained using a cumulative stiffness model based on the UD lay-up axial properties from table 6.8, and the 0-90 lay-up properties from table 6.9 directly with the following equation:

$$\frac{E_{0-90}A_{0-90}}{L} = \frac{E_0 A_0}{L} + \frac{E_{90}A_{90}}{L} \tag{6.6}$$

Where the sub-script 0 represents the properties of the 0° angle part of the lay-up, and the sub-script 0-90 the properties of the 0°-90° balanced lay-up. Using the fact that $A_0 = A_{90}$ and $A_0 + A_{90} = A_{0-90}$ this can be rewritten to:

$$2E_{0-90} = E_0 + E_{90} \tag{6.7}$$

Both methods should give the same transverse modulus properties as long as the slight difference in fibre volume fraction between the two tests is taken into account. Using the equations described the separate fibre and resin moduli are obtained and summarized in table 6.10.

Table 6.10: Calculated fibre and resin moduli based on the test data

Resin modulus (GPa)	2.92
Fibre tensile modulus (GPa)	73.6
Fibre compressive modulus (GPa)	82.5

Abaqus implementation

Since a linear static analysis is used in modelling the tower, there is no possibility to use different elastic properties in tension and compression. The modulus properties used are therefore based on the average modulus property. Since the tower is loaded mainly in bending this would lead to an adequate estimate on deflection, with the data and tools available.

Averaging the modulus properties in tension and compression results in an increase in modulus for tension related properties, and a decrease in modulus for compression related properties. These changes in modulus influences the strength of the material when the strain allowables is kept equal. To solve this issue, the strain allowables in tension and compression are adapted with the inverse of factor with which the modulus changes, hence if the modulus increases the allowable strain in the same direction decreases with the same factor and vice versa. On top of this the typical material knock-downs for composite laminate strength are applied on the strains. Hence a knock-down of 0.8 for material scatter and a knockdown of 0.8 for environmental influences. Furhtermore a knockdown of 0.65 for barely visible impact damage has been implemented, it is acknowlegde that this knock-down of 0.65 might not be appropriate due to the thick and UD lay-up nature of the structure, and therefore has to be verified in future tests. This all together leads to the Abaqus material input as described in tables 6.11 and 6.12.

Table 6.11: Glass laminate moduli input for Abaqus

E_1 (GPa)	32.4
E_2 (GPa)	4.69
v_{12} (-)	0.29
G_{12} (GPa)	2.66
G_{13} (GPa)	2.66
G_{23} (GPa)	1.59

Table 6.12: Glass laminate maximum strain input for Abaqus

$\epsilon_{1_{t,max}}$ (-)	0.0113
$\epsilon_{1_{c,max}}$ (-)	0.0067
$\epsilon_{2_{t,max}}$ (-)	0.0016
$\epsilon_{2_{c,max}}$ (-)	0.0071
$\gamma_{12_{max}}$ (-)	0.0104

6.2.2 Carbon fibre laminate properties

The input data for the property estimation is given in tables 6.7, 6.13 and 6.14. The pure resin and fibre properties are used to determine the transverse and axial moduli of the material. The composite data is used to determine the axial and transverse strength just like is done for the glass fibre laminate. The big difference is that there is no shear test data available on the specific carbon fibre epoxy combination. This excludes the possibility to determine the shear modulus as for glass fibre. The issue is solved by creating a factor based on the influences of fibre modulus on laminate shear modulus using the Halpin-Tsai method. The results are given in table 6.15

Table 6.13: T300 pure fibre properties [5]

Tensile modulus (GPa)	230
Tensile strength (MPa)	3530
Tensile strain (-)	0.015

Table 6.14: T300 laminate properties [5]

Fibre volume fraction (-)	0.6
UD Tensile strength (Mpa)	1790
UD tensile modulus (GPa)	130
UD compressive strength (MPa)	1250
UD compressive modulus (GPa)	125

Based on the data given in tables 6.7 and 6.13 to 6.15. The carbon fibre Abaqus input properties are given in tables 6.16 and 6.17. It must be mentioned that the specific compression modulus for the T300 fibre RIMR 135 epoxy combination, could not be extracted due to a lack of data for the polymer specific properties used to obtain the test data given in table 6.14. Since the difference in compression and tension modulus found in table 6.14 is small, 4%, the tensile modulus of the material, which can accurately be determined based on the data, is directly used as input

Table 6.15: Halpin-Tsai carbon shear modulus factor estimation

Glass laminate shear modulus $f = 0.393$ (GPa)	2.18
Carbon laminate shear modulus $f = 0.393$ (GPa)	2.26
Shear modulus factor (-)	1.04

in Abaqus, and the compression modulus which cannot be determined accurately with the data available is not separately taken into account.

Table 6.16: Carbon laminate moduli input for Abaqus

E_1 (GPa)	92.2
E_2 (GPa)	4.77
v_{12} (-)	0.29
G_{12} (GPa)	2.78
G_{13} (GPa)	2.78
G_{23} (GPa)	1.67

Table 6.17: Carbon laminate maximum strain input for Abaqus

ϵ_{1_t} (-)	0.0052
ϵ_{1_c} (-)	0.0046
ϵ_{2_t} (-)	0.0015
ϵ_{2_c} (-)	0.0070
γ_{12} (-)	0.0100

6.3 Cost influences on design

An interesting effect on the cost of the tower related to tower dimensions is found in land based transportation costs. According to a study performed by the NREL research institute [15], transportation costs increase very rapidly when the diameter of the tower exceeds 4.4m, because towers with a larger diameter cannot be transported in a normal way over roads due to overhead structures and bridges, etc. According to the study cited this currently is avoided by sectioning the tubular tower sections in quarters. But for the fibre reinforced lattice structure considered this would result in complex attachment structures to attach the quarter sections to each other. Therefore it is decided to avoid such types of attachment structures.

Using the data from this reference study the influences of fibre reinforced tower diameter on transport cost is determined by analysing this cost for a tower with a diameter of 6m like the reference tower and a tower which is constraint to a base diameter of 4.4m. The cost estimation of sections below 4.4m diameter is performed based on the total transportation cost estimate generated for the 28 quarter sections in the reference transportation cost study on a land based wind turbine project [15]. The cost figures found in this reference study for this situation are given in table 6.18. A cost estimate for sections with a base diameter above 4.4m can be performed with data from the study in a similar way and is given in table 6.19.

The cost of transporting a composite tower can be determined using this tower dimension dependent transport cost. The composite tower can be transported in four fully cylindrical axial sections with a length of 21.9m each. Sectioning the 6m base diameter tower in four parts, would lead to 3 sections with a diameter above 4.4m and one with a base diameter below 4.4m. The transport costs according to tables 6.18 and 6.19 would amount to 1,234,877 Euro. When the 4.4m

Table 6.18: Tower section transport cost for a tower with a base diameter below 4.4m

Total tower transport cost (Euro)	232,000
Number of quarter sections	28
Section transport cost (Euro)	8286

Table 6.19: Tower section transport cost for a tower with a base diameter above 4.4m

Total tower transport cost (Euro)	2,862,045
Number of quarter sections	7
Section transport cost (Euro)	408,863

base diameter tower would be sectioned in four parts the transport costs would amount to only 33,143 Euro. Since the difference in land based transportation cost according to this reference study is 1.2 million Euro it is decided that the 4.4m base diameter is a hard constrain in the design, to make sure the structure designed in this project can be used for all types of wind turbine locations.

Chapter 7

Detailed design

In the former chapters, manufacturability has been proven, and the design loads and constraints have been determined. The composite lattice design is improved further based on the inputs acquired, using a weight optimisation of the structure to reduce structural weight and material cost. The approach with which this weight optimisation is performed is detailed in this chapter, beginning with a description of the optimisation method in section 7.1, furthermore in section 7.2 it is described how the model is tweaked such that it gives the desired output in an efficient way, and finally in section 7.3 the properties of the resulting most optimal tower found are given.

7.1 Parametric optimisation of the structure

The optimisation is performed using an ATG-Europe in-house developed Genetic Algorithm (GA), based on the Python package called Distributed Evolutionary Algorithms in Python (DEAP) in combination with Catia and Abaqus. The process boils down to a Python script performing the GA with the help of Catia to change parametrized Computer Aided Design (CAD) models and Abaqus to obtain structural weight, stiffness and strength results form the mesh created on these CAD models. The way the Python script determines the fitness and interacts with Catia and Abaqus is described in the following sub-sections.

7.1.1 Description of the Genetic Algorithm

An optimisation logic flowchart is shown in fig. 7.1. It shows how the data in the code is processed. For a user of the code, starting an optimisation begins with defining the input variables, both evolutionary and structurally. The evolutionary variables define the population size, the amount of generations used in the optimisation, the cross-over probability and mutation probability. The evolutionary variables used in the optimisation are given in table 7.1. The structural variables define the composite lattice geometry through the number of helical ribs, the number of hoop ribs, the height of all the ribs, the width of the helical ribs and the width of the hoop ribs.

The structural variables are the variables which change from design to design. The values the structural parameters can be assigned are bounded by variable specific ranges. The initial ranges of the structural variables are determined based on the results form trial runs in which the optimisation is tested. These initial ranges are given in table 7.2. The variable ranges are defined such that the structural properties required can be achieved but also such that the maximum rib number and maximum rib width combinations cannot give physically impossible designs. The minima of the structural parameter ranges are chosen such that enough freedom in parameters is given for reducing the structural weight, without being constrained in the structural parameter minima.

From the values given in table 7.2 the helical and hoop rib width can only be changed in steps of 4mm which is based on the tow width used in this project. Besides that the amount of hoop ribs can only be an even number, this because changing the amount of hoop ribs by just one extra rib has very little influence on the design. This mainly effects the helical rib angle because the rib angle is defined as function of the amount of hoop and helical ribs. But this effect is very small, in the final results a step from 98 to 100 hoop ribs only gives a change in helical angle of 0.2 degrees. Therefore it is found justifiable to restrict the number of hoop ribs to even numbers to reduce the number of possible designs.

Using the defined variable ranges the python code generates a first population by randomly putting the structural variables together to define a group of designs. Each of the individuals in the population is evaluated separately by first updating the CAD design in Catia as described in

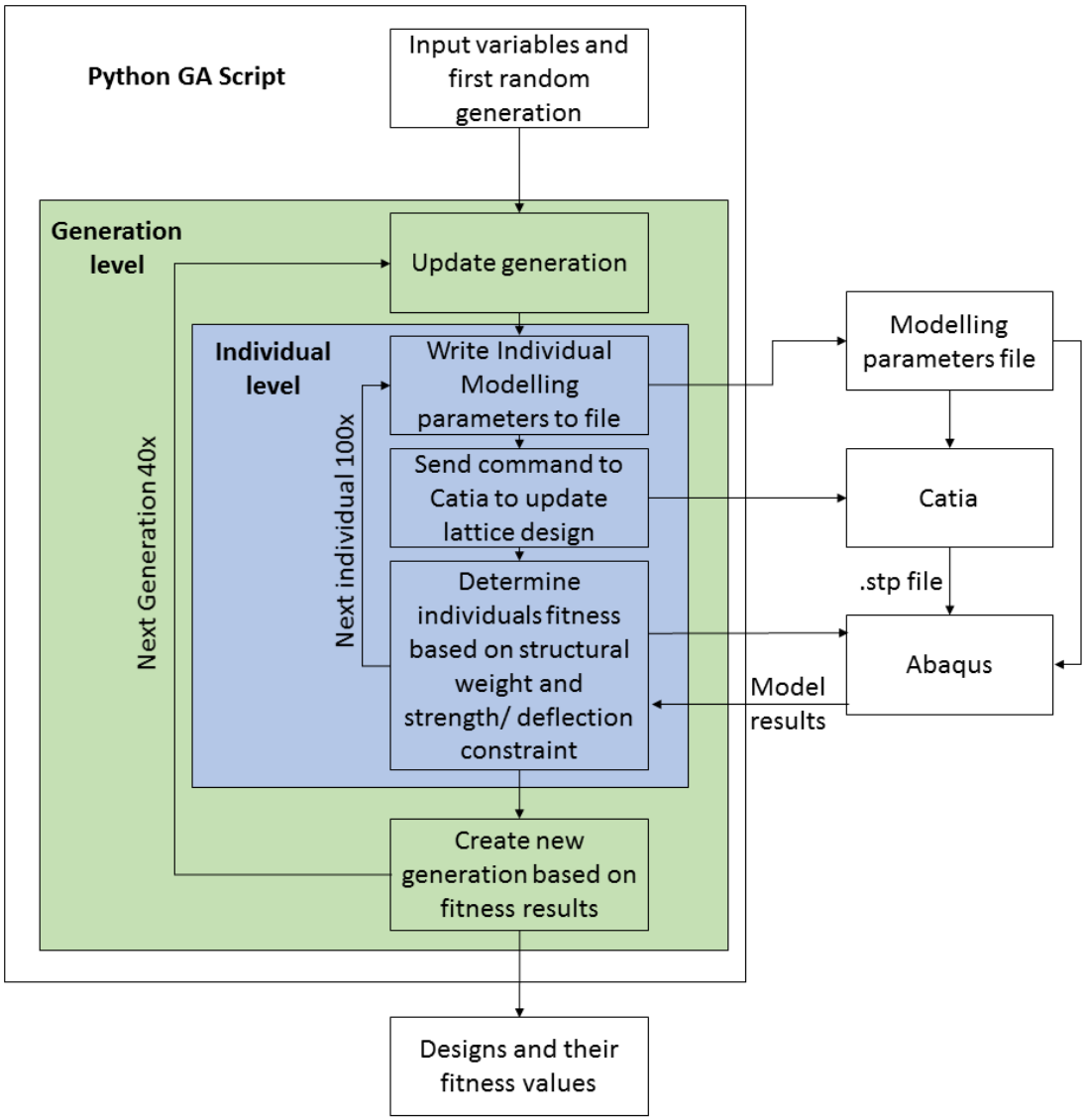

Figure 7.1: Flow chart of the genetic algorithm

Table 7.1: Genetic algorithm evolutionary input variables

Amount of generations (-)	40
Population size (-)	100
Cross-over probability of type double (%)	50
Mutation probability (%)	30

section 7.1.2. And then importing the Catia generated file in Abaqus to mesh and analyse the

Table 7.2: Genetic algorithm structural input variable ranges

	Minimum value	Maximum value
Helical ribs (-)	31	40
Hoop ribs (-)	70	120
Rib height (mm)	200	300
Helical rib width (mm)	12	48
Hoop rib width (mm)	40	76

structures as described in section 7.1.3. The Catia CAD geometry and the Abaqus mesh are shown side by side for comparison in fig. 7.2. From the Abaqus simulation the tower top deflection, the strength based factor of safety, and the total mass of the tower structure are extracted. These variables are used to determine the fitness of each design.

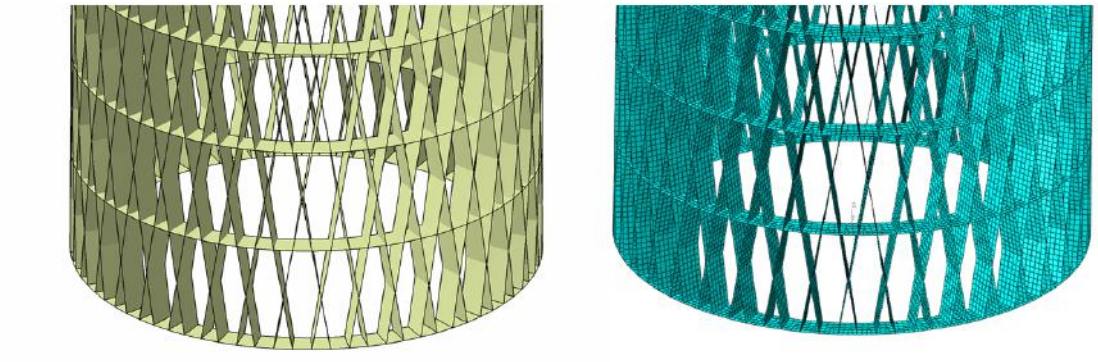

Figure 7.2: The CAD model and FEM mesh side by side, to show how the mesh is generated at the CAD defined geometry

The fitness of the design is determined by the tower weight with penalties on the weight value based on constraints set on the factor of safety and natural frequency. The constraint and penalty values for both of these parameters are given in section 7.2.2. The penalty constraint is defined such that when the constraint is not satisfied a penalty factor is determined based on the mismatch between constraint and design variable. The structural mass of the tower is multiplied by the penalty factor, giving a fitness mass which is used to indicate the quality of the design.

When a full population is analysed in this way, a new population is generated based on the fitness values of the designs, the cross-over probability and the mutation probability. The new population is generated such that the fittest designs have the largest probability to "mate" and therefore have more "offsprings" in the new generation. When all generations are evaluated in this way, an output file is generated with all the designs and their structural properties found from which the best design evaluated in this process can be extracted.

7.1.2 Description of the CAD model

The CAD model is a fully parametrised model of the composite lattice structure consisting of surfaces representing the ribs. Surfaces are used to reduce the computational effort required in analysing the structure, in comparison to a solid volume representation of the structure. The helical rib shape is determined by a set of 100 points which are placed such that they follow a geodesic path on the virtual surface representing the outer dimensions of the tower at any height between tower base and tower top. The initial angle of the geodesic path is dependent on the amount of helical and hoop ribs and the tower base diameter, top diameter and height. Since the outer dimensions are given fixed values in the CAD model the angle of the helical ribs can be changed by only changing the amount of helical and hoop ribs which are design values used in the optimisation.

The points defining the helical rib path are used to make a spline which is extruded towards the centre of the tower by the rib height value to create a helical rib. The helical rib is mirrored to

obtain negative angle helical ribs and circularly patterned around the tower centre to define all the surfaces representing the helical ribs. The intersections of the positive and negative helical ribs are used to determine the location of the hoop ribs. This intersection can be revolved around the tower centre to create the surfaces representing the hoop ribs. The final step is to rotate the negative and positive helical ribs around the tower centre by the angle required to obtain the Hexagonal grid as defined in section 4.2.

In the way the Catia model is set-up the set of 100 points is used to define the complete tower geometry based on the fixed tower outer dimensions, the amount of hoop and helical ribs and the rib height. The position of the points is defined through a Catia macro which can be activated by the GA Python script and reads the required amount of hoop ribs, helical ribs and the rib height from a text file in which the GA-script saved the design variables of the geometry being under investigation. After updating the design the macro automatically saves the new design to a .stp file which is the input required by Abaqus.

7.1.3 Description of the FEM model

The FEM Abaqus model is also defined in such a way that it can be used for every CAD design under consideration. The key here is to make sure the part numbering from the .stp file is consistent such that it can be read and merged in larger parts without manual interventions required. When this consistency is there a script can be written to perform all model preparations without the Abaqus CAE. This script, just like the Catia macro, bases the properties of the structure on the design variables as saved in the text file created by the GA-script

The script imports the geometry from the .stp file in a way that all units are converted such that the distance unit in Abaqus is meters, it furthermore Defines the material as given in section 6.2, and creates sets to assign properties and extract results. Sections are defined based on the material properties and hoop and helical rib width, and orientations are defined based on the helical rib angle. Finally the implementation of constraints, load and mesh is given in a little more detail in the next sections.

Constraint

The constraint used in the model has the purpose to represent the attachment of the tower to the ground based foundation. In this study it is assumed that the foundation to which the tower is connected can be considered infinitely stiff. Therefore the constraint fixing the bottom of the tower can be modelled as a clamp. The clamp is enforced on a point at the bottom of the tower in its centre. This point is coupled through kinematic coupling to the bottom hoop rib which is exactly at the base of the tower.

Loads

The loads are applied as defined in section 6.1. The loads given in this section are defined at the centre of mass of the turbine rotor and nacelle combination. The location of this centre of mass is represented by a point in Abaqus being coupled through kinematic coupling to the tower top edge. The mass of the rotor and nacelle with a total of 350 tonnes is applied in this location as well. Through a gravity force the stresses created by the weight of the rotor and nacelle and by the towers own weight is taken into account. Buckling has been checked in the initial designs, but showed to be far from critical. Therefore buckling is not analysed.

Mesh

The surfaces representing the ribs in the CAD model are meshed with shell elements using a global seed of 0.05m and a structured quad-dominated mesh build up. A shell representation is chosen to reduce computational effort in comparison to solid representation of the model. Using shell elements has the effect of not modelling the nodes in full detail, and can therefore be expected to have slight influence. However the influence of shell modelling has been assessed in previous research and was found to be of little influence on the results [46], therefore shell elements are used to reduce the computational effort for the analysis. The quad-elements in the model are S4R elements and the tri-elements in the model are S3 elements. The mesh is made structured to assure a regular build up of elements which can be used on all rib geometries. The mesh is quad-dominated to make sure the hoop ribs are meshed without problems by allowing a tri-element when required, see section 7.1.3 for an example how the meshing is done throughout the structure on a local scale.

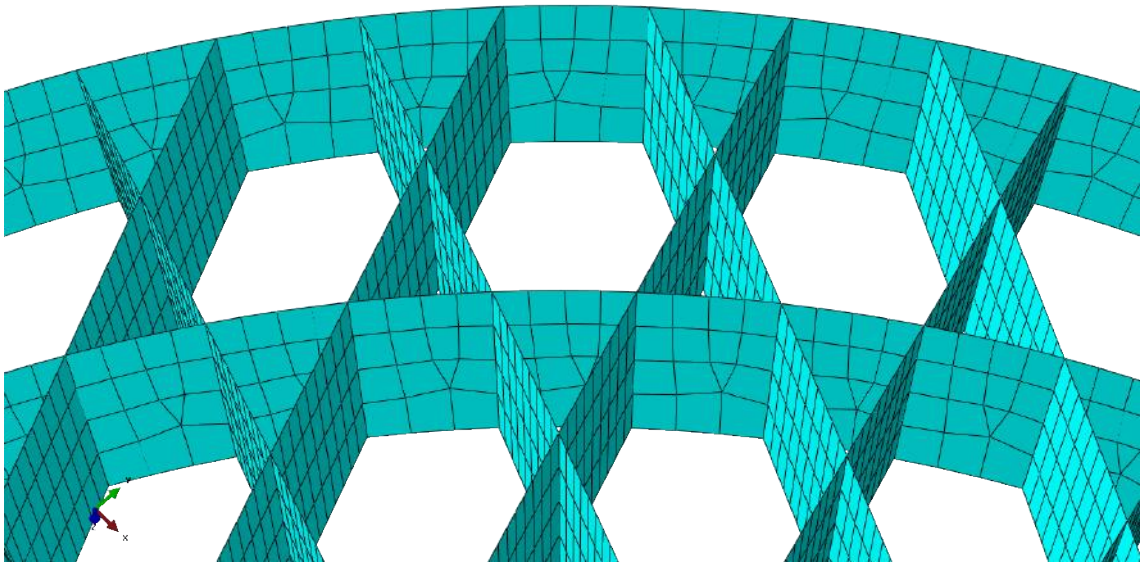

Figure 7.3: Detailed view on rib meshing in tower model

7.2 Model benchmarking

In this section it is explained how the model is benchmarked into its final shape with all the constraints in place such that the results generated with the model is representing the desired results and that theses results are obtained in a way that is as efficient as possible. To explain this, the reasoning behind the final choice of material, glass or carbon fibre, is given section 7.2.1. Model simplifications are described in section 7.2.2, and mesh convergence results are given in section 7.2.2

7.2.1 Final material selection

In the process of determining the penalty constraints it is found that with the dimensional constraints it is impossible to reach the natural frequency limit for a glass fibre tower with a based diameter of 4.4m. This constraint implemented to reduce transport cost as described in section 6.3, could therefore not be satisfied. Ways to improve the results found such as rib tapering as explained in section 7.2.2 did not give enough improvement on its own. This trigged the interest in researching the possibility to have carbon fibre as a more cost efficient material compared to glass fibre.

The comparison of cost efficiency is based on the differences in material cost between a glass fibre design with a base diameter of 6m like the NREL reference tower and a carbon fibre design with a 4.4m diameter. The comparison is made using the 1.2 million Euro of extra transport cost for the glass fibre 6m base diameter design and the difference in material cost for a carbon fibre 4.4m base diameter design. The structural weight of the carbon fibre tower given in this comparison is a weight based on first estimates of feasible designs obtained through a rough preliminary GA optimisation. The geometric parameters for this tower are given in table 7.3. The 6m base diameter glass fibre weight estimate is based on a rough dimensional up-scaling from the carbon fibre design, with an equal number of helical and hoop ribs, to obtain a structurally feasible glass fibre weight estimate. The resulting material weight and costs for the glass fibre tower can be found in table 7.4. the same data for the carbon fibre tower can be found in table 7.5.

It can be seen based on this rough material amount estimation that the carbon fibre tower is expected to be around 35 thousand Euro more expensive in material cost but 1.2 million less expensive in transportation cost. therefore it is concluded that the carbon fibre is the best material choice for the design.

It must be noted that because this estimation is done on non-optimised tower weights, the total material cost of these structures is expected to go down with respect to the references given here for both the glass and carbon fibre design. It is expected that both designs can be weight optimised by a comparable factor which would result in a decrease in the cost gap between glass fibre tower material cost and carbon fibre tower material cost, which strengthens the argument to use carbon fibre as reinforcing material.

Table 7.3: Carbon fibre tower benchmark dimensions

Number of helical ribs (-)	38
Number of hoop ribs (-)	100
Rib height (mm)	188
Helical rib width (mm)	87
Hoop rib widht (mm)	28

Table 7.4: Material weight and cost breakdown of a 6m base glass fibre tower

	Weight (tonnes)	Cost (Euro)
Glass	204	395,775
Epoxy	136	1,430,641
Total	340	1,826,416

Table 7.5: Material weight and cost breakdown of a 4.4m base carbon fibre tower

	Weight (tonnes)	Cost (Euro)
Carbon	83	996,000
Epoxy	82	864,560
Total	165	1,860,560

7.2.2 Model fitting

In order to improve the models computational speeds some modelling simplifications are made. Every simplification is however accounted for in the results by factors on the structural properties affected. Simplifications are made in omitting a natural frequency analysis by fitting the natural frequency of the structure to the top deflection magnitude. A simplification is made in not modelling rib height tapering but accounting for it by a factor based on an optimal rib taper ratio. And similarly a non-linear analysis is omitted by accounting for it by a factor. How these factors are determined and taken into account in the results is shown in this section. The validity of the factors used in this analysis is shown in section 7.3 based on the optimal tower design found in the optimisation.

Frequency fitting

A natural frequency analysis is found to increase the analysis time of the model roughly by a factor two, however the natural frequency of the structure is an important factor to take into account as described in section 6.1.2. Some research is performed using analysis results on random tower geometries.

The natural frequency of the tower is related to the stiffness and mass distribution along the tower. The system has a large point mass placed at the top of the tower, to represent the nacelle and rotor of the turbine, this mass is positioned in the location where movements are the largest, the effect of this point mass on the natural frequency is expected to be relatively large compared to the effect of tower mass. And therefore reducing tower mass is expected to have a relatively small influence on the results.

It is however observed that the bending stiffness of the tower can have a significant effect on the tower natural frequency. The correlation between the effects can be shown by plotting the natural frequencies of the random tower configurations against the tower's top displacement magnitude, as shown in fig. 7.4.

The plot in fig. 7.4 shows a clear trend which can be accurately fitted by a power law trend line. This power law is used to obtain the required tower top deflection magnitude based on the natural

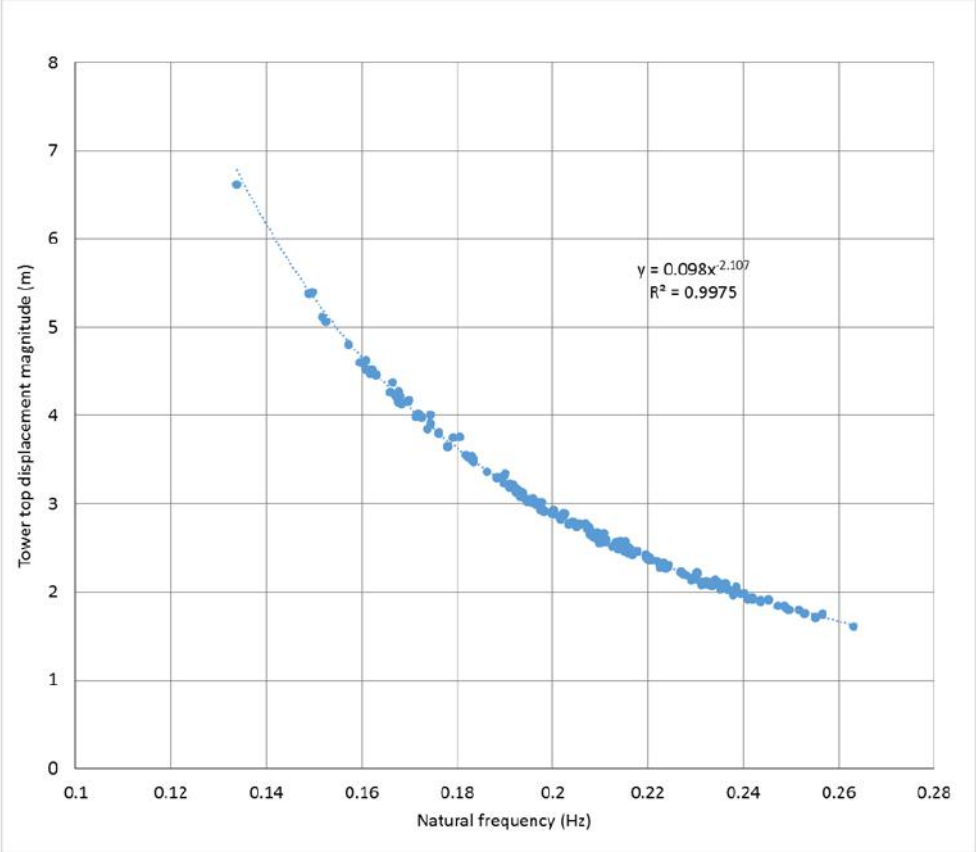

Figure 7.4: Plot of the tower top deflection as function of tower natural frequency

frequency requirements as defined in section 6.1.2. A small uncertainty is taken into account by increasing the natural frequency by 1% to cover the slight spread in the data found. Using this approach a natural frequency analysis can be omitted which reduces the time required to run the optimisation significantly.

Rib width tapering influences

As discussed in section 7.1.1 there are five structural variables used during the optimisations. Based on these parameters alone all ribs would have the same cross-section from tower base to tower top. Since the tower is mainly loaded in bending such a design would be highly inefficient from both a strength and a natural frequency point of view. A design which is able to sustain the bending loads at the bottom of the tower would without tapering be over-designed in strength at the tower top, and this over-designed tower top results in large amounts of material at the tower top, influencing the natural frequency in a negative way.

One could dive into a detailed rib cross-sectional area and rib path optimisation as function of tower height. This would however lead to very complex optimisation study which is left out of scope for this initial feasibility study. In order to capture the effect of the possibility of mass reduction by reducing the amount of material in ribs as function of tower height a rib width reduction factor is defined. The rib width reduction is linearly and discretely implemented by sectioning the tower in eight parts, such that the rib width is constant in every section. The eight sections can be seen in fig. 7.5, which shows strain energy jumps at the location of a section edge. The section thickness is applied in discrete steps to keep the manufacturing of every section simple; the discrete nature makes sure no ply dropping would be required within a section.

The rib width reduction factor is obtained through a simple iteration based on a ratio of tower top rib width over tower base rib width. The ratios finally considered are: 2/3, 1/2, 1/3 and 1/4. The performance of these rib width ratios is determined based on a desired homogeneous distribution of strain energy density table 7.3. The most homogeneous strain energy density distribution is found during benchmarking for the 1/3 taper ratio, the strain energy density distribution for the benchmark tower described in table 7.3, is illustrated in fig. 7.5.

To keep the GA set-up simple the rib width tapering is not directly included in the model

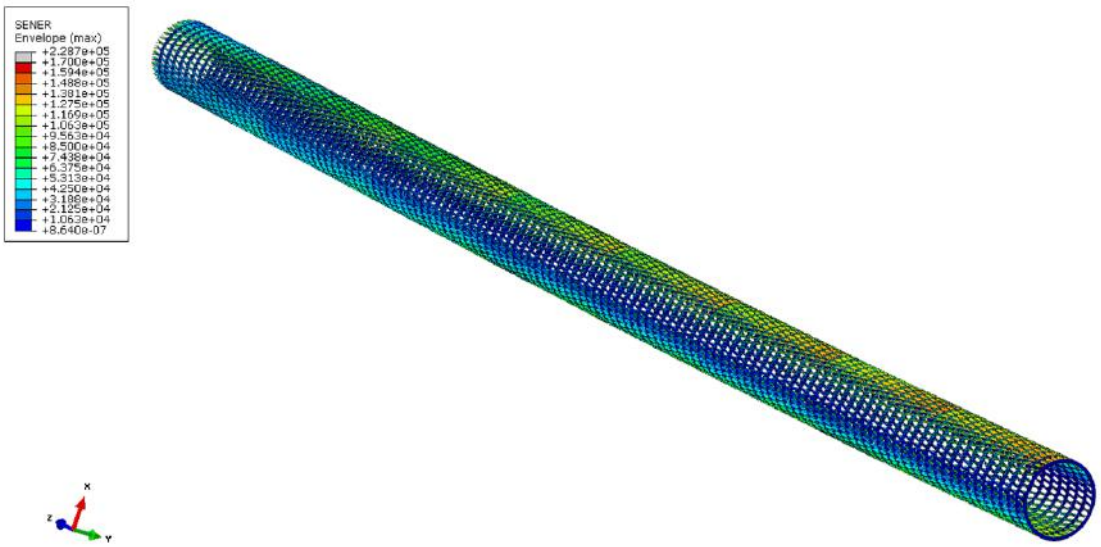

Figure 7.5: Abaqus strain energy density distribution for the statically loaded benchmark tower with a 1/3 tower top over tower bottom rib width ratio.

but the effect is accounted for in the GA model results through factors based on the benchmark structure. These factors are given in table 7.6. It has been verified with other designs that the multiplication factors are relatively constant, and it is shown in table 7.12 that this assumption did not introduce significant errors in the final optimised structure.

Table 7.6: Multiplication factors to take a rib width taper ratio of 1/3 into account

Output type	Multiplication factor
Mass (-)	0.71
Natural frequency (-)	0.93
Tower top deflection (-)	1.22

Non-linear effects

Due to the bending behaviour of the tower under the design loads, geometric non-linear effects influence the behaviour of the tower, however A non-linear analysis is computationally expensive compared to a linear analysis, a non-linear analysis required 25 computation steps while a linear analysis only takes one. Therefore a non-linear analysis is omitted in the genetic optimisation, and the non-linearity effects are estimated based on the benchmark tower.

This approach is considered applicable since the non-linear effect is mainly seen due to bending of the tower. Since natural frequency is the design driver in this process, and it has been shown that the natural frequency is stiffness driven in section 7.2.2, the optimisation algorithm is searching for a lightweight tower design, with a stiffness comparable to the benchmark tower, therefore the non-linear effects in the optimised tower should be comparable to the benchmark tower too. The resulting multiplication factors for non-linear effects are given in table 7.7.

Mesh convergence

The mesh used in the optimisation of the tower is described in section 7.1.3. The global seed size of 0.05 m is determined based on the capabilities of the computer, such that the computer could still be used for other purposes while the optimisation is running in the background. The mesh

Table 7.7: Multiplication factors to take non-linear effects into account

Output type	Linear result	Non-linear result	Multiplication factor
Natural frequency (-)	0.219	0.208	0.949
Tower top deflection (-)	2.455	2.686	1.094
Stress in rib 11 direction (MPa)	164.6	173	1.051

size is checked for convergence for smaller seeds up to the maximum capabilities once to make sure the effects of mesh size are known. The results of the non-linear analyses on tower top deflection, natural frequency and stress is given in table 7.8.

Table 7.8: Global seed size effects

Seed size (m)	0.1	0.075	0.05	0.032	0.025
Number of elements in rib height	2	3	4	6	8
Natural frequency (-)	0.20779	0.20779	0.20777	0.20776	0.20776
Tower top deflection (-)	2.687	2.686	2.686	2.686	2.686
Stress in rib 11 direction (MPa)	170.8	172.4	173.0	173.6	174.0

It can be shown that the stiffness related output of the model is very constant and can therefore be considered converged. For stress this is not the case. Final stress convergence can not be shown for such a large tower model with the computational power available. Based on the trend seen in the rib stress in 11 direction it is assumed that convergence might be reached at 175.0 MPa. Based on the difference between this number and the 173.0 MPa found at a seed size used in the model. A failure criterion multiplication factor of 1.012 is calculated to be used in the constraint determination for the GA model. Such that the effects seen are at least taken into account.

Since the factors of safety found in the optimisation process are high and hence strength is not driving the optimisation, this assumption on stress convergence is considered not to influence the validity of the tower design based on the model described in this section.

Penalty constraint determination

To take the not modelled influences described in this chapter into account the multiplication factors determined in this section are used to determine penalty constraint values for the GA. The GA constraint values are based on the factors determined in this section in combination with the initial constraints. These initial constraints are a minimal natural frequency of 0.222 as determined in section 6.1.2, and a minimum factor of safety of 1. The resulting constraint values with multiplication factors included are given in table 7.9.

Table 7.9: Penalty constraints based on the different influence factors

	Factor of safety (-)	Natural frequency (Hz)
Constraint without knock-downs	1	0.222
Taper influence factor	1.000	0.929
Non-linear influence factor	1.051	0.949
Convergence influence factor	1.012	1.000
Final penalty constrain values	1.063	0.252

The natural frequency constraint is enforced in the GA through the tower top deflection as described in section 7.2.2. Using this tower top deflection to natural frequency relation the deflection

constraint applied in the GA is 1.754 m.

The penalty constraints in the GA are defined such that they start to have an influence on the structural mass of the tower to obtain a fitness mass as soon as the specific constraint is violated. The penalty applied on the structural mass makes sure the fitness of the design is degraded when the constraints are not met. The designs are not entirely removed to make sure potentially good designs with structural behaviour close to the constraint values are still taken into account in the following optimisation steps. When a constraint is not met, a penalty factor of 1.2 is applied to the structural weight of the tower. Besides that a linear mismatch factor purely based on the percentage of mismatch between the constraint and the found value is implemented for the factor of safety constraint, a similar but quadratic mismatch factor is applied at the tower top deflection constraint. The tower top deflection penalty is quadratic because in GA test trials it is found that achieving the required natural frequency requires a lot of additional material. Therefore lightweight designs not complying with the natural frequency constraint, which was linearly defined at the time, were however still found to be able to be the fittest designs. To solve this the penalty is made quadratic based on mismatch.

7.3 Detailed modelling results

The genetic algorithm as described in sections 7.1 and 7.2 is run a total of three times, in which the structural constraints have been tightened based on the results in the former step, to reduce the amount of possible designs and obtain an improved result. The values the structural parameters could initially take are explained in section 7.1.1, and the tightening of constraint per iteration is shown in table 7.10

Table 7.10: Structural variable bounds per GA optimisation run

	GA run 1	GA run 2	GA run 3
Helical ribs (-)	31-40	36-40	38-40
Hoop ribs (-)	70-120	90-120	90-120
Rib height (mm)	200-300	220-300	250-290
Helical rib width (mm)	40-76	40-76	68-76
Hoop rib width (mm)	12-48	12-24	12-20

Table 7.11: Parameters of the most optimal design found by the GA in this study

Tower weight (Tonnes)	134.5
Factor of safety (-)	2.489
Natural frequency (Hz)	0.222
Number of helical ribs (-)	39
Number of hoop ribs (-)	98
Helical base angle (°)	9.97
Rib height (mm)	250
Helical rib height (mm)	76
Hoop rib height (mm)	20

The final design obtained through this optimisation is given in table 7.11. It can be seen that two of the design variables, the rib height and the hoop rib width, ran into the variable bounds in the final design iteration. The hoop rib width was seen to vary very constantly around the values of 12, 16 and 20 mm, it is therefore not expected that the final variable bound has influenced the design. The rib height variable is at the lower bound, which is an interesting result, because it indicates that there might be a slight weight reduction possible. It must however be noted that the final bounds are carefully chosen based on the former GA results, and therefore it is not

expected that significant gain can be achieved by further rib height reductions. Furthermore it can be observed that the helical rib width ran into the maximum rib width allowed in the design, this constraint is used to obtain a geometrically feasible design. And was implemented based on a geometric requirement that the helical rib width should roughly not be larger than the length of the freely hanging parts of the hoop ribs. A picture of the tower based geometry is given in fig. 7.6.

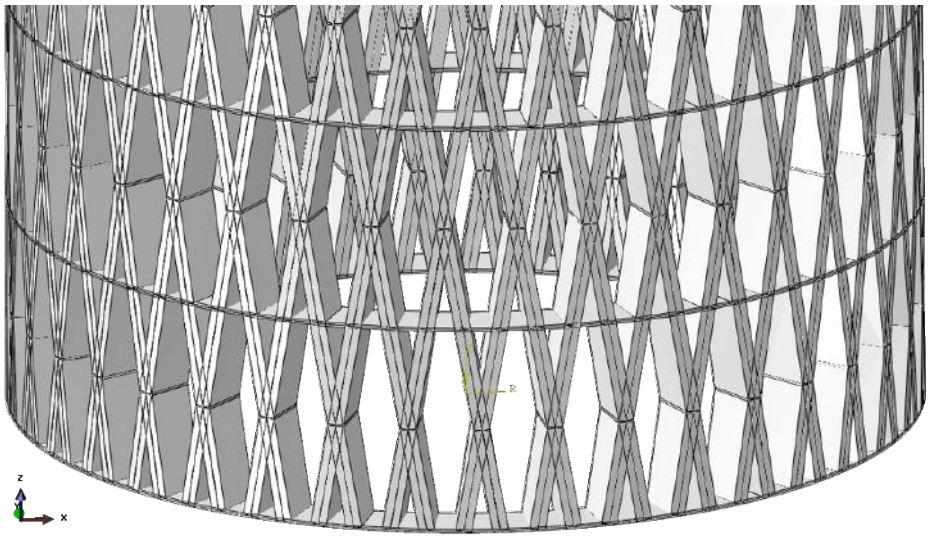

Figure 7.6: Abaqus picture showing the 3D-geometry of the composite lattice at the tower base

It is interesting to validate the simplifications made on rib tapering and natural frequency in the model based on the final output the GA gives and the output of an full Abaqus run in which rib tapering is taken into account in the model and the natural frequency is calculated by Abaqus itself. To make this comparison the GA and full model results without the effect of mesh convergence on the failure criterion are given in table 7.12, the results from the GA and full model, excluding non-linear effects and mesh convergence on the failure criterion are given in table 7.13. And finally the strain energy plot of the optimised tower is given in fig. 7.7.

It can be shown that both the rib tapering an the non-linear simplification have influence on the result, but the influences are small. Therefore it is concluded that the simplifications made in the GA did not have unacceptable influences on the results and hence the optimisation. Furthermore the rib tapering ratio, which is determined based on an homogeneous strain energy density distribution, still shows to have a comparable type distribution compared to the benchmark tower.

Table 7.12: Comparison of the results form the GA and a full analysis run on the final tower

	GA	Full model	Error (%)
Factor of safety (-)	2.518	2.438	3.3
Tower top deflection (m)	2.331	2.400	2.9
Natural frequency (Hz)	0.222	0.225	1.1

Based on the full analysis results from the most optimal tower configuration found, the final performance parameters are given, with the mesh convergence knock-down included, and an estimate for buckling eigenvalue, in table 7.14. During this full analysis it is observed that the failure location shifted from the bottom to the top tower section. The failure however still is found in the helical ribs as axial compressive failure. It is interesting to notice that this shift in failure location seems to have little influence on the magnitude of the factor of safety. This shows that the rib taper ratio is indeed chosen such that the distribution of material over the tower is efficient from a strength perspective. Furthermore notice the buckling eigenvalue estimated based on the static loading. It confirms that buckling is not critical in the tower design.

Considering the final results given here it can be seen that the optimisation is only frequency driven. Based on the strength-wise over-design of the structure it can be concluded that it is

Table 7.13: Comparison of the results form the GA and a full analysis run on the final tower without non-linearity

	GA	Full model	Error (%)
Factor of safety (-)	2.647	2.610	1.4
Tower top deflection (m)	2.131	2.167	1.7
Natural frequency (Hz)	0.234	0.235	0.5

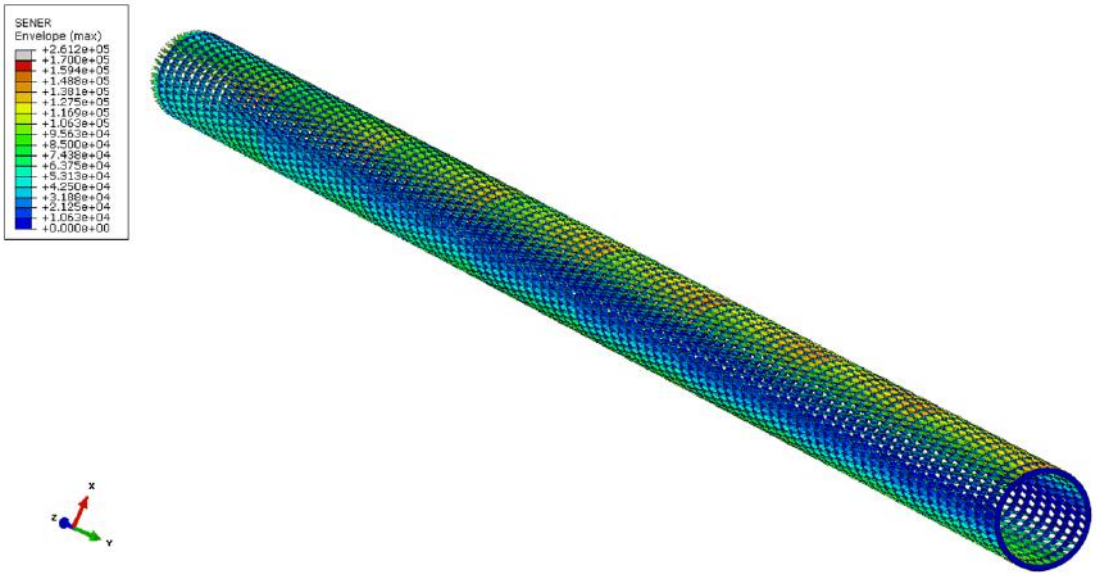

Figure 7.7: Abaqus strain energy density result for the statically loaded optimised tower

judged very unlikely that further convergence of the mesh would give results showing that the currently found design is actually infeasible. However if mechanical test results show the strength of the material is highly overestimated it is desirable to determine a failure knock-down in further research to better estimate the failure characteristics of the structure. This can be done by including differences seen in representative sample test results, accurate mesh convergence results and including effects due to the simplified geometry configuration in the analysis.

Table 7.14: The final tower performance properties as obtained from a full Abaqus analysis with convergence knock-downs on failure

Factor of safety (-)	2.410
Buckling eigenvalue (-)	4.003
Tower top deflection (m)	2.400
Natural frequency (Hz)	0.225

7.4 Final modelling update

In the final stages of the project some additional information influencing the centre of gravity of the rotor and nacelle is obtained. The new centre of gravity coordinate is at the y-symmetry plane at a -0.269m x-coordinate and a 89.55m z-coordinate, as a reference the initially used centre of gravity was located at a -2.635m x-coordinate and a 90m z-coordinate. An Abaqus simulation is performed on the optimised tower design to check the influences of centre of gravity relocation. The results are shown in table 7.15. As can be seen the natural frequency is positively influenced, while the factor of safety slightly drops. Since the natural frequency is driving in design, it indicates that there is some room left for further optimisation to obtain slight weight reductions. The change in natural frequency is 3%, according to the GA data shown in fig. 7.8, this change could lead to mass reductions of 15,000 kg, 11% of the total tower weight, which can significantly reduce material cost as given in chapter 9. However it is considered important to also include more load cases and strength knock-downs based on mechanical tests in further optimisations. When such an expansion of optimisation criteria is made, the effects of the new centre of gravity can easily be included and modelled in detail.

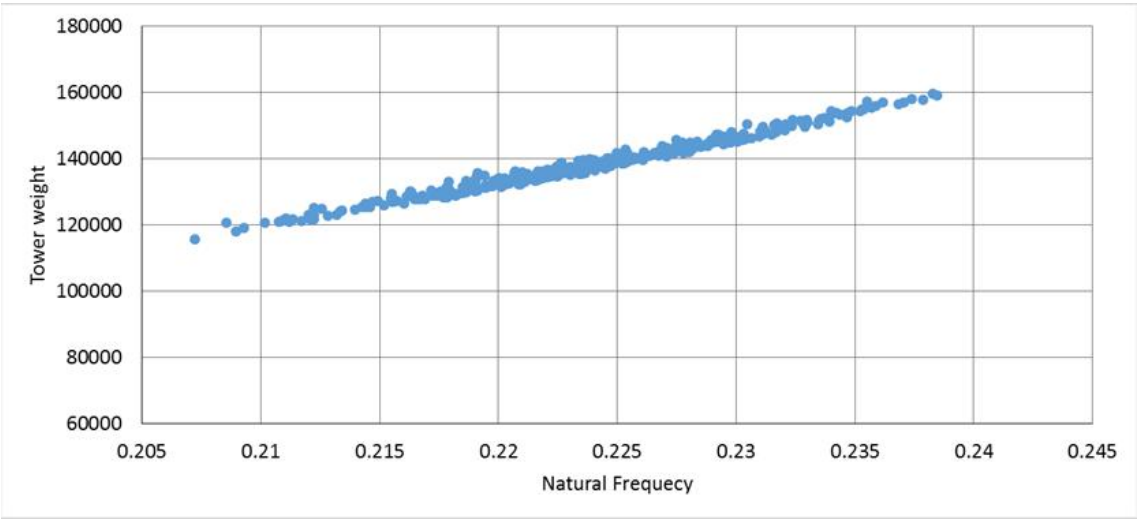

Figure 7.8: Plot of the GA data showing the trend between tower weight and natural frequency

Table 7.15: The updated centre of mass tower performance properties as obtained from a full Abaqus analysis with convergence knock-downs on failure

Factor of safety (-)	2.349
Buckling eigenvalue (-)	3.855
Tower top deflection (m)	2.389
Natural frequency (Hz)	0.232

Chapter 8

Mechanical testing

One of the projects goals is to prove structural feasibility of the structure under consideration. Real life mechanical tests are key in this process to validate the modelling approach. The focus in this chapter is on the in-plane stiffness of the structure, since this is found to be the most critical design parameter in the optimisation process. However the strength is determined in the tests, and the initial failure seen in the final FEM model is determined using a simplified approach to verify predictability of the failure location. In section 8.1 the reasoning behind the design of the sample and the modelling techniques are explained. The production of samples and preparations for the tests are described in section 8.2, and the test results and improvements in model correlation are given in section 8.3.

8.1 Mechanical test sample design

Since the mechanical test campaign is carried out while the optimisation is prepared and running, the most optimum tower found could not be used at the time of test sample design. Furthermore preparations were already in progress when the final design switched from glass to carbon fibre. Therefore glass fibre is already chosen as sample material and is used together with the at that time available benchmark structure as the basis for sample design. Switching to carbon fibre samples is considered not necessary for the validity of these tests with the general purpose to improve the understanding of the global behaviour of vacuum infused fibre reinforced polymer lattice structures. However literature does indicate compressive failure differences between different fibre reinforcements [47], it is therefore acknowledged that additional carbon fibre tests on comparable samples would have a lot of added value for the understanding of possible differences in failure behaviour between carbon and glass fibre reinforced samples.

The parameters obtained from the benchmark structure are converted to a test sample, how this scaling is perfomred is given in section 8.1.1, and the test sample abaqus model is described in section 8.1.2.

8.1.1 Determination of test sample type

The sample is based on the dimensions of the composite lattice found at the bottom of the benchmark tower, and the rib width is constrained by the structural parameter ranges as finally used in the optimisation. This leads to the design parameters for the test sample as given in table 8.1.

Table 8.1: Design parameters for the test sample

Helical angle (deg)	12.22
Rib height (mm)	216
Helical rib height (mm)	76
Hoop rib height (mm)	28

The test campaign under consideration is a six sample compression test campaign. The amount of six samples has be chosen to get a feeling with the magnitude of spread in the sample properties, while the effort for test sample manufacturing was kept within reasonable bounds for this project.

Compression tests are chosen because of the dominance of compressive loads in the bottom section of the tower. For this type of tests a few aspects are driving the design of the sample as given next:

- The compression test bench available is able to go up to a load of 150 kN. This maximum load results in a necessity to scale down the dimensional parameters of the full tower design.
- The dimensional downscaling should not lead to buckling failure of the test sample. Such that the failure type seen in the sample is representative for the full scale structure.
- Main point of interest is the behaviour of the grid influenced by the relatively large helical nodes.

The required downscaling in combination with the buckling constraint are driving the sample dimensions to a large extent. It resulted in a flat test sample with 3 helical rib intersections and two hoop ribs which are potted to have a proper load introduction and a stable sample during the tests.

The first step in downscaling is reducing the dimensions of the grid by a factor of 9.5, and reducing the amount of helical rib intersections to three in which the ribs are placed on a flat surface to simplify manufacturing, this resulted in helical ribs with a width of two tow widths. Scaling the hoop ribs with this factor resulted in hoop ribs with a dimension of 4 mm, because the tow width is constraining the hoop ribs from further down-scaling. The dimensional parameters of such a grid are given in table 8.2.

Table 8.2: Design parameters for the test sample scaled by a factor 9.5

Helical angle (deg)	12.22
Rib height (mm)	22.74
Helical rib width (mm)	8
Hoop rib width (mm)	4

Based on Abaqus simulations made on the geometry given, an expected failure load between 300 kN to 350 kN is found. The failure estimate is based on the load from which the ply-axial strains start to exceed the allowable strains, the allowable strains are calculated using a micro-mechanics approach. The rib and node maximum allowable strains without knock-downs are given in table 8.3. Note that the 3-directions maximum strains are assumed to be equal to the 2-directions ones and that shear strains in the 23-plane are not assessed. The stiffnesses used in these predictions are given in table 8.4

The node fibre volume fraction is assumed to be 65%. Based on found references [48], it can be seen that the relation used to determine the strength in tensile 2-direction starts to underestimate the real strength for high volume fractions because the test data seems to reach a higher limit. Therefore it is assumed that the maximum strain in 2-direction at 65% fibre volume fraction is going to a limit of 0.001 instead of basing this value on the equations used before. The node material properties are as well given in tables 8.3 and 8.4.

Table 8.3: Glass fibre laminate maximum strain input for Abaqus without knock-downs

	Rib	Node
Fibre volume fraction (-)	0.393	0.65
$\epsilon_{1_t,max}$ (-)	0.0272	0.0282
$\epsilon_{1_c,max}$ (-)	0.0161	0.0167
$\epsilon_{2_t,max}$ (-)	0.0037	0.0010
$\epsilon_{2_c,max}$ (-)	0.0171	0.0103
$\epsilon_{3_t,max}$ (-)	0.0037	0.0010
$\epsilon_{3_c,max}$ (-)	0.0171	0.0103
$\gamma_{12,max}$ (-)	0.0251	0.0132
$\gamma_{13,max}$ (-)	0.0251	0.0132

Table 8.4: Glass fibre laminate stiffness input for Abaqus test sample modelling

	Rib	Node
Fibre volume fraction (-)	0.39	0.65
E_1 (GPa)	32.4	51.8
E_2 (GPa)	4.69	7.8
E_3 (GPa)	4.69	7.8
υ_{12} (-)	0.29	0.29
υ_{13} (-)	0.29	0.29
υ_{23} (-)	0.45	0.45
G_{12} (GPa)	2.66	5.05
G_{13} (GPa)	2.66	5.05
G_{23} (GPa)	1.59	3.03

Since the simulations showed no failure before the 150kN maximum of the machine, ways had to be found to further reduce the strength of the sample. It is concluded that in terms of rib width the dimensions could not go down for manufacturing reasons. The amount of nodes is already very dense, 6 nodes on the hoop ribs within a length of 10.5 cm. Increasing this node density further would give problems with the infusion strategy as described in chapter 5.

Further down scaling is therefore done by reducing the rib height, this however increases the risk for buckling failure, which is required to be avoided. The final test sample design based on the design criteria and this final down-scaling resulted in a rib height equal to the rib width. This gave a test sample which is expected to fail at a load between 120 and 150 kN. While buckling was not expected below a load of 223 kN. Since it is hard to predict how the sample would behave in real life on beforehand, this buckling load is considered the minimum desirable buckling load relative to the expected compression failure load. This explains why the sample is not made higher to include longer helical ribs, and non-potted hoop ribs.

Potting is required to ensure stability of the sample in the test bench to have a proper load introduction. The potting type and size determination is performed through iterations based on the effects seen in stress concentrations at the potting rib interface. Besides that the surface on the rib side of the potting is visually checked for the absence of stress influences from the surface on which the sample is compressed.

The selected material for potting is the Huntsman casting epoxy resin RenCast CW 2215 with hardener Ren HY 5160 with a compressive modulus of 3.5-4.0 GPa and a compressive strength of 80-90 MPa [49]. The potting is designed such that the hoop ribs are contained in the middle of the potting fixtures. It has a height of 11mm and a width of four times the rib height (32mm). For this potting material with these dimensions, no stress influences are found from the side on which compression is applied, on the rib side of the potting. At the location where the ribs extend from the potting, strain concentrations in rib axial direction are found with strain values above the failure strains, at an applied loading of 150kN in up to two elements away from potting edge as shown in fig. 8.1. Since in real life the potting rib transition would be way smoother since the potting automatically fillets the edge, the rib-potting interface strains are not considered critical. The sample as described here is shown in table 8.5 and fig. 8.2.

Table 8.5: Design parameters for the test sample scaled to final design dimensions

Helical angle (deg)	12.22
Rib height (mm)	8
Helical rib height (mm)	8
Hoop rib height (mm)	4

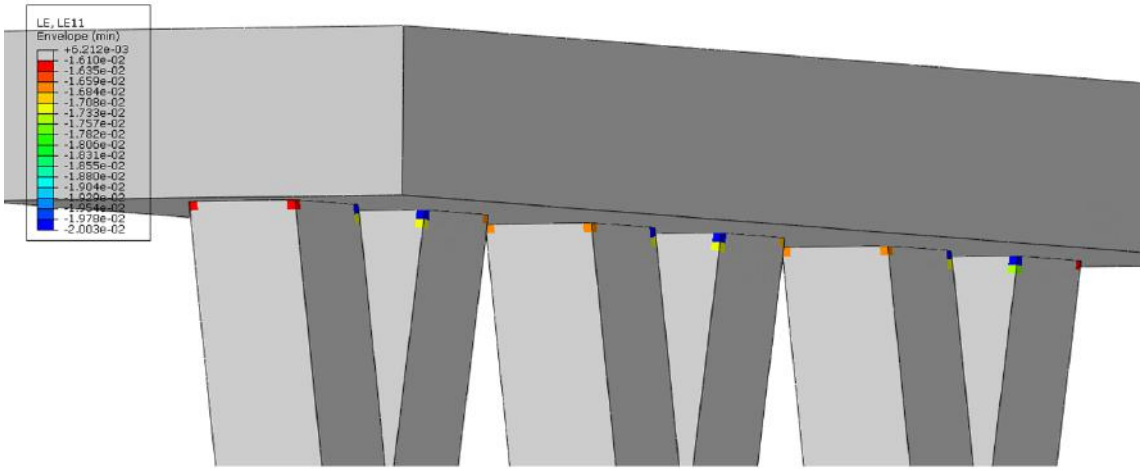

Figure 8.1: Picture of the potting rib interface strain concentrations visualised by elements printed in colour

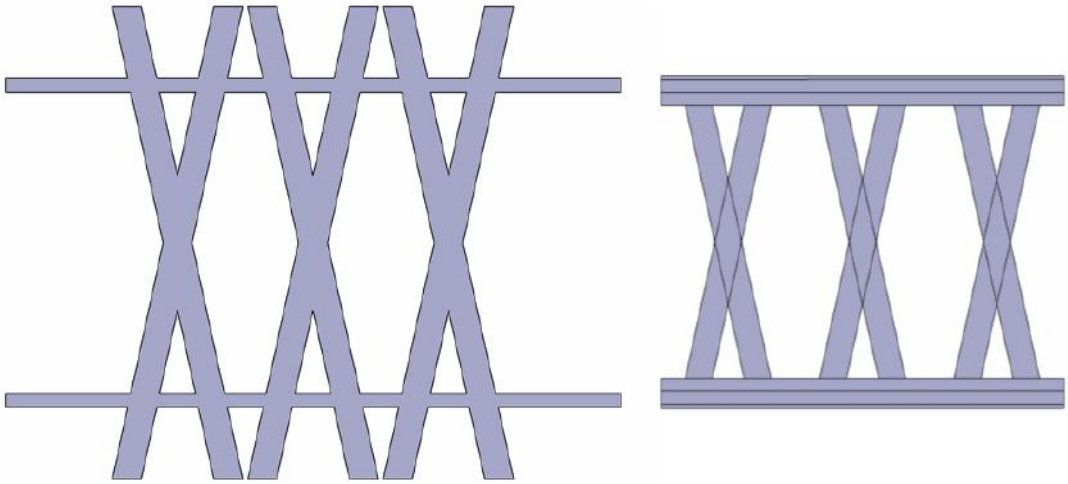

Figure 8.2: Picture of the final test sample design, left shows the infusion geometry, right shows the final test sample geometry with potting

8.1.2 Modelling techniques for the test sample

Modelling of the sample has been done in Abaqus, in which the bottom surface is entirely restricted from movement in all three directions, the top surface is constrained from movement in two directions, allowing the sample to be compressed through an axial force on the top surface. The force and constraints are applied through points which are attached to the surfaces through kinematic-coupling.

The final type of mesh used in correlation had a global seed size of 0.696 mm with local seed sizes of a factor 8 smaller in the areas where the largest strains are found. A picture with the global overview of the mesh is given in fig. 8.3. A picture with a close up of the local node mesh is given in fig. 8.4.

The ribs of the sample are modelled assuming a homogeneous orthotropic material behaviour. The nodes are modelled through composite lay-ups based on 4 plies which are balanced but not symmetric, to represent the lay-up sequence the used manufacturing method would give. The regions with potting material are meshed using a structured technique based on Hex only elements. The regions outside of potting (the free ribs) are all meshed using a sweep advancing front technique. The homogeneous rib sections elements are Hex-dominated, and the composite lay-up nodes elements are Hex only. The solid hex-elements are of the type C3D8R, and the solid wedge-elements of the type C3D6, tet-elements are not present in the mesh.

A geometrical non-linear analysis is carried out, and the strains at strain gauge locations are

measured in the model using one truss-element, with an isotropic stiffness of 0.001 Pa, of which the two nodes are tied to the test sample nodes in the neighbourhood of the truss-element.

Figure 8.3: Overview of the final mesh type on the sample

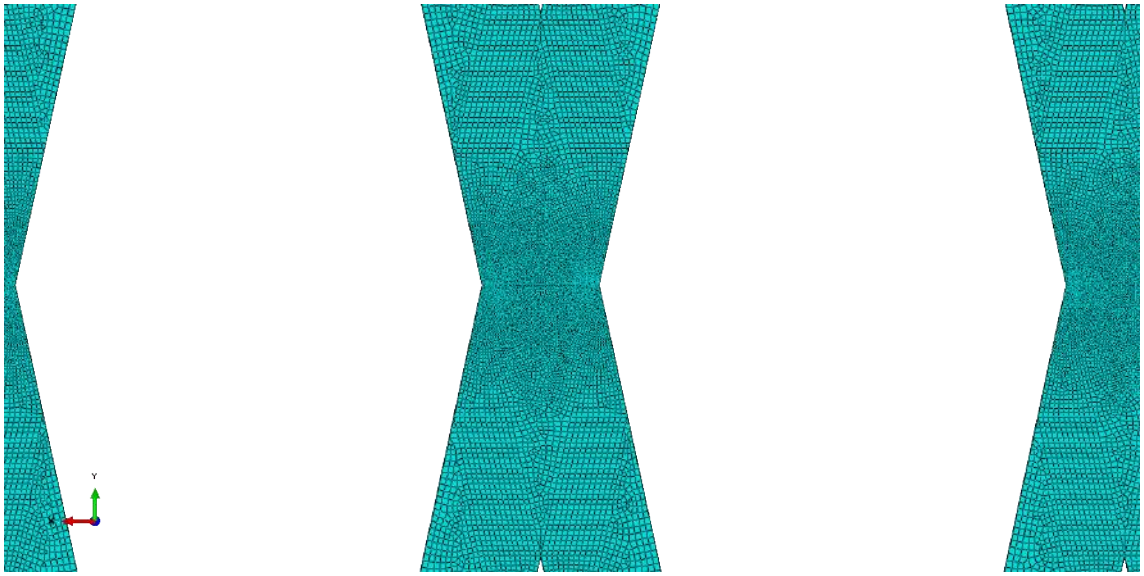

Figure 8.4: Close-up of the mesh at nodes

8.2 Mechanical tests preparation

The necessary production steps to produce the samples and the required test preparations are discussed in this section. First the sample production process is explained in section 8.2.1, secondly the test preparations are described in section 8.2.2.

8.2.1 Production

The designed test samples were produced using the previously developed manufacturing method. The layout of the sample after demoulding is shown in fig. 8.5.

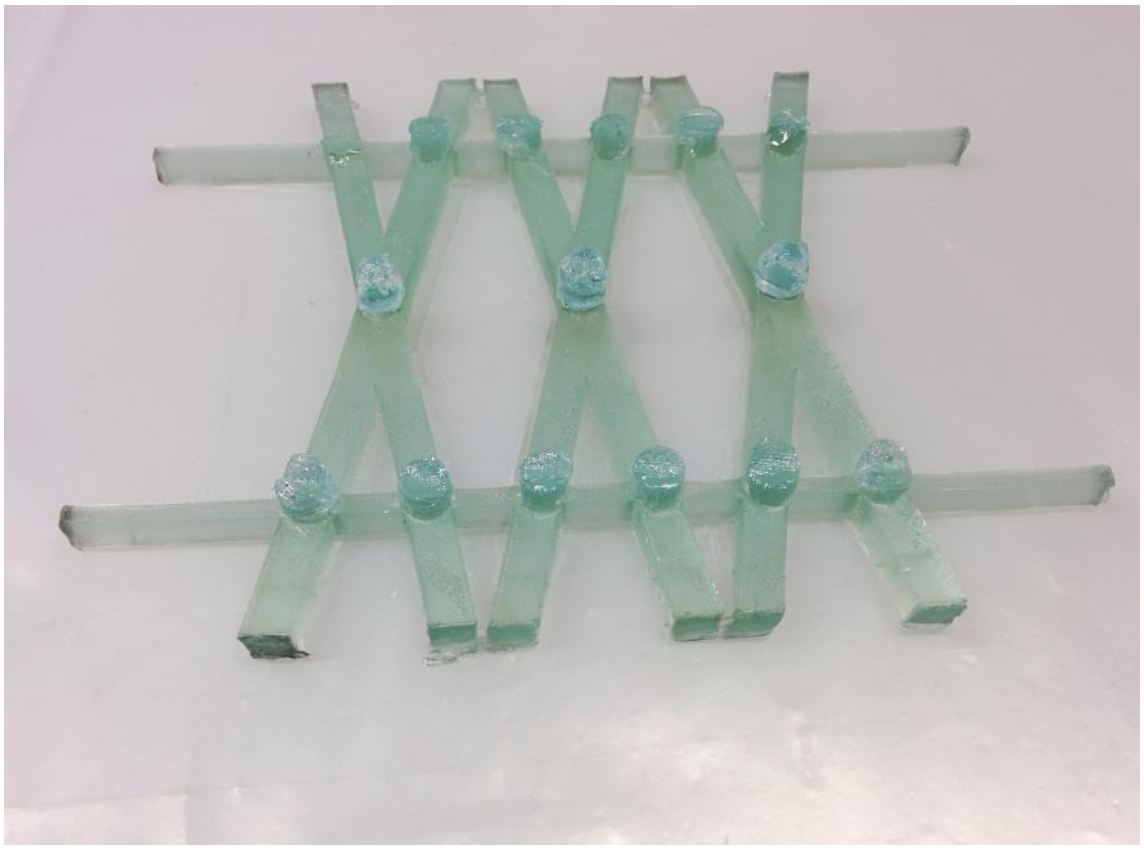

Figure 8.5: Picture of a grid just after infusion

When the infusion of samples was finished the samples are given a post-cure of 15h at 60°C before further processing them. After the post-cure the flash material still attached to the samples is removed using a Dremel tool, and the sample is cut to size using a diamond blade saw. The samples where potted in groups of three, and the curing of the potting is performed overnight in a oven at 40°C for at least 14h. After potting of the samples has been completed, the three samples attached by potting material are cut in individual samples with a band saw, and the surfaces of the potting are milled parallel to each other and perpendicular to the test sample. The potted samples are shown in fig. 8.6.

In the final sample preparation steps six strain gauges are attached to the sample in the locations indicated in figures 8.7 and 8.8. Four strain gauges are placed at the middle four ribs to measure rib axial strain as indicated in fig. 8.7. From the two other strain gauges one strain gauge is placed on the side where Digital Image Correlation (DIC) observations are made to verify the strain gauge and DIC measurements, and one strain gauge is placed next to the node to measure strains in the 3-direction. These two strain gauges are shown in fig. 8.8 A speckle pattern is painted on one side of the specimen for DIC observations.

In the end seven samples were produced of which sample 2 till 7 were used for testing. Sample 1 was used as a sample to test the manufacturing steps before producing the rest of the specimens. Sample 1 is also used for undamaged material microscopy investigations.

8.2.2 Test preparations

The tests are performed on a 150kN compression test bench. The bench has a top head which is adjustable in angle to make sure the machine is not inducing bending loads in the sample. The machine is operated by hand while the load can be read from a screen. Besides strain gauges and DIC measurements, two Linear Variable Differential Transducer (LVDT) measurement devices are used to measure the travel of the testing machine during the test.

Since the minimum gap between the two heads of the bench is too large for the test sample a steel beam is used as support of the sample to reduce the minimum gap. The final set-up is shown in fig. 8.9.

The testing approach is to increase the load in every step by 0.5kN and take measurements from both the strain gauges, LVDT's and the DIC instrumentation after every load increase. This

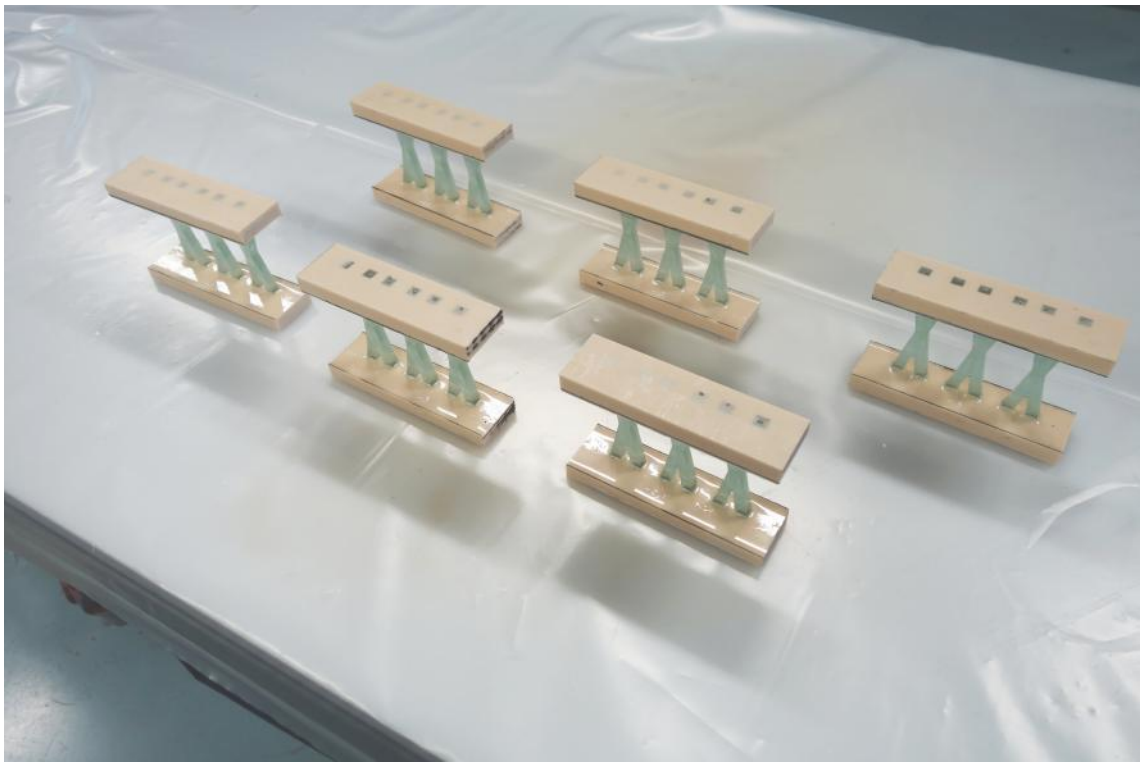

Figure 8.6: The six samples after potting

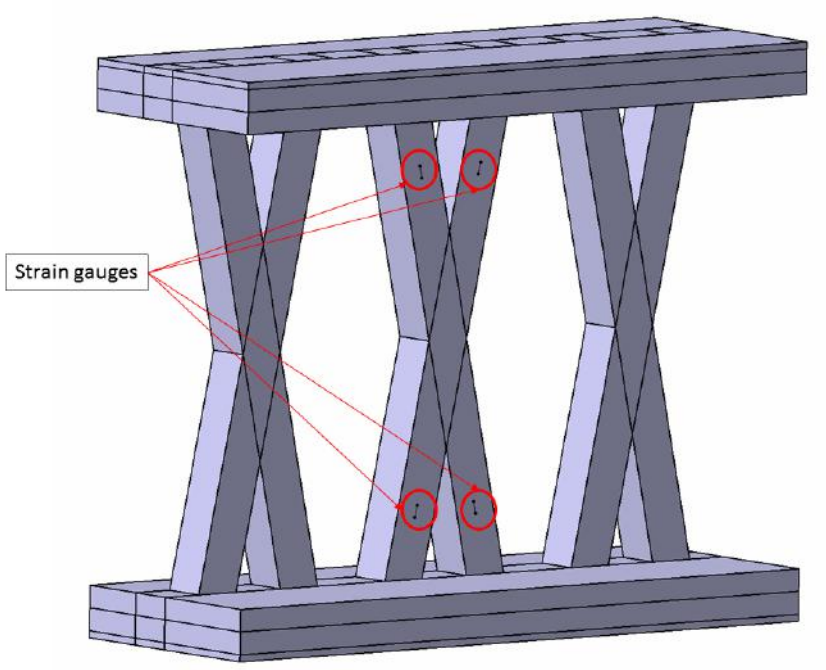

Figure 8.7: The four strain gauges placed on every rib in the middle of the sample

process is continued up until final failure of the sample.

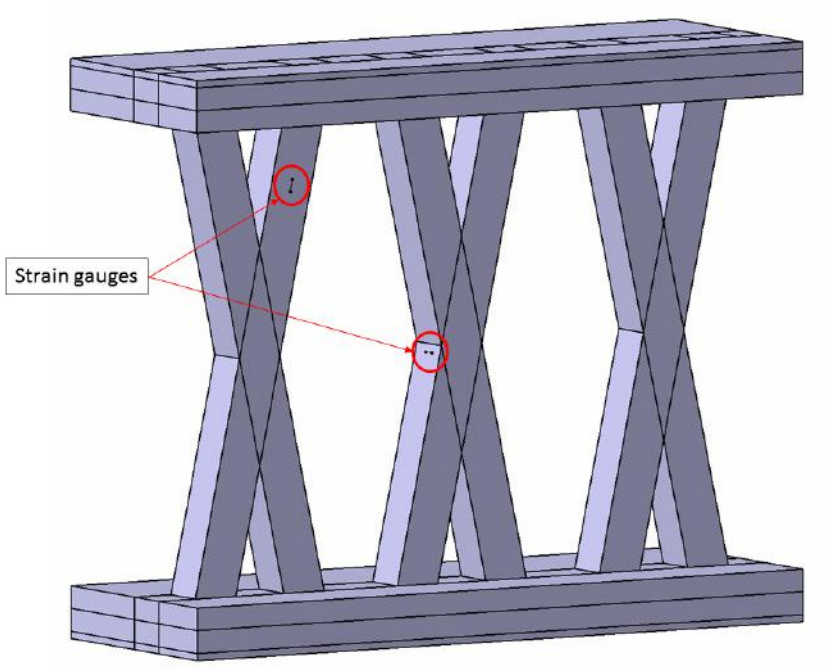

Figure 8.8: The two strain gauges as visible from the DIC side of the sample

8.3 Mechanical test results and analysis

During the execution of the tests it was found out that the final failure mode for the test sample is splitting of the entire rib as shown in fig. fig. 8.10. After final failure the samples are all showing a residual loading of 5±2 kN. The final failure is always preceded by some outer layer fibre buckling at the left and right corners of the nodes as shown in fig. fig. 8.11.

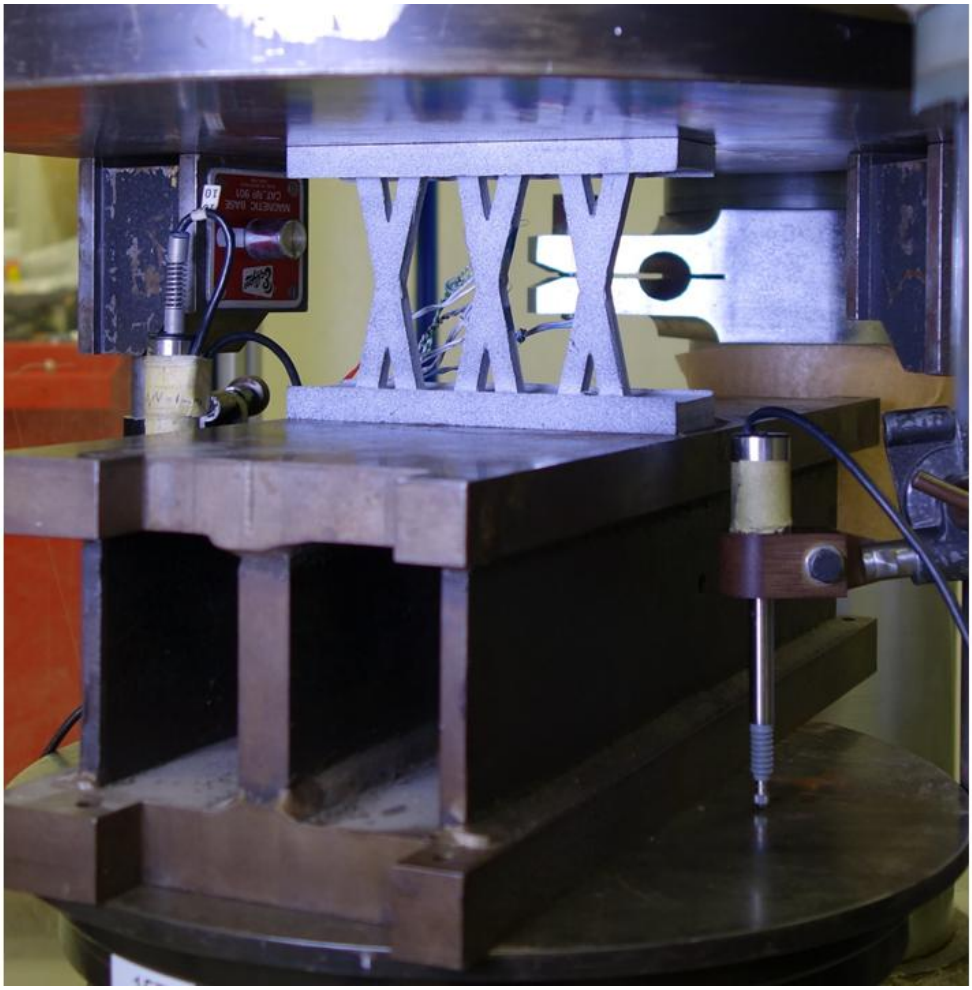

Figure 8.9: The test set-up for compression testing the samples

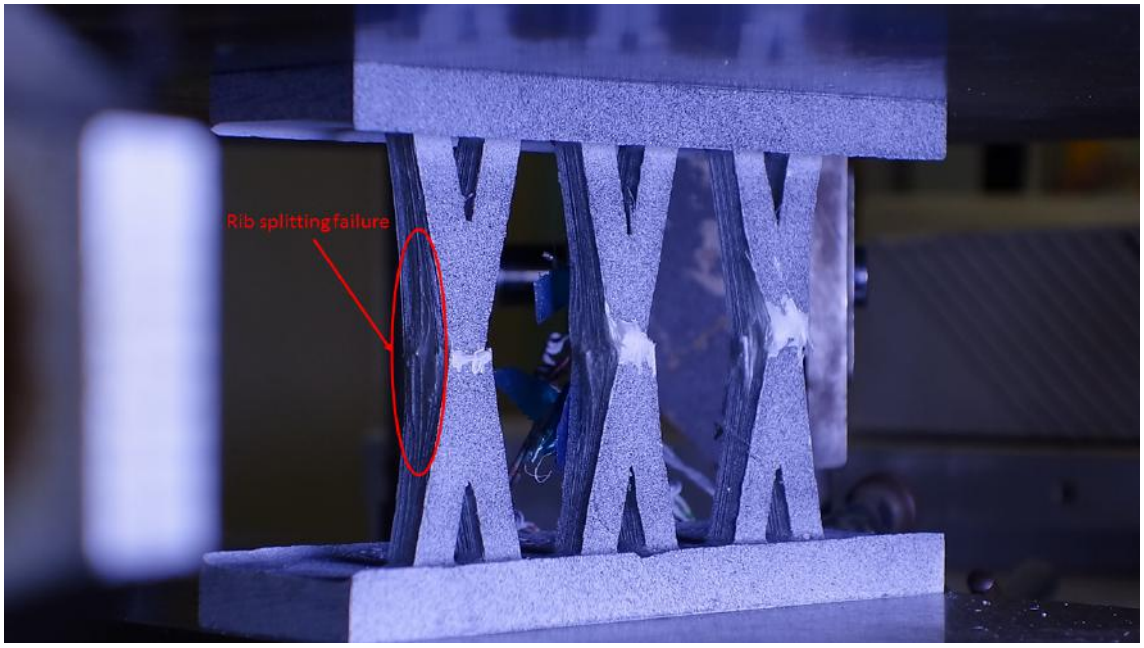

Figure 8.10: A picture showing the final rib splitting failure seen in the test samples while the sample is still loaded with the residual load.

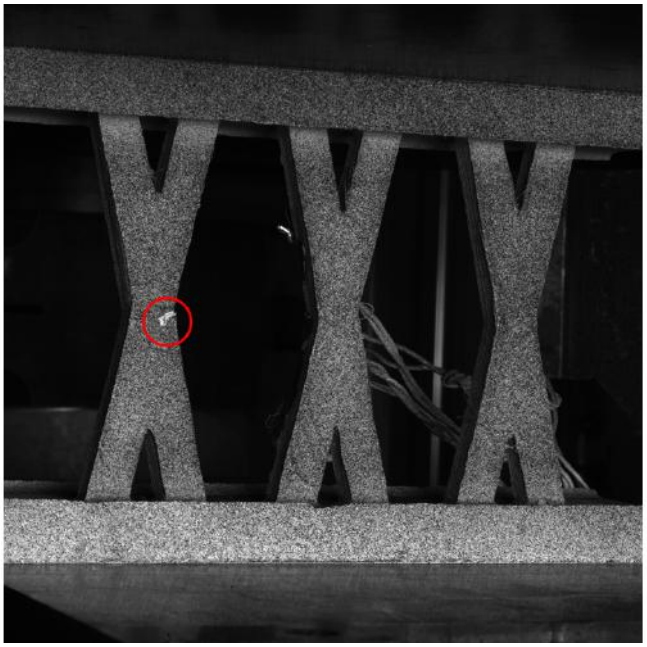

Figure 8.11: A picture taken by the DIC system showing the initial fibre buckling failure at the node, seen as a white mark on the ribs.

In order to correlate the test results with the analysis models a number of improvements with respect to the initial model setup were introduced. These improvements consisted in the following:

- Correction of the geometry for differences in dimensions due to production tolerances, followed by a recalculation of the fibre volume fractions based on the amount of fibre used in production.
- Introduction of node waviness in the model (due to out-of-plane deflections of the fibres passing through the node). This is done to reproduce the bending behaviour of the test samples.
- Implementation of the correct fibre volume distribution as a function the height of the rib.

8.3.1 Correlation results

The simulation results for the improved models together with the test results are given in figures 8.12 to 8.17. The results after applying geometric and fibre volume based improvements alone are given separately, to be able to show the individual influences of modelling bending and membrane stiffness of the sample.

In figures 8.12 to 8.17 the data corresponding to "Abaqus final" is representing the updated model including bending effects, and the data called "Geometry influence" is showing the results for the same model improvements made but without including the effects triggering bending. It can be seen in fig. 8.12 that modelling the bending has very little influence on the global stiffness of the sample, since the in-plane deflection plots for the models with and without bending effects are very close to each other. In fig. 8.13 the stiffness of the final model is shown to be in the range of stiffnesses found in the mechanical tests. The model has an average error compared to the test data in the range of 10 kN to 57 kN of 3.7%. At a load of 40 kN the error to the average is 3.2%, with a test data standard deviation of 4.7%. The 40 kN load will also be used as a comparison reference for the strain gauge data.

The average strain data for the four strain gauges attached to one side of the sample is given in fig. 8.14. It can be seen that the decrease in membrane stiffness improved the result to some extent, but including the features leading to sample bending, shows that the combination of improvements on bending and membrane stiffness leads to a good fit of strain data. At a load of 40 kN the model error with respect to the average of the test data is 4.3% while the standard deviation of the test data at this load is 2.7%.

Strain results for the single strain gauge on the DIC side of the sample where the bending effect creates a tension strain component at the strain gauge location is shown in fig. 8.15. The figure shows that including the geometry corrections leads to larger strains because of the decrease in membrane stiffness, but including bending effects in the model results shows that the model strain data shifts to the range of strains measured in the samples. The error at 40kN is 2.3% compared to the average strain data, and the standard deviation of the test data is 10.1% at this load.

The 3-direction strain results measured next to the node are given in fig. 8.16. The data shows a slight increase in magnitude when the global stiffness decreases, and the bending effect leads to a further strain increase. The final fit of data can be described by an error of 8.2% compared to the test data average with a standard deviation of 11.5% of the test data at 40kN.

The deflection data at 50 kN is shown in fig. 8.17. The results of the model without bending triggering effects show a slightly positive result due to the poisson's effect. Including the bending effects shows an model error of 1.1% in comparison with the maximum out of plane deflection obtained from the average deflection data measured in the tests, with a test data maximum deflection standard deviation of 17.9%. It must be noticed that with the improvements made, a fit with the positive out-of-plane deflection found at the edges of the sample is not achieved. Since modelling the in-plane stiffness of the samples was the main goal of the test and correlation campaign, and has been done with an accuracy of a few percent, and since it has been shown that the out-of-plane deflections only have minor effect on the in-plane stiffness, research on the effect initiating the bending in the outer regions of the sample is left for further research.

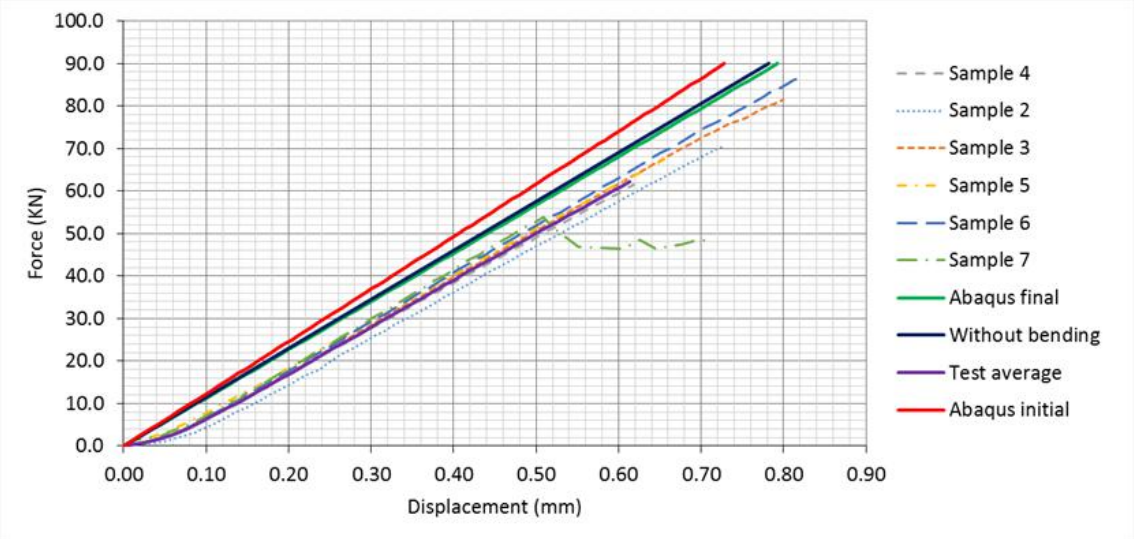

Figure 8.12: Comparison of the deflections found in the final Abaqus model and the mechanical tests

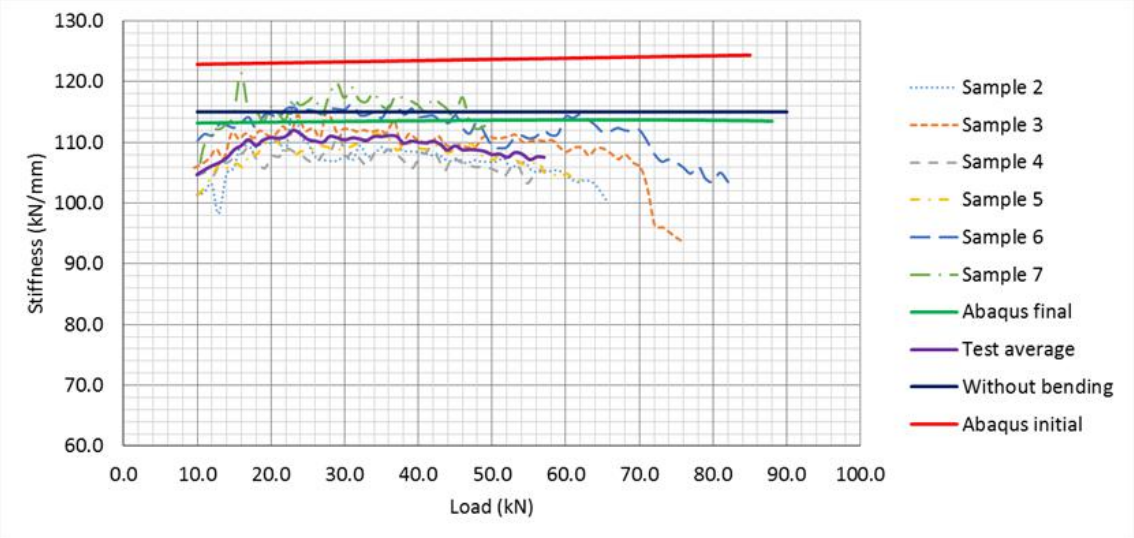

Figure 8.13: Comparison of the stiffness found in the final Abaqus model and the mechanical tests

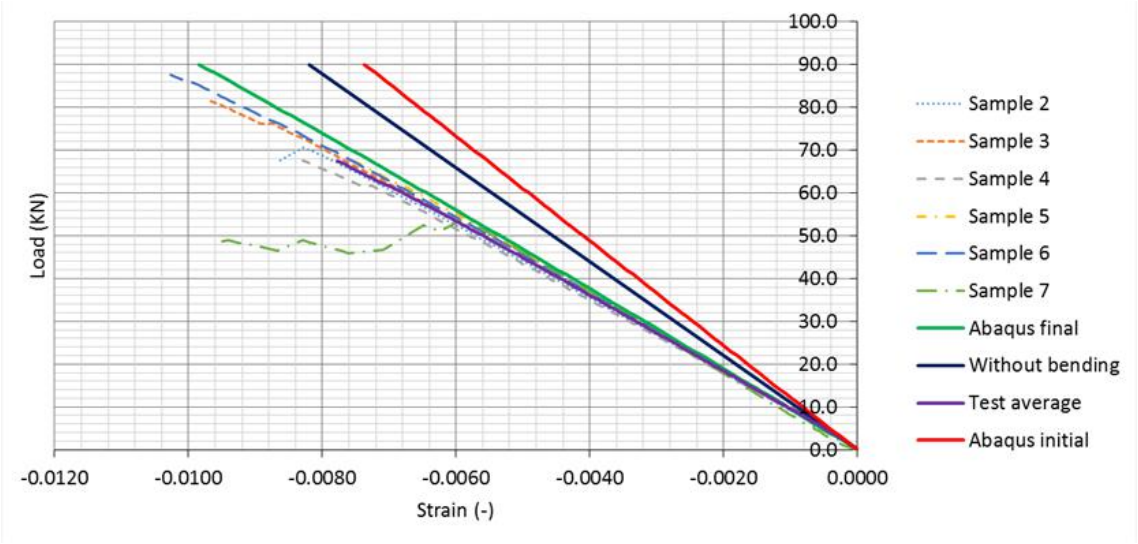

Figure 8.14: Comparison of the strain found at the four ribs in the middle of the sample in the final Abaqus model and the mechanical tests

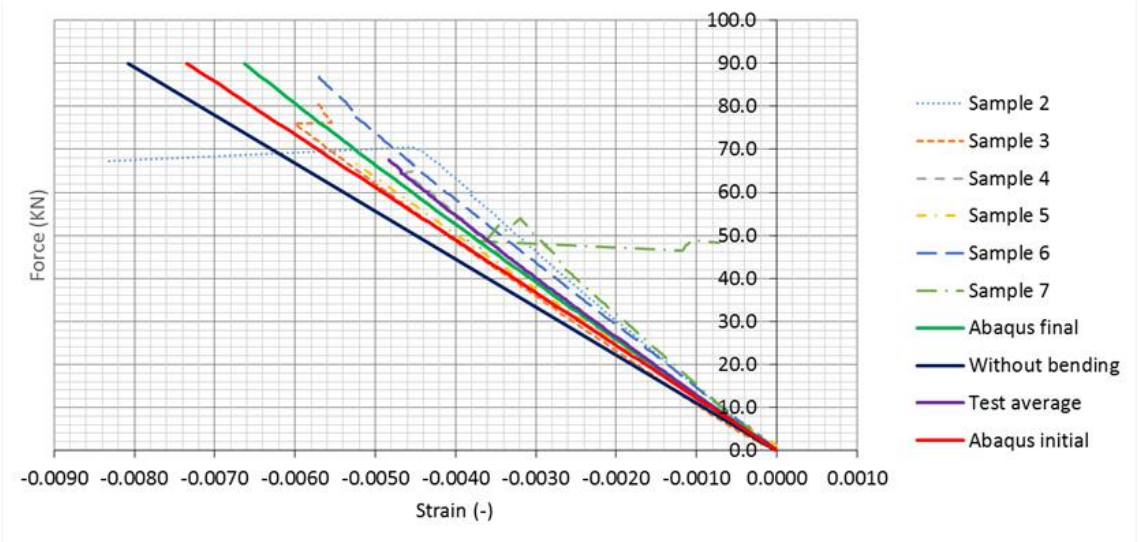

Figure 8.15: Comparison of the strain found at the DIC side of the sample in the final Abaqus model and the mechanical tests

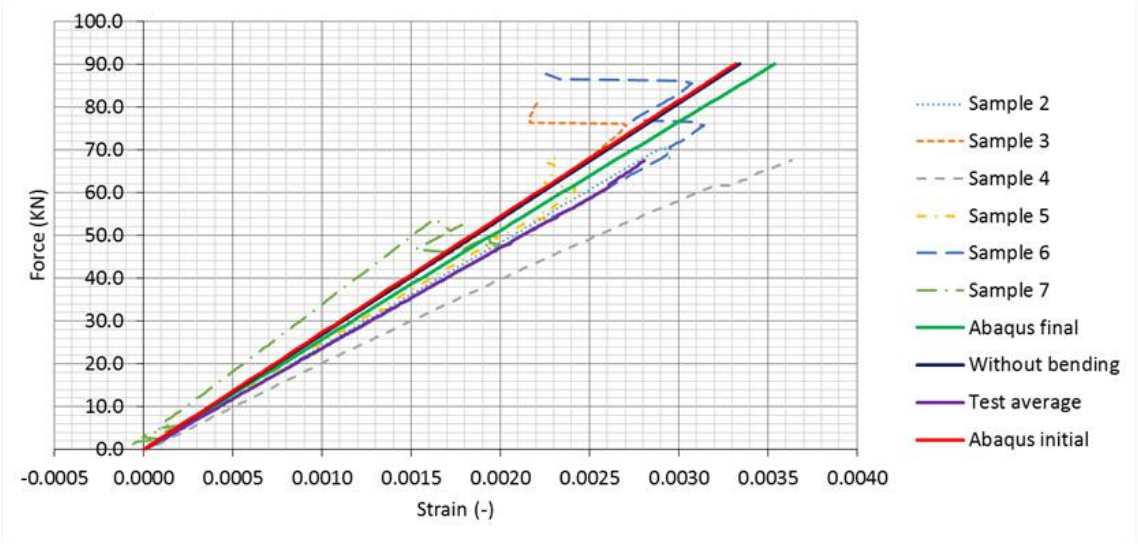

Figure 8.16: Comparison of the 3-direction strains found at the node in the final Abaqus model and the mechanical tests

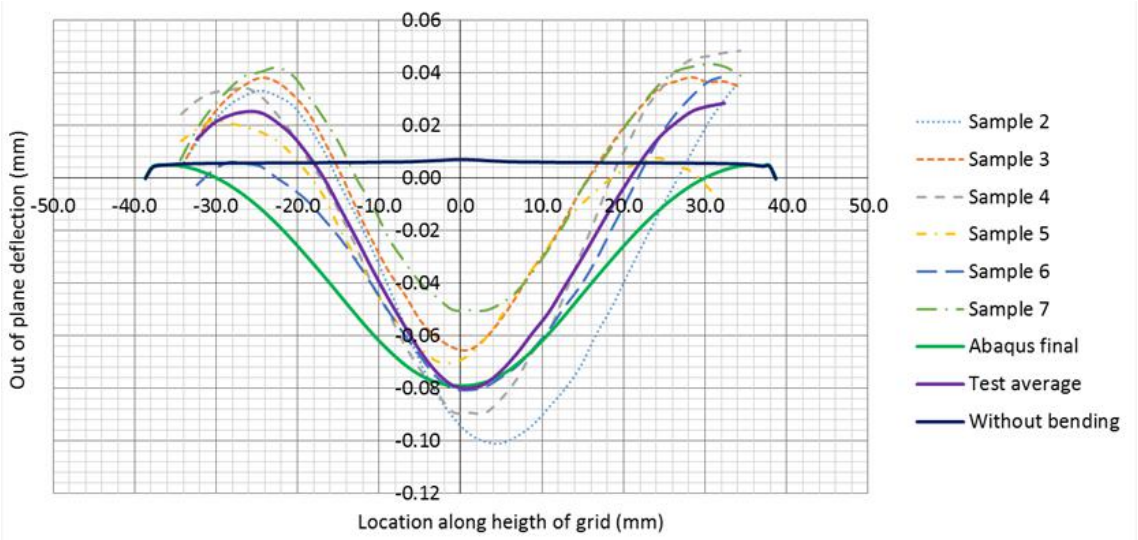

Figure 8.17: Plot of the out of plane deflections found in the mechanical tests at the middle of the sample

8.3.2 Correlation conclusions

The tests performed in this project show how the specific scaled tower section can be predicted in terms of stiffness and what kind of failure behaviour is found in this specific sample. The tests and correlation improvements performed afterwards give a good indication on the properties of small scale samples and how the properties can be modelled. The stiffness of the samples can be accurately modelled, the bending behaviour in the model has improved but cannot completely be represented with the effects included in the final model. However, especially because the bending seen is initiated by fibre waviness, which is expected to be smaller when using automated filament winding with tensioned fibres, these results can be seen as positive feedback for the predictability of a filament wound fibre reinforced lattice structure. Therefore these test results can function as a basis of understanding the composite lattice structure, which is important input for further research on larger filament wound structures. Therefore these tests are an important initial step in the verification of the structural behaviour of the type of structure. However since the sample has been scaled, is not cylindrical, is manually wound and only one load case has been investigated, extensive additional research is definitely required to verify the properties for the full tower.

The additional change in rib height during scaling might have affected the bending behaviour of the samples since this change has impact on the ribs moment of inertia, manual winding of the sample resulted in a lack of fibre tension in comparison to a filament winding process, and the scaling factor of 9.5 might also have significant influences on the resulting structural quality, since it is expected that up-scaling the manufacturing would result in large difficulties in air removal at the nodes, and possible heat build-up in the structure due to the exothermic reaction. Furthermore the samples have only been tested in compression while some shear loading is present on the tower, which especially has quite some contribution to the total loading at the tower top. Therefore to get a better insight into these effects it is recommended that further tests are performed on larger test machines which allow the ribs to have their real life cross-sectional aspect ratios, and allow the samples to be larger such that the behaviour of the hoop rib - helical rib interaction can be taken into account as well. In the most ideal case these tests are performed on fully cylindrical filament wound structures to represent the structure even more accurately, and furthermore it is recommended that shear (or for a cylindrical specimen torsion) tests are performed since this type of loading becomes a more dominant design load at the tower top. With these tests the real life out-of-plane bending and stress concentrations can be much more accurately assessed.

Chapter 9

Cost and performance considerations

In this chapter the secondary benefits and the cost estimation for the composite wind turbine tower from the start of production to the installation of the wind turbine are described. The cost estimation is performed to enable a comparison of cost between a composite tower and the steel reference tower. The economic feasibility for the concept can be determined based on this comparison. This cost estimation is broken down into three parts as described in section 9.1. Some further foreseen additional performance considerations with possible influences on the cost of a composite lattice structure are given in section 9.2.

9.1 Cost comparison

The composite tower cost estimation broken down in three separate topics is given in this section. The material cost of the composite wind turbine is based on the final design in section 9.1.1. The productions cost estimation is described in section 9.1.2. The transport and assembly cost is given in section 9.1.4. The cost of the reference tower is determined in section 9.1.3, and the cost of the reference and composite tower is compared in section 9.1.5. When in this section cost numbers had to be converted from Dollar to Euro, the exchange rate of 1.10 Euro/Dollar is used as found at 26-02-2016.

9.1.1 Material cost estimation

The material cost of the tower configuration found in the optimisation is based on its total weight and the fibre weight fraction of the material used in this optimisation as described in table 6.6. With a price per kilogram added to these numbers the material cost for a tower can be obtained. The costs of fibre used in this estimation are based on quotes obtained from material suppliers. According to these and based on the projected order quantities the cost of carbon fibre is 12 EURO/kg whereas the cost of resin is 3.5 EURO/kg

The weight breakdown of the tower based on the 134.5 tonnes tower design, and the 0.502 carbon fibre weight fraction is given in table 9.1. Considering the carbon fibre and epoxy cost per kg given above the material cost of the tower can be calculated and is given table 9.2.

Table 9.1: Weight breakdown of tower

Tower weight (tonnes)	134.5
Carbon weight (tonnes)	67.5
Epoxy weight (tonnes)	67.0

Table 9.2: Material cost estimation for the composite tower

Carbon cost (Euro)	810,000
Epoxy cost (Euro)	234,000
Total cost (Euro)	1,044,000

9.1.2 Production cost estimation

The estimation of total production cost of a tower as designed in this project is hard because of the lack of research and especially commercialisation of vacuum infused fibre reinforced grid structures. Because of this lack of direct references to this type of structure, reference cost estimates are sought in other types of large vacuum infused structures. Such a good example for large vacuum infused structures can be found in wind turbine blades, both because of the large size of the infused parts and the similar industry (wind energy) in which they are produced. The production cost estimation of the composite tower is therefore based on research performed on the influences of wind turbine blade size on cost [51]. In this cost study three sizes of blades are compared on material cost, labour cost, plant cost and tooling cost. The production cost for the composite tower is extrapolated, based on the growth in cost compared to the growth in product weight in this reference study. Of course not all the types of cost as described in the reference study can directly be used as a reference for a vacuum infused wind-turbine tower because of the differences in types of structure. How these differences are taken into account can be explained with the following points of attention:

- Material cost as determined in the reference study is not used. The types of material and the way in which they are used in the structure are different. The material cost estimation for the composite tower is performed separately and is based on the real material usage as determined through the wind turbine tower optimization.
- The reference weight of the blades is based on the glass fibre and epoxy weight in the blade only. Other materials are excluded since they are not representative for the material in the tower.
- The labour cost in the reference study is determined for the complete process of wind turbine blade production, including transport, and assembly of the different parts of the blade, two skin sides and shear webs. Such a step is not required for tower production, tower sections are infused in one shot. Furthermore since the cost of transport and assembly of separate tower sections is taken into account in section 9.1.4, the labour cost for transport and assembly as defined in the reference study are omitted.
- The labour involved in installing the attachment transition structure and the cost of this structure is treated separately since a blade only has one attachment zone, while the tower consists of eight sections with 16 attachments zone. It is assumed that the installation of the attachment at the end of a tower section and the attachment structure itself is comparable in complexity to that of a wind turbine blade. Therefore the attachment part and labour cost is multiplied with a factor 16 from the reference.
- Plant cost for wind turbines is determined based on floor area required to produce blades for on average 640 MW of wind turbine capacity. Based on this criterion less blades are required when they become larger to produce 640 MW of wind turbine capacity. This means that for larger (heavier) infused structures a scaling based on blade weight would automatically assume a decrease in parts produced per year based on the trend in required amount of blades produced. The plant cost per blade is therefore used as a reference for plant cost per tower under the assumption that required floor area for tower production is linearly dependent on the amount of towers to be produced per year. This means that producing more towers would not influence the plant cost per tower.
- To scale the plant cost from wind turbine blades to towers it is assumed that the floor area aspect ratio required to produce a wind turbine blade or a full tower is comparable.
- To scale the plant cost from wind turbine blades to towers the assumption is made that producing the tower in sections compared to the blade being produced in full length does not have influence on the plant size. This assumption is found to be reasonable because smaller sections would both have positive and negative effects on plant size. Infusing a larger amount of smaller parts would require more area. But smaller parts would also be easier to move through the plant, requiring less area to be left free for transport.
- Tooling cost is directly scaled based on weight under the assumption that tooling complexity is comparable. Both positive and negative effects on tooling complexity for blades and towers can be defined. For instance blades have a relatively complex shape which should be accurately represented by the mould for aerodynamic reasons. The tower mould should

on the other hand be separable to allow for removal of the mould form the inside of the cylindrical structure.
- The number of mould cycles for the tower is 400 just like the assumed mould cycle count for wind turbine blades in the reference study.

Based on the assumptions above the blade production cost is adapted to fit the needs to extrapolate the tower cost based on structural weight. The adapted cost figures and weight references for wind turbine blades ready to be used for extrapolation to tower production cost are given in tables tables 9.3 to 9.7. Based on previous experience by ATG-Europe, the cost of labour in the cost estimate is rated at 50 Euro per hour, and attachment labour is not implemented in the labour estimate given here. Attachment labour is separately determined later on in this section.

Table 9.3: Cost scaling part reference weight

Part size	30m	50m	70m
Part weight (tonnes)	3.8	17.4	46.4

Table 9.4: Labour cost

Part size	30m	50m	70m
Cost per blade (Euro)	16,936	48,091	116,176
Cost per kg (Euro)	4.49	2.77	2.50

Table 9.5: Plant cost for different part sizes

Part size	30m	50m	70m
Cost per year (Euro)	1,199,971	1,672,873	2,217,600
Cost per blade (Euro)	833	3,485	9,240
Cost per kg (Euro)	0.22	0.20	0.20

Table 9.6: Tooling cost for different part sizes

Part size	30m	50m	70m
Cost per mold (Euro)	2,178,810	600,803	1,213,787
Cost per blade (Euro)	544	1,502	3,034
Cost per kg (Euro)	0.14	0.09	0.07

The total production cost per part shows to be linearly related to part weight and is therefore linearly extrapolated to obtain the cost of the wind turbine tower. For the 134.5 tonnes tower this comes down to a production cost of 388,366 Euro per tower.

Not included in this cost assumption is the automation of the production of wind turbine tower through filament winding. A cost reduction factor is determined based on a paper in which the manufacturing costs of different production methods are compared [52]. This paper gives a cost indication for small parts being manufactured by different manufacturing methodologies in large quantities. Using the cost data given in the paper for a manual process with autoclave curing, a filament winding process with autoclave curing, and a filament winding process without autoclave curing, allows for extraction of the autoclave cost in this comparison. This enables the comparison

Table 9.7: Total production cost for different part sizes

Part size	30m	50m	70m
Cost per blade (Euro)	20,008	57,886	140,068
Cost per kg (Euro)	5.30	3.33	3.02

Table 9.8: Automation cost scaling per part

Manual with autoclave process cost (Euro)	294.14
Winding with autoclave process cost (Euro)	153.40
Winding without autoclave process cost (Euro)	129.40
Autoclave cost (Euro)	24.00
Manual out of autoclave process cost (Euro)	270.14
Manual to filament winding cost ratio (Euro)	0.48

of a manual process without autoclave and a filament winding process without autoclave. The data is given in the table 9.8.

The cost ratio between a manual and winding process given in table 9.8 would reduce tower production cost to 186,031 Euro as an estimate for the automated production cost. It must be said that production of a tower would lead to way larger parts in way lesser quantities to be manufactured by winding than discussed in the reference paper. This would lead to a smaller amount of time required for start-up and finishing of the winding process and might therefore influence the cost effectiveness of the winding process positively for the tower. On the other hand the manual reference cost is also affected by start-up and finishing effects in a similar way. It is therefore assumed the effect of this on the cost ratio is small and is not taken into account. Another assumption in determining this knock-down factor is made in the type of winding process. The reference process is considering wet winding which consists of winding wet fibres and having an elevated temperature oven cure cycle afterwards. This is different compared to the dry winding vacuum infusion process considered for the tower. No detailed cost studies on dry wound vacuum infused parts are known to the author. It is for now assumed that the differences in cost between the dry and wet winding techniques are small. The exact influences of the dry winding with vacuum infusion on the cost of composite lattice towers has to be detailed in further research.

Finally the attachment labour cost as determined from the reference under the assumptions stated before would boil down to the data in tables 9.9 to 9.11.

Table 9.9: Attachment zone labour cost

Part size	30m	50m	70m
Cost per blade (Euro)	11,880	22,097	38,114
Cost per kg (Euro)	3.15	1.27	0.82

Table 9.10: Attachment zone structure cost

Part size	30m	50m	70m
Cost per blade (Euro)	794.55	4136.36	11,773
Cost per kg (Euro)	0.21	0.24	0.25

Table 9.11: Attachment zone total cost

Part size	30m	50m	70m
Cost per blade (Euro)	12,675	26,233	49,887
Cost per kg (Euro)	3.36	1.51	1.08

The total attachment cost per blade again scales linearly with total part weight. The trend is therefore linearly extrapolated to get the tower attachment cost of 126344 Euro. Bringing the total production cost to 312,375 Euro.

It must be noted that this way of estimating the production cost is very rough. However it gives an insight in the expected order of magnitude of production cost. It is shown in section 9.1.5 that the total cost is highly dominated by material cost and therefore inaccuracies in the current production cost estimation are not expected to influence the concluding total cost picture.

9.1.3 Reference tower material and production cost

The material and production cost of the reference tower is relatively easy to establish because it is a conventional design. A study is found into cost scaling of wind turbines based on basic parameters wind turbine such as rotor swept area and hub height [16]. The tower cost in this study is based on the mass of wind turbine and a production cost of rolled steel of 1.50 Euro/kg. The NREL 5MW reference turbine tower has a mass of 347.5 kg. This brings the production and material cost of the entire reference steel turbine tower to 510,000 Euro.

9.1.4 Transport and assembly cost comparison

The transport and assembly cost estimation is based on the differences in transport and assembly between steel towers and composite towers. Hence only the aspects on which extra or less cost is expected for a composite wind turbine tower are highlighted in this section. This makes sense since the final goal is to make a cost comparison in this chapter. The transport and assembly cost comparison is based on a report written by the Sandia National Laboratories on wind turbine logistics [15]. As mentioned before in section 6.3 the maximum transport dimensions are a limiting factor for the design because of the high increase in transport costs related to overshooting a diameter of 4.4m. This leads to a design for which full tower sections would be transportable on a truck at once. This dimension limitation is not found in steel towers since these can be transported in quarter sections and welded together on side. This difference is where the transport and assembly difference between the steel reference tower and the composite tower come from. Not having quarter section tower parts for the composite design yields less parts to be transported and no assembly cost for attaching the quarter sections.

The total cost of quarter section welding can be extracted from the wind turbine logistics report for the tower under investigation. The tower consists of 7 tubular sections which are all transported in quarter tubes. Combining this gives the cost of assembling one tubular section and is given in table 9.12

Table 9.12: Quarter tower assembly cost

Total uarter tower assembly cost (Euro)	226,374
Amount of tubular sections	7
Quarter tower assembly cost per tubular section (Euro)	32,339

To determine the quarter tower assembly cost of the NREL 5MW reference tower, the minimum number of sections in which the tower can be transported is determined to be four. This leads to sections of 21.9m long of which one section has a diameter below 4.4m. Hence three section have to be transported in quarter section leading to a total quarter section assembly cost for the NREL 5MW reference tower of 97,017 Euro.

A comparable reasoning can be applied to the transport cost of the NREL 5MW reference tower. As discussed before in section 6.3 the cost of transporting a tower in sections fitting a normal truck are given in table 6.18. Based on this the cost involved with transporting the 13, 3*4

quarter + 1 tubular, sections of the NREL reference turbine amount to 107,714 Euro. The cost of transporting the composite tower with a base diameter below 4.4m has already been given in section 6.3 and is 33,143 Euro. Based on the truck transport cost of the composite and the steel reference tower and the extra cost in assembly for the steel tower a total savings on transport cost and assembly made by using the composite tower is given in table 9.13

Table 9.13: Composite tower transport and assembly savings

Transport cost savings (Euro)	74,571
Assembly cost savings (Euro)	97,017
Total cost savings (Euro)	171,589

9.1.5 Total cost comparison

Based on the cost estimations done in the previous sections of the chapter, a cost comparison can be made based on the cost related to the process of manufacturing the wind turbine tower to installing it on-site. The production costs of both the composite and the steel reference tower have been estimated and a cost saving on transport and assembly for the composite tower has been determined. These numbers are summarised in table 9.14.

Table 9.14: Total cost comparison of a steel and composite wind turbine

	Steel tower	Composite tower
Material cost (Euro)	510,000	1,044,000
Production cost (Euro)		312,000
Transport and assembly savings (Euro)	0	-171,000
Total (Euro)	510,000	1,185,000

It is interesting to notice that the composite tower cost is very dominated by material cost. And that this material cost therefore also drives the cost increase of a composite tower compared to the steel reference. The total cost increase for a composite tower is roughly 675 thousand Euro, however based on the increase of fibre reinforced materials being used in industry, it can be expected that the prices of especially carbon fibres might drop in the future, and that therefore the cost increase for a composite tower would drop as well.

To put the cost increase of 675 thousand Euro into perspective, the number should be compared with the cost of wind energy. The cost of wind energy indicates the cost per certain amount of energy generated, therefore to convert the increase in cost found for the carbon tower to an increase in cost of energy, the amount of energy a wind turbine can produce should be determined. To do this a capacity factor, indicating the factor of energy generated by a turbine, compared to the theoretical maximum amount of energy the turbine could have generated, is determined based on reference studies on wind energy production in Germany [53, 54]. It is found the German wide wind turbine capacity factor is 0.175. By using this capacity factor of 0.175 and assuming a wind turbine life expectancy of 25 years, the 5MW turbine would be able to generate 191.9 GWh in its entire life. Based on this expected amount of energy generated, the expected cost of energy increase due to the composite lattice tower would be 3.52 Euro/MWh. The German research furthermore indicates the current cost of energy ranges for both land and off-shore based wind energy, which enables the determination of a cost increase percentage as given in table 9.15. It can be concluded from the numbers that off-shore is the market where the composite lattice towers have the most potential. Furthermore it is concluded that the composite wind turbine tower can be a cost effective solution when the secondary benefits as described in section 9.2, can together generate wind turbine cost savings of 5-10%.

It must furthermore be noted that the transport and assembly savings only apply to land based wind turbines, and are dependent on the distance of land based transport. Hence for short distance land based transportations it leads to lower transportation cost increases when the 4.4m constraint is not met. This implies that the transport and assembly savings would not be an effect in off-shore projects, because the dimensional limitations on the towers in transport would

Table 9.15: Composite lattice tower cost increase percentage

Location	German energy cost (Euro/MWh)	Composite tower increase (%)
On-Land	45 - 107	7.8 - 3.3
Off-shore	119 - 194	3.0 - 1.8

not apply here. However this also means that for short distance land based transportation and for off-shore applications the tower might even be optimised to a higher degree by releasing the maximum diameter constraint, which can enable the use of glass fibre as reinforcement or getting further weight savings on the carbon fibre tower. Additionally, the potential for further weight reductions up to 11% have been indicated in section 7.4, an 11% reduction in tower mass would lead to significant material cost reductions.

9.2 Additional performance considerations

As indicated before additional benefits are foreseen for the wind turbine tower. The most important one is the possibility in reducing the tower-blade interaction induced cyclic loading of the blade because of the air transparent nature of the composite lattice structure. Based on further research on this effect, conclusions can be drawn on the magnitude of this effect and the resulting impact on the blade design. A reduction in cyclic loading on the blade could result in blade weight reductions, which can result in tower weight reductions, due to the lower mass at the tower top, which increases the natural frequency. When the influence of the tower on the airflow is sufficiently small a so called down wind blade design can even be considered, in which the bending flexibility of the blades is not constrained by the risk of hitting the tower in high loading situations, this also has potential to result in wind turbine blade mass reductions.

To give an indication on potential material cost decreases by this effect, the full tower model has been checked for changes in natural frequency when the blade mass is reduced by 10%. It was found that this influences the natural frequency of the system by 0.8%, and based on the optimisation data it can be found that this roughly results in a tower weight decrease potential of 2.6%. Calculation of the possible cost reductions based on the wind turbine blade scaling study [51], and section 9.1.1, results in total cost reduction of 70,000 Euro, which is 10% of the total cost increase of 675 thousand Euro.

Furthermore corrosion resistance has been indicated as a potential benefit compared to steel. However to make a fair comparison in this area, a broader study on material degradation should be performed since fibre reinforced polymer material can also degrade through for instance water absorption.

Finally also the recycling of composite towers should be taken into account. Steel can effectively be recycled but for fibre reinforced polymers this is more complicated. Further research should indicate to which extend recyclability of the structure is possible and what the influence of recycling and/or waste cost at the end of wind turbine life is.

Chapter 10

Conclusions and impact

Based on the research performed in this project conclusions and recommendations are described in this chapter.

10.1 Conclusions

In this project a feasibility study on fibre reinforced lattice structures for wind turbine towers is performed. The goal of the study is to assess the feasibility based on the objectives to:

1. Design a full scale composite lattice tower structure fulfilling the design requirements obtained from references.
2. Show manufacturability of representatively scaled samples of the structure.
3. Evaluate the real life mechanical performance and behaviour of composite lattice geometries under wind turbine typical design loads.
4. Obtain a relative cost figure for the composite design in comparison to a reference tower, based on the cost related to the process of tower production up to the assembly on-site.

A full scale tower design is performed based on the expected loads in normal wind turbine operations with an occurrence probability of once per 50 years, and a constraint on natural frequency of 0.222 Hz. The tower dimensions are constraint by the dimensions of the "NREL 5MW reference wind turbine", except for the base diameter which is reduced to 4.4m for road transportation cost reductions. Based on the base diameter requirements it is found that a glass fibre design is not feasible for stiffness reasons. Therefore a glass fibre design with a base diameter of 6m is compared to a carbon fibre design with a base diameter of 4.4m. It is concluded that the carbon fibre design is 35,000 Euro more expensive in material cost, but that not meeting the 4.4m base diameter requirement with a glass fibre reinforced tower results in a 1.2 million Euro cost increase in tower transportation. Therefore the carbon fibre 4.4m base diameter is favoured in this research.

A tower complying to the design requirements as stated has been designed and optimised to a weight of 134.5 tonnes, as compared to the steel reference weighing 347.5 tonnes. This shows that objective 1 has been achieved. It must however be noted that the optimisation is done based on two important basic structural properties: structural strength based on the specified loads and natural frequency of the tower. Since there are more load cases described by regulations for more detailed loading aspects than these two it can not be ruled out that the design and hence the optimum might be affected by one of the other load cases defined. Expanding the set of load cases is left for further research.

Test samples have been manufactured based on the preliminary and detailed tower designs. Samples based on the preliminary design scaled with a factor 6, and samples based on the detailed design scaled with a factor 9.5 plus an additional reduction in rib height are successfully manufactured using vacuum infusion as a low cost production method. This shows that objective 2 has been achieved. Achieving objective 2 does not mean that the technology is ready to produce a full scale tower. It does however indicate that the manufacturing technology is ready to be tested on a larger scale samples.

The scaled samples based on the detailed design considerations are tested in compression. Differences between the test results and the initial finite element model build before the tests are found. The test samples have a lower stiffness, a lower strength and show out of plane deflections, compared tot the initial finite element model. Changing the initial model based on geometry differences, fibre volume distributions, fibre angles in the node and a non-uniform fibre volume distribution over the height of the grid improve the modelling results significantly. This shows that the real life sample behaviour is better understood, and that the strength and stiffness can be explained more accurately by the model. The test results and improvements in sample modelling

show that objective 3 is achieved. It must be noted that the bending observed in the samples comes from the fibre waviness in the sample. This waviness is partly allowed by the lack of fibre tension. With a filament winding process fibre tension would be applied and therefore has the potential to decrease the fibre waviness. Further research should be performed to determine this effect.

The cost of a carbon fibre tower has been compared to the steel reference tower based on material cost, production cost and transport and assembly savings. It has been concluded that the final carbon tower design is 675 thousand Euro more expensive than the steel reference tower. This cost estimate proofs completion of objective 4. It is furthermore observed that potential for more efficient material usage, and for glass fibre reinforcement is there when the design constraint of 4.4m can be dropped in for instance off-shore applications. Based on this cost figures found it is concluded that the composite lattice wind turbine tower becomes economically attractive when the secondary benefits of the composite lattice tower have the potential of further cost reductions of 5-10

Further cost reduction might be found in several areas of interest. The current carbon fibre cost estimation is done based on a 12 Euro/kg carbon fibre cost assumption. Carbon fibre prices are rather high at this moment in time, however when the carbon fibre prices drop over time, due to general industry using the material more and more, this could lead to potential fibre reinforce lattice wind turbine tower material cost reductions, therefore this type of structure has the potential to become more interesting over time. Furthermore potential composite lattice structure influences on cost are seen in a different tower-blade interaction. Due to the air transparent nature of the composite lattice structure, cyclic loading on the blades might be reduced, these reductions in blade cyclic loading might lead to weight and cost savings. And finally the different corrosive/degradation properties of the composite material compared to steel could have influences on the cost as well. The exact determination of the magnitude of these effects on cost is however left for further research.

Based on the expectations beforehand as described in the introduction it can be concluded that the a composite lattice structure can be designed with a lower weight than the steel reference tower. The design had the effect of transport and assembly cost reductions, however this cost reduction did not come from the difference in weight but from the lower number of parts to be transported and assembled when the tower is designed with a base diameter of 4.4m. The material cost at this moment in time did show to be the driver in composite tower cost, making the composite tower economically less competitive with respect to the steel tower. Glass fibre was expected to be the most cost efficient fibre for this application, which turned out not to be true in any case. Since the design turned out to be stiffness driven, carbon fibre turned out to be the material leading to the most cost efficient design for towers requiring a small base diameter.

As a final conclusion, a composite lattice structure for wind turbines seems to be structurally feasible and shows potential secondary benefits. However material cost seems to be a weakness at this moment in time. Ways to improve the cost figure of this concept should be found in the secondary benefits, potentially further weight optimisations, and potential material cost reductions over time, to make the composite lattice wind turbine tower economically competitive.

10.2 Recommendations

Based on the results multiple recommendations can be made for further research. The recommendations follow from the conclusions of this project, but also indicate how further research can broaden the understanding of the effects a composite lattice tower has on the entire wind turbine system.

Based on the full tower design it is recommended to expand the number of load cases for which the tower design is optimised. Especially fatigue is considered important to be included in further research. Furthermore since the structural model of the complete tower is analysed using shell elements the effects of node regions on especially stress concentrations is not taken into account in the complete tower model. Therefore further research is recommended for determining the exact differences in modelling results between such a simplified surface model, a solid model with accurate methods for local failure determination and test samples. Knock-downs to improve the strength and stiffness estimations of the tower can be determined based on this. The knock-downs are useful in further composite lattice tower design studies.

Attachment structures are not taken into account in the current model. The attachment structures are expected to have little influence on the global stiffness of the tower but can however have significant effects on stress concentrations. It is therefore recommended to include the effects of an attachment structures in the model.

Based on lessons learned from the testing campaign, it is recommended to perform tests on samples with a representative rib heigh to rib width ratio and tensioned fibres to better represent the composite lattice geometry and the filament winding process. Based on such tests it can be determined if the bending seen originates from the down scaling and manufacturing differences or that the behaviour is really an inherent property of the structure. It would also be very valuable

to perform tests with carbon fibre samples to observe possible differences between the carbon fibre and glass fibre sample behaviour.

To determine further structural performance of the composite lattice geometry it is considered important to perform shear/ combined loading tests to represent the different types of load the structure has to resist. Fatigue tests are considered to be an important next step in structural property determination. Furthermore strength after impact tests are considered to be of importance since the composite lattice geometry does not have fibres in other directions than the rib direction, making it a weak type of structure in irregular loading conditions.

Considering the cost of the structure, potential is observed in further weight optimisation of the structure, especially of off-shore applications. This potential should be further investigated with an expanded form of the optimisation approach, to include a larger amount of load cases and strength knock-down factors.

Improvements in cost estimation can especially be made on the production cost, by further detailing the origin of costs, and as such determine a tower specific cost estimation, instead of using a wind turbine blade scaling study to extrapolate to tower production cost. Furthermore post-curing effects on the structural performance should be studied in further research, to determine if post-curing is a necessary production step. When post-curing turns out to be a necessary extra production step this could translate to an increase in production cost.

Furthermore potential is seen in reducing the cost of a composite lattice tower wind turbine because of the air transparent nature of the structure. This could lead to reduced cyclic loading on the blade, which might reduce blade mass and cost. It is therefore recommended to research the effect the composite lattice tower has on the airflow using wind tunnel tests. This can be the basis of a more global optimisation of the entire composite lattice tower based wind turbine system, leading to further cost reductions.

Furthermore studies on the cost effects of the corrosion resistance but also on specific fibre reinforced polymer material degradation factor should be performed. It is also advised to study the recyclability of the structure and account for the effect of cost through recycling and/or waste processing of the structure at the end of wind turbine life.

Chapter 11

Project implementation

This chapter describes the problems (technical and organizational) that have occurred during the project and how these issues were resolved (where applicable).

- **Explanation of changes to the project plan**
  The project was delayed by half a year due to unavailability of resources at the time of foreseen kick-off (KO). A shift of the KO date was requested and granted, allowing for necessary actions to be taken internally. From the new starting date, the project ran on schedule.
- **Explanation method of dissemination**
  The output of the project is this report plus manufacturing samples of the technology under consideration. It is not foreseen to use the current report in any method of dissemination, however parts of its contents will be used for presentations and (potentially) scientific papers. For PR purposes, the samples are displayed at ATG Europe HQ and results from the project may be published on the company website or in company presentations. Given the outcome of the project (results of the feasibility) it is also foreseen to get in contact with potential end-users of the technology in the wind energy industry and beyond. It goes without saying that the output of this projects will serve as a basis for talks and discussions with interested parties. If and when applicable ATG Europe will be more than willing to present the results at dedicated industry platforms (WoZ meetings/b2b meetings/matchmaking events/)

There were no significant deviations from the project budget or plan. Some additional work was done beyond the one initially planned and budgeted, but this was handled internally by ATG Europe.

Chapter 12

Acknowledgements

Het project is uitgevoerd met subsidie van het Ministerie van Economische Zaken, Nationale regelingen EZ-subsidies, Topsector Energie uitgevoerd door Rijksdienst voor Ondernemend Nederland.

Bibliography

[1] Huybrechts, S. M., Meink, T. E., Wegner, P. M., and Ganley, J. M., "Manufacturing theory for advanced grid stiffened structures," *composites: Part A*, Vol. 33, 2002, pp. 155–161.

[2] Barone, M., Paquette, J., Resor, B., and Manuel, L., "Decades of Wind Turbine Load Simulation," *50th AIAA Aerospace Sciences Meeting*, Nashville, 2012.

[3] "EPIKOTE Resin MGS RIMR 135 and EPIKURE Curing Agent MGS RIMH 134-137," Tech. rep., Hexion, 2006.

[4] Peters, L., Adolphs, G., Bech, J. I., and Brøndsted, P., "HiPer-tex WindStrand: A new generation of high performance reinforcement," Tech. rep., Owens Corning, 2006.

[5] Toray, "T300 Data Sheet," Tech. rep.

[6] Polyzois, D. J., Raftoyiannis, I. G., and Ungkurapinan, N., "Static and dynamic characteristics of multi-cell jointed GFRP wind turbine towers," *Composite Structures*, Vol. 90, 2009, pp. 34–42.

[7] Lim, S., Kong, C., and Park, H., "A Study on Optimal Design of Filament Winding Composite Tower for 2 MW Class Horizontal Axis Wind Turbine Systems," *International Journal of Composite Materials*, Vol. 3, No. 1, 2013, pp. 15–23.

[8] Hou, A. and Gramoll, K., "Compressive Strength of Composite Lattice Structures," *Journal of Reinforced Plastics and Composites*, Vol. 17, No. 5, 1998.

[9] Vasiliev, V. V. and Razin, A. F., "Anisogrid composite lattice structures for spacecraft and aircraft applications," *Composite Structures*, 2006.

[10] Vasiliev, V. V., Barynin, V. A., and Razin, A. F., "Anisogrid composite lattice structures - Development and aerospace applications," *Composite Structures*, 2012.

[11] R.R. Pedersen, S.R.K. Nielsen, P. T.-C., "Stochastic analysis of the influence of tower shadow on fatigue life of wind turbine blade," *Structural Safety*, Vol. 35, 2012, pp. 63–71.

[12] International Electrotechnical Commission, "IEC 61400-1 Wind turbines Part1: Design requirements," Tech. rep., IEC, Geneva, 2014.

[13] Buhl, M. L. and Manjock, A., "A Comparison of Wind Turbine Aeroelastic Codes Used for Certification," *AIAA Aerospace Sciences Meeting and Exhibit*, Reno, Nevada, 2006.

[14] Jonkman, J., Butterfield, S., Musial, W., and Scoot, G., "Definition of a 5-MW Reference Wind Turbine for Offshore System Development," Tech. rep., NREL, Golden, 2009.

[15] Smith, K., "WindPACT Turbine Design Scaling Studies Technical Area 2: Turbine, Rotor, and Blade Logistics," Tech. Rep. June, 2001.

[16] Fingersh, L., Hand, M., and Laxson, A., "Wind Turbine Design Cost and Scaling Model," Tech. rep., 2006.

[17] Huybrechts, S. and Tsai, S. W., "Analysis and Behavior of Grid Structures," *Composites Science and Technology*, Vol. 56, 1996, pp. 1001–1015.

[18] Chen, H.-J. and Tsai, S. W., "Analysis and Optimum Design of Composite Grid Structures," *Journal of composite Materials*, Vol. 30, No. 4, 1996, pp. 503–534.

[19] Vasiliev, V., Barynin, V., and Rasin, A., "Anisogrid lattice structures, survey of development and application," 2001.

[20] Huybrechts, S. M., Hahn, S. E., and Meink, T. E., "Grid Stiffened Structures: A Survey of Fabrication Analysis and Design Methods," *International Conference on Composite Materials*, 1999.

[21] Gurdal, Z. and Gendron, G., "Optimal design of geodesically stiffened composite cylindrical shells," *Composites Engineering*, Vol. 3, No. 12, 1993, pp. 1131–1147.

[22] Wodesenbet, E., Kidane, S., and Pang, S.-S., "Optimization for buckling loads of grid stiffened composite panels," *Composite Structures*, Vol. 60, 2003, pp. 159–169.

[23] Reddy, A. D., Valisetty, R., and Rehfield, L. W., "Continuous filament wound composite concepts for aircraft fuselage structures," *Journal of Aircraft*, Vol. 22, No. 3, 1985, pp. 249–255.

[24] Jaunky, N., Knight, N. F., and Ambur, D. R., "Formulation of an improved smeared stiffener theory for buckling analysis of grid-stiffened composite panels," *Composites Part B: Engineering*, Vol. 27, No. 5, 1996, pp. 519–526.

[25] Zhang, B., Zhang, J., Wu, Z., and Du, S., "A load reconstruction model for advanced grid-stiffened composite plates," *Composite Structures*, Vol. 82, 2008, pp. 600–608.

[26] Jaunky, N., Knight, N., and Ambur, D., "Optimal design of general stiffened composite circular cylinders for global buckling with strength constraints," *Composite Structures*, Vol. 41, No. 3-4, 1998, pp. 243–252.

[27] Baker, D. J., Fudge, J., Ambur, D. R., and Kassapoglou, C., "Optimal Design and Damage Tolerance Verification of an Isogrid Structure for Helicopter Application," *44th AIAA/ASME/ASCE/AHS Structures, Structural Dynamics, and Materials Conference*, No. April, Norfolk, 2003, pp. 1–19.

[28] Holopainen, T. P., "Finite element free vibration analysis of eccentrically stiffened plates," *Computers & Structures*, Vol. 56, No. 6, 1995, pp. 993–1007.

[29] Kolli, M. and Chandrashekhara, K., "Finite element analysis of stiffened laminated plates under transverse loading," *Composites Science and Technology*, Vol. 56, 1996, pp. 1355–1361.

[30] Kumar, Y. V. S. and Mukhopadhyay, M., "A new triangular stiffened plate element for laminate analysis," *Composites Science and Technology*, Vol. 60, 2000, pp. 935–943.

[31] Zhifeng Zhang, Haoran Chen, and Lin Ye, "A Stiffened Plate Element Model for Advanced Grid Stiffened Composite Plates/Shells," *Journal of Composite Materials*, Vol. 45, No. 2, 2011, pp. 187–202.

[32] Kassegne, S. K. and Reddy, J. N., "Local behavior of discretely stiffened composite plates and cylindrical shells," *Composite Structures*, Vol. 41, 1998, pp. 13–26.

[33] Guo, M.-W., Harik, I. E., and Ren, W.-X., "Buckling behavior of stiffened laminated plates," *International Journal of Solids and Structures*, Vol. 39, 2002, pp. 3039–3055.

[34] Jadhav, P. and Mantena, P. R., "Parametric optimization of grid-stiffened composite panels for maximizing their performance under transverse loading," *Composite Structures*, Vol. 77, 2007, pp. 353–363.

[35] Totaro, G. and De Nicola, F., "Recent advance on design and manufacturing of composite anisogrid structures for space launchers," *Acta Astronautica*, Vol. 81, 2012, pp. 570–577.

[36] Shroff, S., *Design, Analysis, Fabrication and Testing of Grid-Stiffened Structures for Fuselage Applications*, Ph.D. thesis, TU Delft, 2014.

[37] Cain, J. J., Post, N. L., Lesko, J. J., Case, S. W., Lin, Y.-N. N., Riffle, J. S., and Hess, P. E., "Post-curing effects on marine VARTM FRP composite material properties for test and implementation," *Journal of Engineering Materials and Technology-Transactions of the Asme*, Vol. 128, No. 1, 2006, pp. 34–40.

[38] Venditti, R. a. and Gillham, J. K., "A relationship between the glass transition temperature (Tg) and fractional conversion for thermosetting systems," *Journal of Applied Polymer Science*, Vol. 64, No. 1, 1997, pp. 3–14.

[39] Abdelkader, A. and White, J., "Water absorption in epoxy resins: The effects of the crosslinking agent and curing temperature," *Journal of applied polymer science*, Vol. 98, No. 6, 2005, pp. 2544–2549.

[40] De'Nève, B. and Shanahan, M. E. R., "Water absorption by an epoxy resin and its effect on the mechanical properties and infra-red spectra," *Polymer*, Vol. 34, No. 24, 1993, pp. 5099–5105.

[41] Boisseau, A., Davies, P., and Thiebaud, F., "Sea Water Ageing of composites for ocean energy conversion systems: Influence of glass fibre type on static behaviour," *Applied Composite Materials*, Vol. 19, No. 3-4, 2012, pp. 459–473.

[42] Boisseau, a., Davies, P., and Thiebaud, F., "Fatigue behaviour of glass fibre reinforced composites for ocean energy conversion systems," *Applied Composite Materials*, Vol. 20, No. 2, 2013, pp. 145–155.

[43] Valery V. Vasiliev; Evgeny V. Morozov, *Advanced mechanics of composite materials*, second edi ed., 2007.

[44] Rene Bos, "PHd in the TU Delft wind energy group," 2015.

[45] 3B-Fibreglass, "SE 1500 Direct Rovings data sheet," Tech. rep., 3B-Fibreglass.

[46] Maes, V. K., *Design, Analysis, Optimization and Testing of Grid-Stiffened Composite Structures*, Ph.D. thesis, Delft University of Technology, 2015.

[47] Lee, S. and Waas, A. M., "Compressive response and failure of fiber reinforced unidirectional composites," *International Journal of Fracture*, Vol. 100, No. 3, 1999, pp. 275–306.

[48] Clyne, B., Kiatlertpongsa, J., Brook, D., Barber, B., Best, C., and Sallows, L., "Strength of long fibre composites, http://www.doitpoms.ac.uk/tlplib/fibre_composites/index.php," .

[49] Huntsman, "RenCast CW 2215 / Ren HY 5160 Data sheet," Tech. rep., Hunstman, 2007.

[50] Lange-Ritter, "Lange Ritter Preisliste," 2016.

[51] TPI-Composites, "Cost Study for Large Wind Turbine Blades : WindPACT Blade System Design Studies," Tech. rep., 2003.

[52] Krolewski, S. M., "Study of the application of automation to composites manufacturing," Tech. rep., 1989.

[53] Kost, C., Mayer, J. N., Thomsen, J., Hartmann, N., Senkpiel, C., Philipps, S., Nold, S., Lude, S., Saad, N., and Schlegel, T., "Levelized Cost of Electricity Renewable Energy Technologies," Tech. Rep. November, 2013.

[54] Burger, B., "Electricity Production from solar and wind in Germany in 2012," Tech. rep., 2013.

[55] Bryan Harris, *Engineering composite materials*, The institute of materials, London, 1999.